Coordination Chemistry Reviews xxx (2017) xxx–xxx

Contents lists available at ScienceDirect

Coordination Chemistry Reviews

journal homepage: www.elsevier.com/locate/ccr

Review

Coordination chemistry of 1,3,5-triaza-7-phosphatricyclo[3.3.1.1]decane (PTA) and derivatives. Part III. Variations on a theme: Novel architectures, materials and applications

Antonella Guerriero, Maurizio Peruzzini *, Luca Gonsalvi *

Consiglio Nazionale delle Ricerche, Istituto di Chimica dei Composti Organometallici (CNR-ICCOM), Via Madonna del Piano 10, 50019 Sesto Fiorentino (Firenze), Italy

ARTICLE INFO

Article history:
Received 12 June 2017
Received in revised form 18 September 2017
Accepted 22 September 2017
Available online xxxx

Dedicated to Prof. Pierre Braunstein, in recognition of his outstanding contributions in organometallic chemistry, homogeneous catalysis and much more, on occasion of his 70th birthday.

Keywords:
1,3,5-Triaza-7-phosphatricyclo[3.3.1.1]decane
Water soluble ligands
Coordination chemistry
X-ray crystallography
Catalysis
Materials science
Medicinal inorganic chemistry

ABSTRACT

This review paper covers the recent (2010–2017) synthetic modifications of the water soluble cage-like aminophosphine ligand 1,3,5-triaza-7-phosphatricyclo[3.3.1.1]decane (PTA) and their application in coordination chemistry, with a focus on applications in the fields of selected catalytic processes, 1D–3D materials and mention to novel use as anticancer and antimicrobial agents in medicinal inorganic chemistry.

© 2017 Elsevier B.V. All rights reserved.

Abbreviations: PTA, 1,3,5-triaza-7-phosphatricyclo[3.3.1.1]decane; HPTA, 1-H-1,3,5-triaza-7-phosphatricyclo[3.3.1.1]decane; mPTA, 1-methyl-1,3,5-triaza-7-phosphatricyclo[3.3.1.1]decane; PTA—Bn, 1-benzyl-1,3,5-triaza-7-phosphatricyclo[3.3.1.1]decane; PTA═S, 1,3,5-triaza-7-phosphatricyclo[3.3.1.1]decane-7-sulfide; PTA═O, 1,3,5-triaza-7-phosphatricyclo[3.3.1.1]decane-7-oxide; PTA—SO_2, 2-thia-1,3,5-triaza-7-phosphatricyclo[3.3.1.1]decane-2,2-dioxide; dmoPTA, 3,7-dimethyl-1,3,7-triaza-5-phosphabicyclo[3.3.1]nonane; HdmoPTA, 3,7-H-3,7-dimethyl-1,3,7-triaza-5-phosphabicyclo[3.3.1]nonane; DAPTA, 3,7-diacetyl-1,3,7-triaza-5-phosphabicyclo[3.3.1]nonane; PZA, phenyl-(1,3,5,-triaza-7-phosphatricyclo[3.3.1.1]dec-6-yl)methanol; PZA-NMe_2, 4′-(dimethylamino)phenyl-(1,3,5,-triaza-7-phosphatricyclo[3.3.1.1]dec-6-yl)methanol; CAP, 1,4,7-triaza-9-phosphatricyclo[5.3.2.1^{4,9}]tridecane; p-cymene, η^6-$C_{10}H_{14}$; Tp, κ^3-tris(pyrazolyl)borate; Tpm, κ^3-tris(pyrazol-1-yl)methane; Tpms, tris(pyrazol-1-yl)methanesulfonate; *m*TPPMS, *meta*-(triphenylphosphine)monosulfonate; *m*TPPTS, *meta*-(triphenylphosphine)trisulfonate; THP, tris(hydroxymethyl)phosphine; RAPTA, generic Ru–arene-PTA complex; RAPTA-C, [$RuCl_2$(p-cymene)(PTA)]; Na[$H_2B(pz)_2$], κ^2N-dihydrobis(pyrazolyl)borate sodium salt; K[$H_2B(tz)_2$], dihydrobis(triazolyl)borate potassium salt; K[$H_2B(tzNO_2)_2$], dihydrobis(3-nitro-1,2,4-triazolyl)borate potassium salt; $CH_2(pz)_2$, bis(pyrazol-1-yl)methane; H[bdmpza], κ*N,N,O*-bis(3,5-dimethylpyrazol-1-yl)acetic acid; Hba, benzoic acid; Hcba, 4-cyanobenzoic acid; Haba, 2-aminobenzoic acid; H_2tpa, terephthalic acid; H_2suc, succinic acid; H_2adip, adipic acid; H_2mal, malonic acid; Hchc, cyclohexanecarboxylic acid; H_2chdc, 1,4-cyclohexanedicarboxylic acid; H_4chtc, 1,2,4,5-cyclohexanetetracarboxylic acid; H_2pga, 3-phenylglutaric acid; H_2dmga, 3,3-dimethylglutaric acid; H_2pma, phenylmalonic acid; bipy, 2,2′-bipyridine; dtbpy, 4,4′-di-*tert*-butyl-2,2′-bipyridine; phen, 1,10-phenanthroline; neocup, 2,9-dimethyl-1,10-phenanthroline; dione, 1,10-phenanthroline-5,6-dione; tht, tetrahydrothiophene; Spy, pyridine-2-thiolate; Spyrim, pyrimidine-2-thiolate; Smepyrim, 4-methylpyrimidine-2-thiolate; SMe_2pyrim, 4,6-dimethylpyrimidine-2-thiolate; MNP, metal nanoparticles; salphen, *N,N′*-bis(salilcylidene)imine-1,2-phenylenediamine; MOF, metal organic framework; LC_{50}, median lethal concentration required to kill half the members of a tested cell population after a specified test duration; LD_{50}, median lethal dose required to kill half the members of a tested cell population after a specified test duration; GI_{50}, concentration for 50% of maximal inhibition of cell proliferation; IC_{50}, half maximal inhibitory concentration for a specific biological or biochemical function; NMR, multiplicities; s, singlet; d, doublet; dq, doublet of quartets; t, triplet; dt, doublet of triplets; tt, triplet of triplets; br, broad; brs, broad singlet; q, quartet; sept, septuplet; m, multiplet; TON, turnover number; TOF, turnover frequency (h^{-1}); ^{t}BuDAD, *tert*-butyldiazadiene; OTf^-, $CF_3SO_3^-$, triflate anion; CORM, carbon monoxide releasing molecules; Mb, myoglobin; phen, 1,10-phenanthroline; pbt, 2-(pyridyl)benzothiazole; CV, cyclic voltammetry; TCNE, tetracyanoethylene; DMAD, dimethylacetylenedicarboxylate; DEAD, diethylacetylenedicarboxylate; DBMH, dibenzoylmethane; HRMS, high resolution mass spectrometry; EPR, electron spin resonance spectroscopy; ET-dmbaH, 17-α-[4′-ethynyldimethylbenzylamine]-17-β-testosterone.

* Corresponding authors.
E-mail addresses: maurizio.peruzzini@iccom.cnr.it (M. Peruzzini), l.gonsalvi@iccom.cnr.it (L. Gonsalvi).

https://doi.org/10.1016/j.ccr.2017.09.024
0010-8545/© 2017 Elsevier B.V. All rights reserved.

Please cite this article in press as: A. Guerriero et al., Coordination chemistry of 1,3,5-triaza-7-phosphatricyclo[3.3.1.1]decane (PTA) and derivatives. Part III. Variations on a theme: Novel architectures, materials and applications, Coord. Chem. Rev. (2017), https://doi.org/10.1016/j.ccr.2017.09.024

Contents

1. Introduction

After the first comprehensive reports on the chemistry of 1,3,5-triaza-7-phosphatricyclo[3.3.1.1]decane (PTA, also denoted in the literature as 1,3,5-triaza-7-phosphadamantane) published in 2004 and 2010, respectively [1], the use of this cage-like water-soluble phosphine and its derivatives, often obtained by cage functionalisation and introduction of different substituents (Chart 1) was expanded further by many research groups worldwide, beyond their established role as ligands for coordination chemistry to noble and base metals. Further to use in catalysis, luminescence studies and medicinal applications, novel approaches were described in the literature, including for example the synthesis of 1D and 3D materials, novel bimetallic complexes endowed with peculiar characteristics, the use as capping agent to stabilise metal nanoparticles (MNPs) and further derivatisations of the adamantyl cage.

In this review article, recent (2010–2017) contributions in the field of synthetic coordination chemistry of PTA and its novel derivatives and use in catalysis will be summarised.

In the field of medicinal inorganic chemistry, the number of reports on the use of ruthenium(II)–arene PTA (RAPTA-type) complexes grew dramatically in the reference years due to their activity as antitumour agents. The synthetic chemistry and the most effective derivatisations of RAPTA complexes, together with studies of the mechanisms of interaction with cells obtained by different experimental techniques and theoretical calculations, has been recently reviewed [2]. Thus, these literature data will not be included in the present review article. The antitumour activity of other classes of PTA complexes will be mentioned in the chapters related to the corresponding syntheses. Finally, the use of (mainly) Group 11 coordination compounds of PTA as antimicrobial agents has recently emerged as a viable application, and selected examples will be here described.

2. Recent ligand structural variations and functionalisations

As previously reviewed [1], PTA can be functionalised either at the "upper rim", on P or C atoms, or at the "lower rim", essentially through quaternisation of a N atom (Chart 1). Whereas the target of C-atom functionalisation is mainly to introduce a pendant arm with donor atoms in such a way to obtain a bidentate P-element ligand, the formation of N—C bonds is generally thought as a suitable way to tune water-solubility and add the desired degree of lipophilicity to the parent compound. Novel PTA analogues and miscellaneous synthetic reactions will be briefly reported below. Table S1 (Supporting Information) summarises ^{1}H and $^{31}P\{^{1}H\}$ NMR data reported in the literature cited, including deuterated solvents used, for the novel ligands and complexes.

2.1. Upper rim functionalisations

P-atom derivatives: Iminophosphorane PTA analogues **1a** and **1b** were obtained by Staudinger-type reaction of PTA with thiophosphoryl azides $(RO)_2P(=S)N_3$ (Scheme 1, R = Et, **1a**; Ph, **1b**) [3]. The products were fully characterised and showed $^{31}P\{^{1}H\}$ NMR doublets with $^{2}J_{PP}$ = 8.9 Hz, at −27.92 ppm for the iminophosphorane and at 62.38 ppm for the thiophosphoryl group in the case of **1a**,

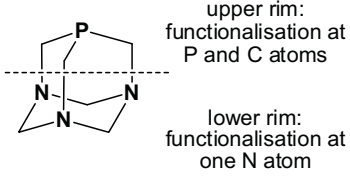

Chart 1. 1,3,5-Triaza-7-phosphatricyclo[3.3.1.1]decane (PTA).

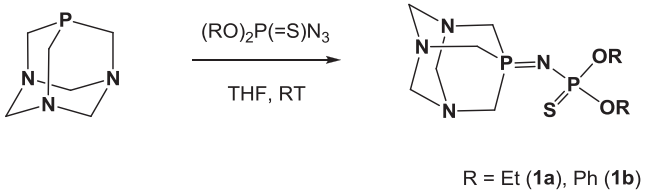

Scheme 1. PTA–iminophosphorane derivatives.

Please cite this article in press as: A. Guerriero et al., Coordination chemistry of 1,3,5-triaza-7-phosphatricyclo[3.3.1.1]decane (PTA) and derivatives. Part III. Variations on a theme: Novel architectures, materials and applications, Coord. Chem. Rev. (2017), https://doi.org/10.1016/j.ccr.2017.09.024

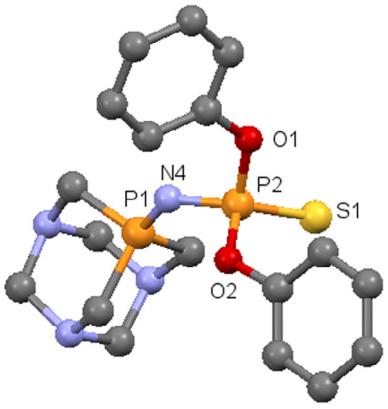

Fig. 1. X-ray crystal structure of PTA–iminophosphorane derivative **1b**. Adapted from Ref. [3b].

while **1b** showed $^{31}P\{^{1}H\}$ NMR doublets with $^{2}J_{PP}$ = 14.7 Hz, at −34.27 ppm for P═N and at 55.64 ppm for the P═S group, respectively. For **1b**, the corresponding X-ray crystal structure was obtained (Fig. 1). The structure showed P—N bond lengths in line with a P═N double bond P(1)—N(4) at 1.569(3) Å and a P—N single bond P(2)—N(4) at 1.584(3) Å [3b]. Reaction of $(RO)_2P(=S)N_3$ with DAPTA (DAPTA = 3,7-diacetyl-1,3,7-triaza-5-phosphabicyclo[3.3.1]nonane) also gave the corresponding iminophosphorane derivatives. The X-ray crystal structure determination for R = Ph confirmed the proposed structure in the solid state, with P—N bond lengths very similar to those of **1b** [3b]. Remarkably, only the products with R = Et were found to be water-soluble, with $S(H_2O)_{20°C}$ = 201 g L^{-1} for **1a** and 312 g L^{-1} for the DAPTA analogue, respectively.

Another iminophosphorane-PTA ligand, namely PTA═N—C(O)-2-BrC_6H_4 (**1c**) was obtained in 86% yield by the Pomerantz method reacting PTA with 2-bromobenzaldehye and ^{t}BuDAD (tert-butyl diazadiene) [4].

Reactions of PTA and mPTA (mPTA = 1-methyl-1,3,5-triaza-7-phosphatricyclo-[3.3.1.1]decane) with four different unsaturated dicarboxylic acids (maleic, fumaric, citraconic and mesaconic acids, Scheme 2) showed the selective formation of the corresponding phosphonium alkanoate zwitterions **2a–b** in water in the absence of added strong acids. NMR studies using D_2O and DFT calculations helped to unravel the lack of reactivity upon N-atom protonation. In details, N-atom quaternisation decreases the reactivity at P atom due to distortion of the cage electron density distribution. The higher reactivities observed for the *E*-isomers were attributed to the more favourable steric and electronic parameters of the corresponding carbanions. As expected, the reaction of PTA with mesaconic acid gave **2b** in very low yields (<10%) after very long reaction time at room temperature [5].

C-atom derivatives: In order to obtain "upper rim" PTA derivatives, introducing binding atoms on pendant arms close to P atom, the lithium salt of PTA (with a formal carbanion on a C atom adjacent to P) was synthesised and reacted with electrophiles by our group and others in the recent past [6]. Expanding on the scope of electrophiles which could react cleanly with PTA–Li, we reported on the synthesis of the water soluble β-phosphino alcohol 4′-(dimethylamino)phenyl-(1,3,5-triaza-7-phosphatricyclo[3.3.1.1]dec-6-yl)methanol, (PZA–NMe_2, **3**) and the corresponding phosphine oxide O═PZA—NMe_2 (**4**) and sulfide S═PZA—NMe_2 (**5**), as shown in Scheme 3 [7]. For **3**, a value of $S(H_2O)_{20°C}$ = 1.9 g L^{-1} was measured.

The compounds were fully characterised in solution by NMR spectroscopy. $^{31}P\{^{1}H\}$ NMR signals were observed for **3** as singlets at −102.72 and −106.27 ppm (3:1 ratio), due to the presence of two distinct diastereoisomers. By fractional crystallisation, the pure (*SR,RS*) isomer was recovered and the corresponding X-ray crystal structure was obtained (Fig. 2). $^{31}P\{^{1}H\}$ NMR signals at 2.09(s) and −14.07(s) ppm were observed for **4** and **5**, respectively.

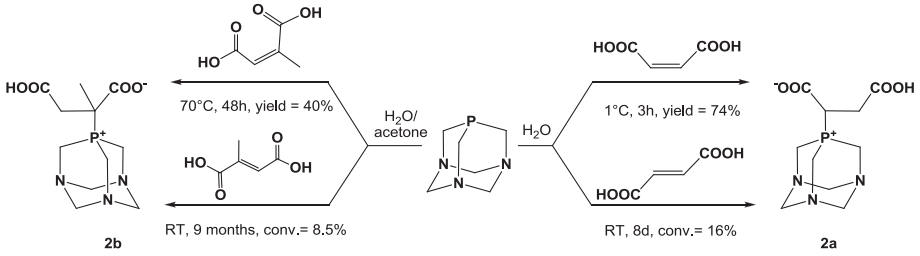

Scheme 2. Phosphonium alkanoates **2a–b** from reaction of PTA with dicarboxylic acids.

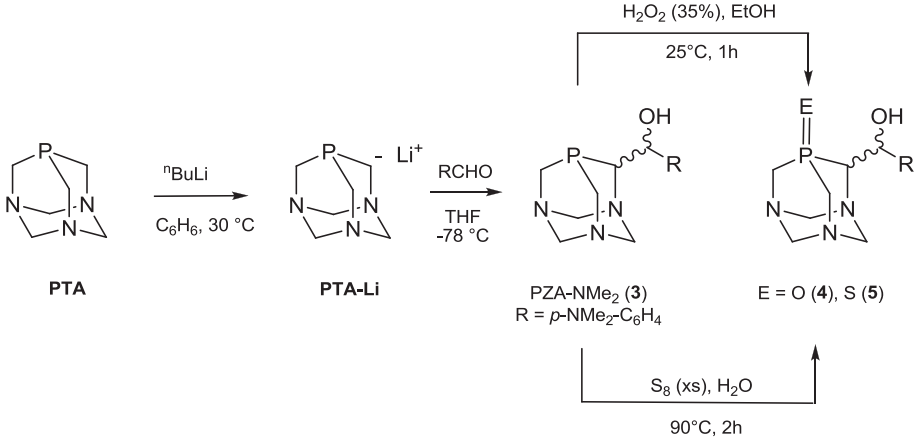

Scheme 3. Synthesis of β-phosphino alcohol **3** and the corresponding oxide **4** and sulfide **5**.

Please cite this article in press as: A. Guerriero et al., Coordination chemistry of 1,3,5-triaza-7-phosphatricyclo[3.3.1.1]decane (PTA) and derivatives. Part III. Variations on a theme: Novel architectures, materials and applications, Coord. Chem. Rev. (2017), https://doi.org/10.1016/j.ccr.2017.09.024

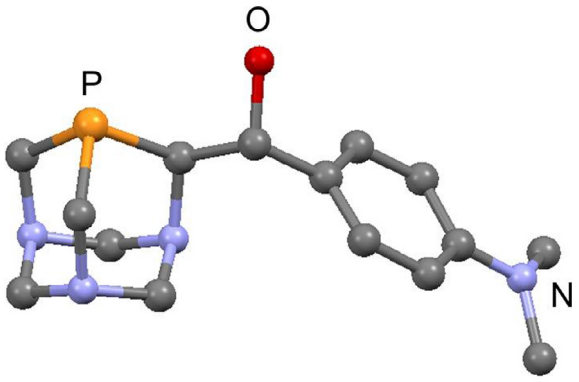

Fig. 2. X-ray crystal structure of (*SR*,*RS*)-PZA-NMe_2 (**3**). Adapted from Ref. [7]. Copyright 2011 American Chemical Society.

Reaction of PTA–Li with 1-methyl-2-imidazole carboxyaldehyde and bis(N-methylimidazole-2-yl)ketone gave the first imidazolyl "upper rim" PTA derivatives, namely 1-methylimidazolyl-(1,3,5-triaza-7-phosphatricyclo[3.3.1.13,7]dec-6-yl)methanol (**6**) and bis(1-methylimidazolyl)(1,3,5-triaza-7-phosphatricyclo[3.3.1.13,7]dec-6-yl)methanol (**7**), as shown in Scheme 4, together with the corresponding phosphine oxides **8** and **9**, the latter obtained in NMR scale quantities by simple reaction of the parent compounds with H_2O_2 in D_2O [8].

Compounds **6** and **7** showed good water solubility, with $S(H_2O)_{20°C} = 320$ and 78 g L^{-1}, respectively. As for **3**, the $^{31}P\{^1H\}$ NMR pattern for **6** showed two singlets, at −103.39 and −104.65 ppm, due to the presence of two diastereoisomers in solution. In the case of **7**, a singlet at −97.55 ppm was present. Phosphine oxides **8** and **9** showed two singlets at 0.59 and −0.48 ppm for **8**, and a singlet at −0.20 ppm for **9**.

Three different (racemic) P,N bidentate "upper rim" PTA β-aminophosphine derivatives **10**–**12** were obtained by reaction of PTA–Li with aryl imines (Scheme 5) in THF at −78 °C followed by quenching with water [9]. Water solubilities were measured at 20 °C in the range 2.7–4.9 g L^{-1}.

The $^{31}P\{^1H\}$ NMR patterns and chemical shift values closely resemble those observed for other "upper rim" derivatives described above, with values at −102.4 and 105.9 ppm (**10**), −102.1 and −105.9 ppm (**11**) and −97.7 ppm (**12**). As previously described for related compounds, the corresponding P-oxides (**13**–**15**) could be obtained by simple reaction of **10**–**12** with aqueous H_2O_2, showing $^{31}P\{^1H\}$ NMR singlets at −2.9 and −5.7 ppm (**13** and **14**) and −1.5 ppm (**15**). X-ray crystal structures were obtained for **10** (both *SR* and *RS* diastereoisomers) and **12** (both *R* and *S* enantiomers). Fig. 3 shows the X-ray crystal structures of *SR*-**10** and *R*-**12**.

Two chiral PTA derivatives (Scheme 6) were synthesised in racemic form upon reaction of PTA–Li with ClP^iPr_2 or $ClP(N^iPr)_2(CH_2)_2$ [10]. The corresponding P,P bidentate ligands PTA–P^iPr_2 (**16**) and PTA–$P(N^iPr)_2(CH_2)_2$ (**17**) showed moderate water solubilities at 25 °C (13.3 and ca. 10 g L^{-1} for **16** and **17**, respectively). Compound **16** showed a pair of $^{31}P\{^1H\}$ NMR doublets at −3.3 (P^iPr_2) and −98.3 ppm (PTA) with a $^2J_{PP} = 50$ Hz, whereas **17** was characterised by a similar pattern with chemical shift values of 100.4 (PR_2) and −100.2 ppm (PTA) with a $^2J_{PP} = 38$ Hz. For both compounds, X-ray crystal structures of *R*-enantiomers were obtained (Fig. 4).

By reaction of **16** and **17** with H_2O_2, as expected, both P atoms were oxidised to give the corresponding bis(P═O) oxide derivatives **18** and **19**, respectively, characterised by $^{31}P\{^1H\}$ NMR doublets at

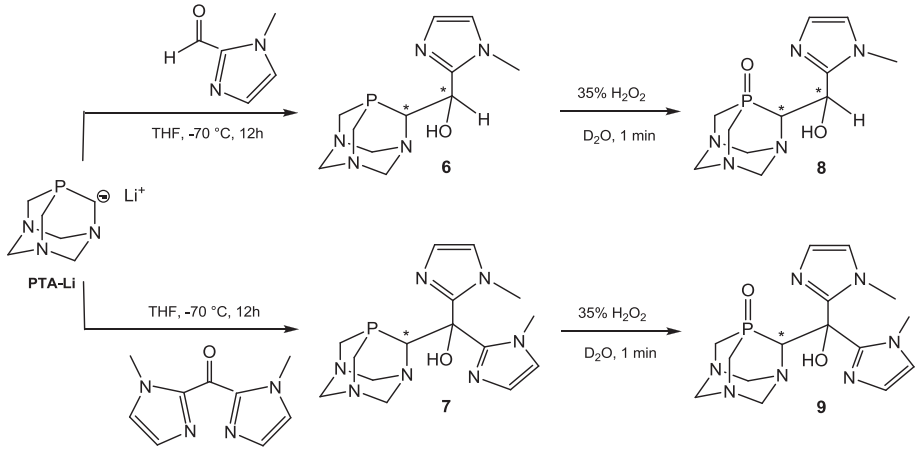

Scheme 4. Synthesis of "upper rim" imidazolyl derivatives **6** and **7** and the corresponding oxides (**8**, **9**).

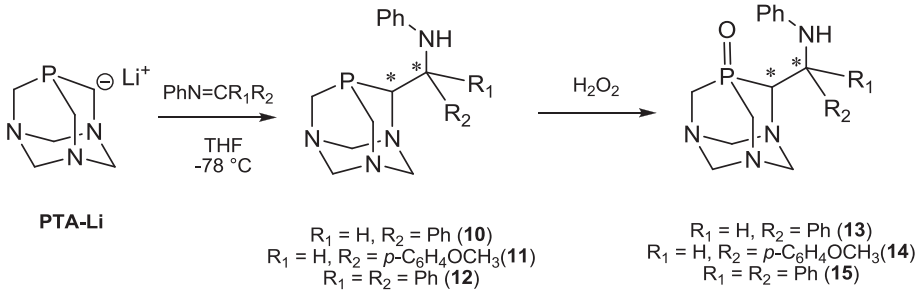

Scheme 5. Synthesis of P,N bidentate "upper rim" PTA β-aminophosphine derivatives **10**–**12** and the corresponding phosphine oxides **13**–**15**.

Please cite this article in press as: A. Guerriero et al., Coordination chemistry of 1,3,5-triaza-7-phosphatricyclo[3.3.1.1]decane (PTA) and derivatives. Part III. Variations on a theme: Novel architectures, materials and applications, Coord. Chem. Rev. (2017), https://doi.org/10.1016/j.ccr.2017.09.024

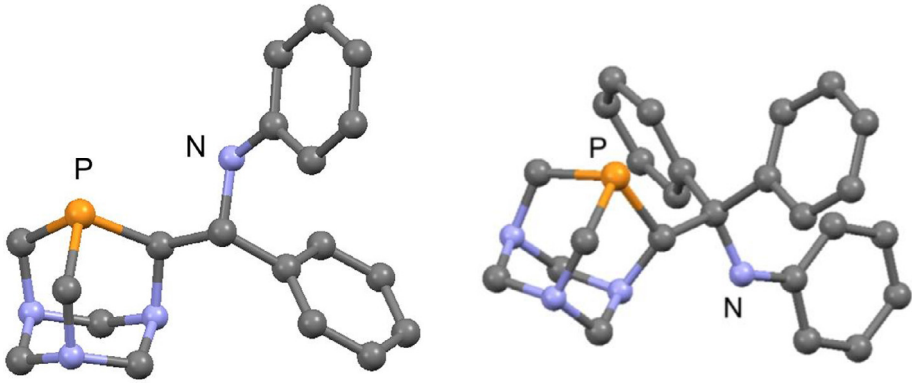

Fig. 3. X-ray crystal structures of *SR*-**10** (left) and *R*-**12** (right). Adapted from Ref. [9]. Copyright 2013 American Chemical Society.

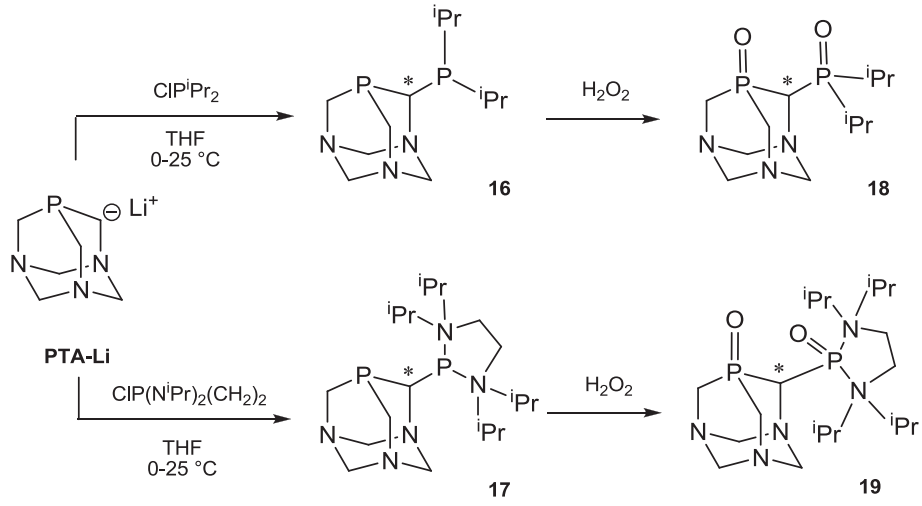

Scheme 6. Synthesis of P,P bidentate "upper rim" bis(phosphine) derivatives **16** and **17** and the corresponding bis(phosphine) dioxides **18** and **19**.

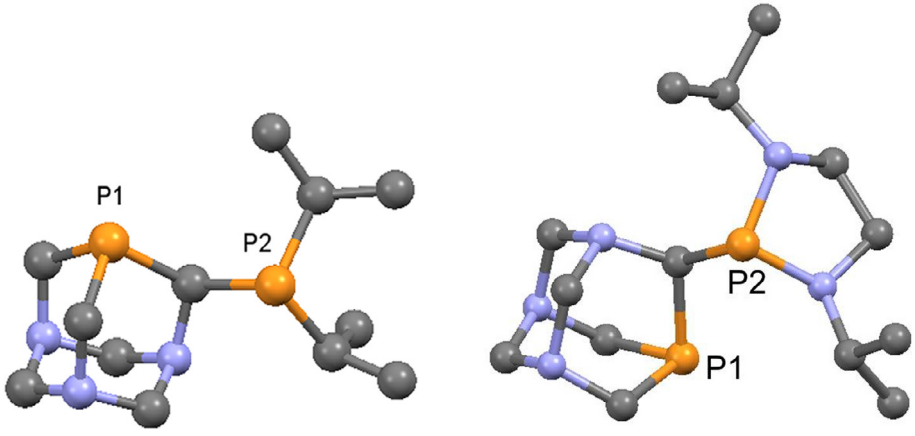

Fig. 4. X-ray crystal structures of *R*-**16** (left) and *R*-**17** (right). Adapted from Ref. [10]. Copyright 2015 Elsevier Science B.V.

57.0 (O=P^{i}Pr$_2$) and −8.8 ppm (O=PTA) with a $^2J_{PP}$ = 5 Hz for **18**, and by two singlets at 24.9 (O=PR$_2$) and −10.5 ppm (O=PTA) for **19**.

2.2. Lower rim functionalisations

N-atom quaternisations: A common and generally facile PTA derivatisation consists of alkylation/benzylation on a N atom of the cage "lower rim" using terminal organohalides. The water solubility is usually higher than the parent compound due to the ionic nature of product and, when appropriate, to the presence of polar groups on the quaternising group attached. On the other hand, the introduction of long-chain alkyl group can be used to modulate the degree of lipophilicity of the N-derivative. A summary of the selected recent N-functionalised PTA derivatives is shown in Scheme 7.

Please cite this article in press as: A. Guerriero et al., Coordination chemistry of 1,3,5-triaza-7-phosphatricyclo[3.3.1.1]decane (PTA) and derivatives. Part III. Variations on a theme: Novel architectures, materials and applications, Coord. Chem. Rev. (2017), https://doi.org/10.1016/j.ccr.2017.09.024

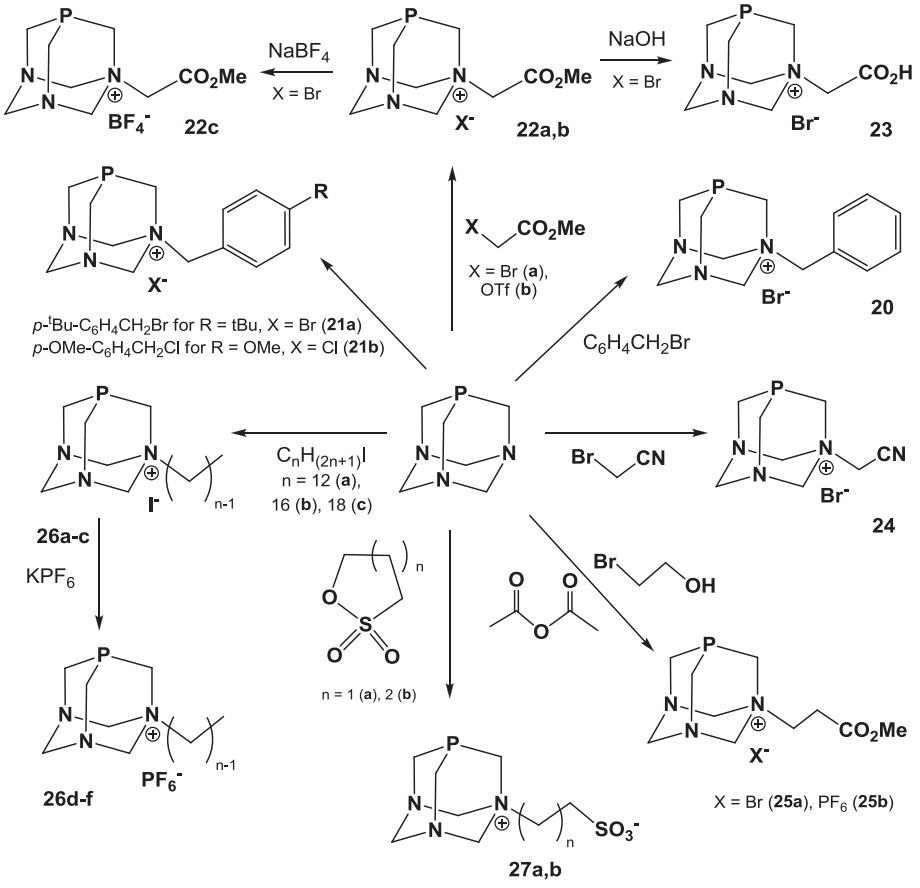

Scheme 7. Some PTA reactions to give N-functionalised PTA derivatives.

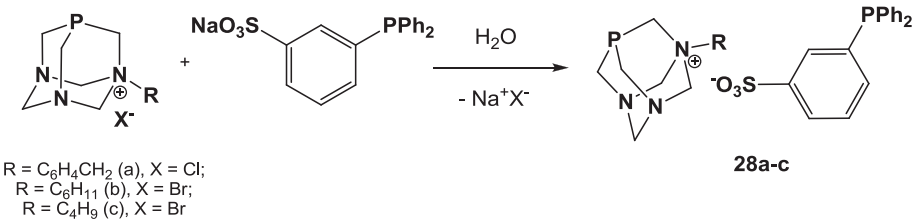

Scheme 8. Ion pairs **28a–c** obtained from N-functionalised PTA and *m*TPPMS.

Straightforward reaction of PTA with either benzyl bromide [11] or p-(*t*-butyl)benzyl bromide [12] gave the corresponding N-benzylated PTA derivatives **20** and **21a** as bromide salts. Similarly, the *p*-methoxybenzyl derivative **21b** was obtained using *p*-methoxybenzyl chloride. The strategy used for **21b** was also employed to graft PTA onto chloride-ending dendrimers (generations G_1–G_3) and the corresponding water-soluble macromolecular ligand was used for catalytic and medicinal applications [13].

N-alkylations with different electrophiles were described in the literature. Reaction of PTA with methyl bromoacetate and (methoxycarbonyl)methyltrifluoromethane sulfonate in acetone at 0 °C gave compounds **22a** and **22b**, respectively, in high yields after workup. Anion exchange by salt metathesis in **22a** with KBF_4 gave the corresponding BF_4^- derivative **22c**. The corresponding analogue with a terminal carboxylic acid group (**23**) was obtained by reaction of **22a** with NaOH. Another terminal polar group such as nitrile was introduced in a similar way by reacting PTA with bromoacetonitrile to give compound **24** [11]. A slightly different procedure was used to obtain the methyl ester derivatives **25a**,**b** (X = Br, **a**; PF_6, **b**, obtained by anion exchange with KPF_6) bearing a —$(CH_2)_2$— spacer between N and the carboxylic group, namely reacting PTA with bromoethanol in the presence of acetic anhydride. [14] Ligand **25** was used to coordinate to CpRu moieties by phosphine ligand exchange from $[RuCpCl(PPh_3)_2]$ [14].

Long-chain alkyl groups were introduced onto PTA at the N atom by reaction with C_{12}, C_{16} and C_{18} primary iodides, giving compounds **26a–c**, together with the corresponding PF_6^- salts **26d–f** by anion exchange [15]. A ca. 20 ppm shift in the $^{31}P\{^1H\}$ NMR spectra was observed compared to PTA, with singlets at −84.32 ppm for **26a**, −84.27 ppm for **26b** and −84.26 ppm for **26c**, respectively.

Zwitterionic PTA derivatives were obtained by reaction of the parent compound with 1,3-propanesultone and 1,4-butanesultone. The corresponding products, $PTA^+C_3H_6SO_3^-$ (**27a**) and $PTA^+C_4H_8SO_3^-$ (**27b**) are endowed with moderate to good water solubility, with $S(H_2O)_{25°C} = 50$ and 504 g L^{-1}, respectively. The $^{31}P\{^1H\}$ NMR chemical shift values resemble those observed for the long-chain derivatives **26a–c**, namely at −83.67 and −82.86 ppm in D_2O [16]. Other examples of PTA-based ligands in the form of ion pairs, with the positive charge on the N-alkylated or benzylated lower rim atom, and *meta*-monosulfonated triphenylphosphine (*m*TPPMS) as anion (**28a–c**, Scheme 8) were also described [17].

Please cite this article in press as: A. Guerriero et al., Coordination chemistry of 1,3,5-triaza-7-phosphatricyclo[3.3.1.1]decane (PTA) and derivatives. Part III. Variations on a theme: Novel architectures, materials and applications, Coord. Chem. Rev. (2017), https://doi.org/10.1016/j.ccr.2017.09.024

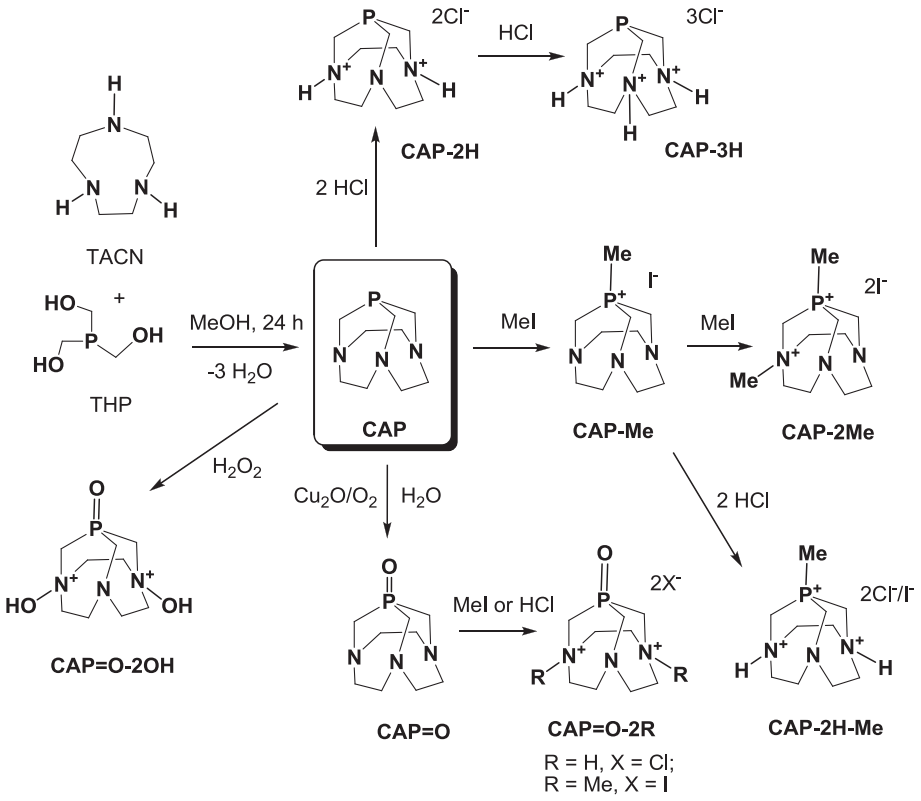

Scheme 9. Synthesis of CAP and its reactivity towards protonation, alkylation and oxidation.

2.3. PTA analogues and other reactions

Recently, the novel tris-(homoadamantane) cage compound 1,4,7-triaza-9-phosphatricyclo[5.3.2.1^{4,9}]tridecane (CAP), formally a higher homologue of PTA, was obtained [18]. As for PTA, the synthesis of CAP involves a Mannich-type condensation, using 1,4,7-triazacyclononane (TACN) and tris-(hydroxymethyl)phosphine (THP), as shown in Scheme 9. An alternative synthesis using the easier-to-handle tetrakis-(hydroxymethyl)phosphonium chloride salt (THPC) from which THP is generated *in situ* was also demonstrated [19]. CAP is air-stable and can be stored in glass vials without the need of a protecting atmosphere at room temperature for at least one year. It is soluble in MeOH, EtOH, ^{i}PrOH and MeCN, and insoluble in acetone, THF, benzene, toluene and hexane. Water solubility of CAP was measured as $S(H_2O)_{25°C} = 20\ g\ L^{-1}$, ca. one order of magnitude lower than PTA ($235\ g\ L^{-1}$), having a melting point of ca. 50 °C.

Although CAP formally differs from PTA only by the presence of —$(CH_2)_2$— spacers between the lower rim N atoms, this has profound implications on its reactivity and donor properties, together with unexpected NMR chemical shift values [20]. The $^{31}P\{^{1}H\}$ NMR spectrum for CAP shows a singlet at 46.72 ppm in D_2O and 47.49 ppm in $CDCl_3$, in contrast to the value observed for PTA (−96.20 ppm in D_2O). In addition, most $^{31}P\{^{1}H\}$ NMR resonances of CAP derivatives are displaced well upfield relative to the parent compound ($\Delta\delta$ = ca. −34 ppm). The authors concluded that this behaviour is due to a closer resemblance of CAP to Verkade's base (hexahydro-2*a*,4*a*,6*a*-triaza-6*b*-phosphacyclopenta[*cd*]pentalene, Chart 2) than to PTA, and related to the flexible bi-/tricyclic atrane-type conformations.

DFT calculations followed by electron density distribution analysis, using molecular electrostatic potential (MESP) and atoms-in-molecules (AIM) approaches, substantiate the unusual NMR pattern. Calculations showed that, as in azaphosphatranes, the lone pairs on bridgehead P and the N atoms in CAP derivatives are involved in four-centred intrabridgehead interactions, with transannular P ← N bonds arising from substitution-induced shrinkage of the bicyclic[3.3.3]pro-atrane cages. The small cone-angle of CAP, 109° for the symmetrical [3 3 3] cage conformation, slightly larger than for PTA (103°), approaches the value calculated for $P(OEt)_3$.

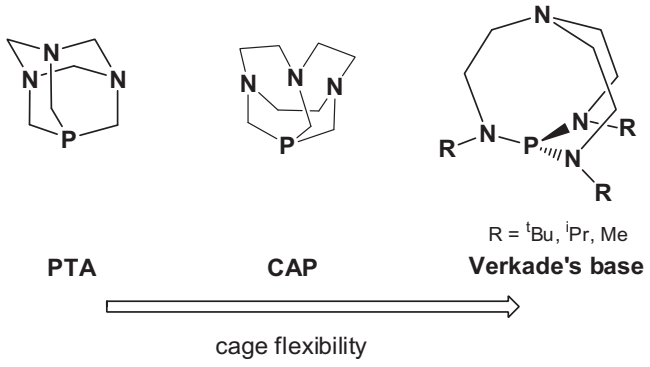

Chart 2. Cage flexibility trend from rigid adamantane-type PTA to azaphosphatrane-type Verkade's base.

Rather striking differences between PTA and CAP were observed in protonation, methylation and oxidation reactions. While PTA can be selectively protonated with strong acids at one N atom only, CAP is prone to tris-protonation, giving compounds CAP-2H and CAP-3H by addition of up to 3 equiv. of HCl (Scheme 9). CAP methylation by MeI (1 equiv.) gives selectively P-methylation instead of N-methylation, in contrast with the known behaviour of PTA, where only a single N-methylation is obtained. Compound (CAP-Me)I displays a $^{31}P\{^{1}H\}$ NMR singlet at 25.56 ppm and ^{1}H

Please cite this article in press as: A. Guerriero et al., Coordination chemistry of 1,3,5-triaza-7-phosphatricyclo[3.3.1.1]decane (PTA) and derivatives. Part III. Variations on a theme: Novel architectures, materials and applications, Coord. Chem. Rev. (2017), https://doi.org/10.1016/j.ccr.2017.09.024

NMR doublets at 1.52 and 1.35 ppm ($^2J_{PH}$ = 17.3 Hz) for the Me group due to the coupling of P and H atoms. Reaction of (CAP–Me)I with 1 equiv. of MeI gave the P,N dimethylated species CAP–2Me. Even more remarkable is the reactivity of CAP towards oxidation. Whereas PTA cleanly reacts with aqueous H_2O_2 to give selective P oxidation to PTA=O, P-oxidation and double N-hydroxylation were observed for CAP under the same conditions, to give the bis-hydroxylated phosphine oxide CAP=O—2OH. Compound CAP=O, the P-oxidised analogue of PTA=O, could be obtained by a milder route, namely reaction with O_2 in the presence of Cu^{2+} salts. Also this compound is endowed with reactivity towards HCl and MeI at N atoms, giving the corresponding bis-protonated and bis-methylated CAP=O—2H and CAP=O—2Me, respectively (Scheme 9). In the words of the authors, CAP can be thus defined either as a "Verkade's ligand with bridging P—C—N atoms" or as a "macrocyclic counterpart of PTA".

Finally, PTA=O reduction is a potentially interesting reaction to recover PTA, for example at the end of catalytic reactions, where the water-soluble ligand is often found in its oxidised form. Together with other authors, we disclosed a sustainable, simple and cheap method to achieve this reaction in ca. 83% yield, using polymethylhydrosiloxane (PMHS, a by-product of silicon industry) as reductant, without the need of added solvents, in a metal-free process run under nitrogen at 220 °C for 1 h [21].

3. Recent examples of transition metal complexes of PTA and derivatives

In the following chapter, selected recent examples of PTA coordination compounds and related applications will be summarised, divided by groups of the Periodic Table to which the corresponding transition metals belong. Examples of bi- and polymetallic coordination compounds will also be described.

3.1. Group 7 complexes

Novel Group 7 coordination compounds of PTA were described in the recent literature (Chart 3). The Mn(I) complex *fac*-[Mn(κ^2*S*-S_2CNEt_2)(PTA)$(CO)_3$] (**29**) was obtained by reaction of [$MnBr(CO)_5$] with 1 equiv. of PTA and 1 equiv. of Na(S_2CNEt_2), and characterised by a singlet at −36.9 ppm in the corresponding $^{31}P\{^1H\}$ NMR spectrum. In the solid state, **29** shows an octahedral environment around the metal centre, with a chelating diethyldithiocarbamate ligand, one P-coordinated PTA and three carbonyl ligands in *fac*-arrangement. The Mn—P bond length was measured as 2.3049 (6) Å and the angle C(3)—Mn—P(1), where C(3) belongs to CO trans to PTA, was of 175.9(8)°. The intended use of **29** as CO releasing molecule (CORM) evaluated by standard myoglobin (Mb) assay was hampered by the low solubility of the complex in water [22].

Two PTA–Mn(I) carbonyl complexes bearing co-ligands 2-(pyridyl)benzothiazole (pbt) and 1,10-phenanthroline (phen), namely *fac*-[$Mn(CO)_3$(L)(PTA)](OTf) (L = pbt, **30a**; phen, **30b**; OTf = $CF_3SO_3^-$), were obtained in a two-step synthesis from [MnX$(CO)_3$L] (X = Br, L = pbt; X = Cl, L = phen), at first by reaction with MeCN/AgOTf to obtain the intermediates [Mn(MeCN)L$(CO)_3$]OTf, which were then reacted with excess PTA to obtain the desired complexes. The Re(I) analogues *fac*-[$Re(CO)_3$(L)(PTA)](OTf) (L = pbt, **31a**; phen, **31b**) where similarly obtained [23]. All compounds were characterised in solution by NMR and UV–vis spectroscopies and in the solid state by single-crystal X-ray diffraction. The coordination geometries display distorted octahedrons at the metals, three CO ligands in *fac*-disposition, the chelating N,N ligands and one P-coordinated PTA molecule. The planes constituted by the metal, two N atoms and two C atoms of the carbonyl ligands are relatively distorted from planarity in the case of L = phen, by 0.023 Å for **30b** and 0.029 Å for **31b**, respectively. Complexes **30** and **31** were applied as photoCORMs (photo-induced CORMs) and their CO releasing properties upon illumination were evaluated by a number of spectroscopic techniques, standard Mb assay and evaluation of dose-dependent eradication of breast cancer cells MDA-MB-23. Mn complexes **30a** and **30b** showed exhaustive photolysis with broad-band visible light, resulting in the release of all three CO molecules, whereas the Re analogues **31a** and **31b** release only one CO molecule under UV-A irradiation.

The Re(I) analogue of complex **29**, namely *fac*-[Re(κ^2*S*-S_2CNEt_2)(PTA)$(CO)_3$] (**32**), was obtained in nearly quantitative yield by reaction of either [$ReCl(CO)_5$] or [$Re(CO)_3(H_2O)_3$]Br with 1 equiv. of PTA and 1 equiv. of Na(S_2CNEt_2) [24]. The corresponding X-ray crystal structure showed a geometry similar to **29**.

Reaction of [$ReBr_2(MeCN)_3(NO)$] with PTA in dioxane gave the water soluble complex *cis*-[$ReBr_2(PTA)_3(NO)$] (**33**), with $^{31}P\{^1H\}$ NMR signals at −88.0 (d, $^2J_{PP}$ = 10.7 Hz) and −70.4 ppm (t, $^2J_{PP}$ = 11.0 Hz). Reaction of **33** with excess of HBr yielded *cis*-[$ReBr_2(HPTA)_3(NO)$]Br_3 (**34**) by N-atom protonation at all three PTA ligands. On the other hand, complex *trans*,*trans*-[$ReBr_2(MeCN)(PTA)_2(NO)$] (**35**), showing a $^{31}P\{^1H\}$ NMR singlet at −89.4 ppm, could be obtained by reduction of [$Me_4N]_2$[$ReBr_4(NO)$] in acetonitrile with Zn in the presence of PTA [25]. Stepwise protonation of **35** with HBr gave sequentially complexes *trans*,*trans*-[$ReBr_2(MeCN)(PTA)(HPTA)(NO)$]Br (**36a**) and *trans*,*trans*-[$ReBr_2(MeCN)(HPTA)_2(NO)$]Br_2 (**36b**). Complex **35** was also used as precursor for the bis-hydrido species *cis*,*trans*-[$Re(H)_2(PTA)_2(NO)(THF)$] (**37**) by reaction with $NaHBEt_3$ in THF at −30 °C. Complex **37** was characterised by a $^{31}P\{^1H\}$ NMR singlet at −68.5 ppm and two doublets of triplets (dt) signals in the negative region of the ^1H NMR spectrum at −1.93 (dt, $^2J_{HH}$ = 8 and $^2J_{HP}$ = 32 Hz) and −6.97 ppm (dt, $^2J_{HH}$ = 8 and $^2J_{HP}$ = 36 Hz). X-ray crystal structures were obtained for both **33** and **35**. Exposure of **37** to ethylene under pressure gave complex *trans*-[$ReH(CH_2CH_3)(\eta^2$-$C_2H_4)(PTA)_2(NO)$] (**38**), whereas reaction of **35** with RCH=CH_2 (R = H, Ph) gave complexes *cis*,*trans*-[$ReBr_2(\eta^2$-RCH=$CH_2)(PTA)_2$(NO)] (R = H, **39a**; R = Ph, **39b**) [25a].

The previously reported cluster complex [$Re_6(\mu_3$-$Se)_8(PEt_3)_5$(PTA)]$(SbF_6)_2$ was used to coordinate Zn(II) and Cu(II) by one N atom of PTA, giving complexes [M{$Re_6(\mu_3$-$Se)_8(PEt_3)_5$(PTA)$(NO_3)_3$}](SbF_6) (M = Zn, **40a**; Cu, **40b**). Complex **40a** was characterised in solution by NMR techniques, with a $^{31}P\{^1H\}$ singlet at −105.35 ppm for PTA. Single-crystal X-ray diffraction data confirmed the proposed coordination of PTA and showed significant distortions of the cage upon N-coordination to hard metals [26].

The water soluble oxorhenium(VII) complexes [$ReO_3(PTA)_2$][ReO_4] (**41**), [ReO_3(mPTA)][ReO_4]I (**42**), [$ReO_3(\eta^2$-Tpm)(PTA)][ReO_4] (**43**), were obtained by reaction of Re_2O_7 in MeOH at room temperature with PTA only in Re:PTA = 1:3 ratio (in case of **41**), with the N-methyl derivative (mPTA)I using Re:ligand = 1:2 ratio (for **42**) and with PTA together with the scorpionate ligand hydrotris(pyrazol-1-yl)methane (Tpm) using Re:PTA:Tpm = 1:2:1 ratio for **43**, respectively. A PTA-based Re(III) complex, namely [$ReCl_2${=N=NC(O)Ph}$(PTA)_3$] (**44**), was instead obtained by ligand exchange reacting precursor [$ReCl_2${=N=NC(O)Ph}(Hpz)$(PPh_3)_2$] with a 10:1 excess of PTA (Hpz = pyrazole) [27].

3.2. Group 8 complexes

Recent examples of Group 8 coordination compounds of PTA are largely dominated by ruthenium, also due to the application of such complexes in catalysis and medicinal inorganic chemistry. As stated above, the literature covering Ru–arene PTA complexes (RAPTA), with a focus on arene (for example with the introduction of fluorinated and hydrophilic or hydrophobic substituents, acetals,

Please cite this article in press as: A. Guerriero et al., Coordination chemistry of 1,3,5-triaza-7-phosphatricyclo[3.3.1.1]decane (PTA) and derivatives. Part III. Variations on a theme: Novel architectures, materials and applications, Coord. Chem. Rev. (2017), https://doi.org/10.1016/j.ccr.2017.09.024

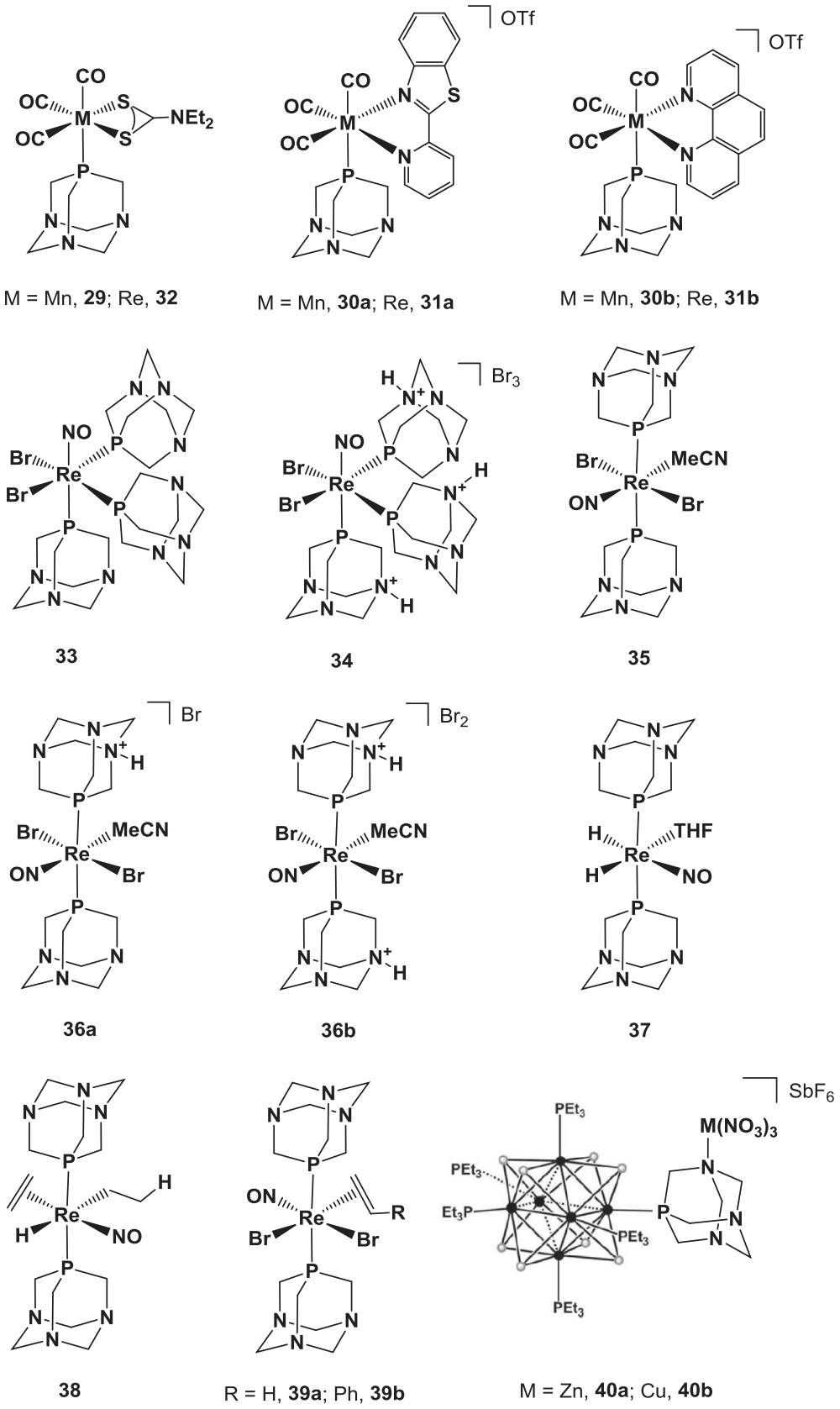

Chart 3. Group 7 complexes **29**–**40** bearing PTA and derivatives.

aldehydes, amino-, amido-, peptido groups and oximes) and co-ligands variations (including for example triazole–imidazole, β-ketoamine, maleimide, etc.) has been already reviewed [2,28]. RAPTA-type complexes were also recently encapsulated into polymeric matrixes or degradable micelles, obtaining macromolecular complexes that increase drug resistance, solubility and cell uptake

Please cite this article in press as: A. Guerriero et al., Coordination chemistry of 1,3,5-triaza-7-phosphatricyclo[3.3.1.1]decane (PTA) and derivatives. Part III. Variations on a theme: Novel architectures, materials and applications, Coord. Chem. Rev. (2017), https://doi.org/10.1016/j.ccr.2017.09.024

[29]. Incorporation and release of metallodrug RAPTA-C (RAPTA-C = [$RuCl_2$(p-cymene)(PTA)]) in the highly robust MOF (metal organic framework) [$Ni_8(OH)_4(H_2O)_2$(4,4′-(buta-1,3-diene-1,4-diyl)bispyrazolato)$_6$]$_n$ was also reported [30].

Apart from these aspects, novel Ru–arene complexes bearing PTA and derivatives were synthesised for different applications. New structural analyses to investigate ligand effects on the properties of RAPTA complexes were described, mainly using ion mobility mass spectrometry, collision-induced dissociation and DFT calculations [31]. Ligand (PTA–Bn)Cl was reacted with [$RuCl_2$(p-cymene)]$_2$ in 2:1 ratio in MeOH at room temperature to give [$RuCl_2$(p-cymene)(PTA–Bn)]Cl (**45**), which was also characterised in the solid state by single-crystal X-ray diffraction, showing two water molecules in the unit cell [17]. In the same article, the authors also described the synthesis of two related Ru–arene complexes using ligand **28a**. Using a 1:1 ratio to the Ru precursor, each phosphine in the ligand ion pair coordinate a Ru–arene moiety giving the bimetallic ion-pair complex {[$RuCl_2$(p-cymene)(PTA–Bn)][$RuCl_2$(*m*TPPMS)(p-cymene)]} (**46**) after 1 h in 70% yield. At longer reaction time (10 h) using a 2:1 ligand to Ru dimer ratio, the monometallic complex [RuCl(*m*TPPMS)(p-cymene)(PTA–Bn)]Cl (**47**), with both phosphine ligands binding to the same Ru atom, was instead obtained in 82% yield.

Ru–arene complexes of general formula [$RuCl_2$(η^6-arene)(mPTA)]Cl (**48**, η^6-arene = C_6H_6, **a**; p-cymene, **b**; 1,3,5-$C_6H_3Me_3$, **c**; C_6Me_6, **d**) were obtained by reaction of the corresponding [$RuCl_2$(η^6-arene)]$_2$ precursors with (mPTA)Cl. Successful heterogenisation of **48a** was obtained by wet impregnation of Montmorillonite K-10, at different Ru weight percentages ranging from 0.7% to 3.1% [32].

The cationic half-sandwich guanidinatoruthenium(II) complex [Ru{κ*N*,*N*′-(ArN)$_2$C—N(H)Ar}](p-cymene)(PTA)](OTf) (**49**, Ar = 2-MeC_6H_4, Chart 4) was isolated from the reaction of neutral [RuCl{κ*N*,*N*′-(ArN)$_2$C—N(H)Ar}(p-cymene)] with PTA in the presence of AgOTf. It was characterised in solution by NMR techniques and in the solid state by single-crystal X-ray diffraction [33]. Variable temperature (VT) $^{31}P\{^1H\}$ NMR spectroscopy of **49** revealed the presence of a mixture of four isomers in CD_2Cl_2, in a ratio of approximately 1.4:11.0:1.6:0.1 at 238 K. DFT calculations were performed on the *syn–syn*, *syn–anti*, *anti–syn*, and *anti–anti* conformers of **49**, imparted by the guanidinate ligand, and revealed that the *syn–anti* was the most stable conformer, both in the gas phase and in solution.

Ru–arene complexes bearing either PTA or other water-soluble monodentate phosphines and a N-heterocyclic carbene (NHC) ligand were also reported. The complexes of general formula [RuCl(NHC)(p-cymene)(L)]$^{n+}$ (**50**, NHC = bmim = 1-butyl-3-methyl-imidazole-2-ylidene; L = PTA, **a**; *m*PTA, **b**; PTA–Bn, **c**; *m*TPPMS, **d**; *m*TPPTS, **e**; *n* = 1–2, Chart 4) were obtained *in situ* by reaction of [$RuCl_2$(NHC)(p-cymene)] with ligands L. Complex **50a** was characterised in solution by NMR spectroscopy, showing a $^{31}P\{^1H\}$ singlet at −38.50 ppm in DMSO-d_6. NMR analysis, using DMSO-d_6, of the crude reaction mixture (carried out in MeOH) showed other two $^{31}P\{^1H\}$ singlets at −37.55 ppm and −35.54 ppm. The authors attributed the singlet at −35.54 ppm to [$RuCl_2$(p-cymene)(PTA)] and the singlet at −37.55 ppm to [Ru(solv)(NHC)(PTA)(p-cymene)]$^{2+}$ (solv = MeOH, DMSO). Thus it can be concluded that in solution **50a** could either exchange the NHC ligand with PTA or the coordinated Cl^- ligand with a solvent molecule [34].

More recently, the same group obtained the novel complex [Ru(η^2-O_2CO)(p-cymene)(PTA)] (**51**) from simple exchange of chloride with carbonate ligands from [$RuCl_2$(p-cymene)(PTA)]. The presence of the carbonato ligand was confirmed by solution $^{13}C\{^1H\}$ NMR spectroscopy, showing a singlet at 166.8 ppm in CD_3OD and by IR spectroscopy with sharp bands at 1663 and 1613 cm^{-1}. The $^{31}P\{^1H\}$ NMR signal due to PTA was observed at −34.4 ppm. Complex **51** was characterised in the solid state by single-crystal X-ray diffraction as dihydrate adduct, with a Ru(1)—P(1) bond distance of 2.309(5) Å [35].

Another class of Ru(II) complexes bearing PTA and derivatives is represented by (substituted) η^5-cyclopentadienyl (Cp) complexes. The long-chain N-alkyl PTA ligands **26** were used to obtain the corresponding complexes [RuCpCl(PPh_3)(L)]X (L = **26a–c**; X = I^-; L = **26d–f**; X = PF_6^-), namely **52a–c** (X = I^-) and **52d–f** (X = PF_6^-) [15]. Two different synthetic routes were applied, the first by direct alkylation of PTA in complex [RuCpCl(PPh_3)(PTA)] using the corresponding terminal iodides, the second by ligand exchange from [RuCpCl(PPh_3)$_2$] with ligands **26d–f** bearing PF_6^- as counter anion (Scheme 7). The reaction was monitored by $^{31}P\{^1H\}$ NMR spectroscopy, showing that the initial signals at 40.52 ppm due to PPh_3 and −81 ppm (free ligands) gradually turned upon formation of the products into an AM pattern at ca. 47 and −14 ppm, with a $^2J_{PP}$ = 43.7 Hz. The stability of the known complex [RuCpCl(mPTA)$_2$](OTf)$_2$ towards aquation was assessed by mass spectrometry and UV–vis spectroscopy. Coordination of water molecules was found to occur, following chloride and mPTA exchange with water, hydroxide or triflate anions, to give a series of different substitution products. Stabilisation of the parent compound towards water coordination and ligand exchange was obtained with dilute HCl or isotonic neutral 0.15 M NaCl solutions [36].

The coordination chemistry of the lower-rim open PTA analogue dmoPTA (dmoPTA = 3,7-dimethyl-1,3,7-triaza-5-phosphabicyclo[3.3.1]nonane) was expanded to the synthesis of heterobimetallic complexes, exploiting the ligand heteroditopic behaviour [37]. Synthetic pathways to Ru–Ni, Ru–Zn were devised, together with a high-yielding synthesis of precursor [RuCpCl(κ*P*-HdmoPTA)(PPh_3)](OTf), previously reported by the same authors (HdmoPTA = 3,7-H-3,7-dimethyl-1,3,7-triaza-5-phosphabicyclo[3.3.1]nonane). In these complexes, of general formula [RuCpCl(PPh_3){μ-dmoPTA-1κ^1*P*:2κ*N*,*N*′-M(κ^2*O*-acac)$_2$}] (M = Ni, **53a**; Zn, **53b**; Co, **53c**), the P atom of dmoPTA coordinates the "soft" Ru(II) centre, while the "open" lower rim binds the "hard" metals in a bidentate N,N fashion. The reactions were performed in a two-step synthetic pathway, passing through intermediate [RuCpCl(κ*P*-dmoPTA)(PPh_3)]. The Co(II) complex **53c** could instead be obtained directly from [RuCpCl(κ*P*-dmoPTA)(PPh_3)](OTf). This reactivity is shown in Scheme 10.

The isostructural complexes **53a** and **53b** were also characterised in the solid state by X-ray crystal structure determination as mono-aquo species (Fig. 5).

The geometry around the Ru atom does not substantially deviate from that of the parent compound and related complexes. A slightly distorted octahedral geometry is adopted by the metal coordinated by the N,N open lower rim atoms in a pseudo-chair conformation. In solution, the diamagnetic Ru–Zn complex **50b** was fully characterised by NMR spectroscopy at 193 K as two

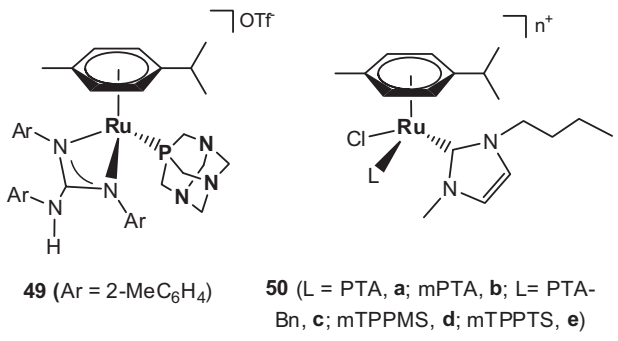

49 (Ar = 2-MeC_6H_4) **50** (L = PTA, **a**; mPTA, **b**; L= PTA-Bn, **c**; mTPPMS, **d**; mTPPTS, **e**)

Chart 4. Ruthenium complexes **49** and **50a–e**.

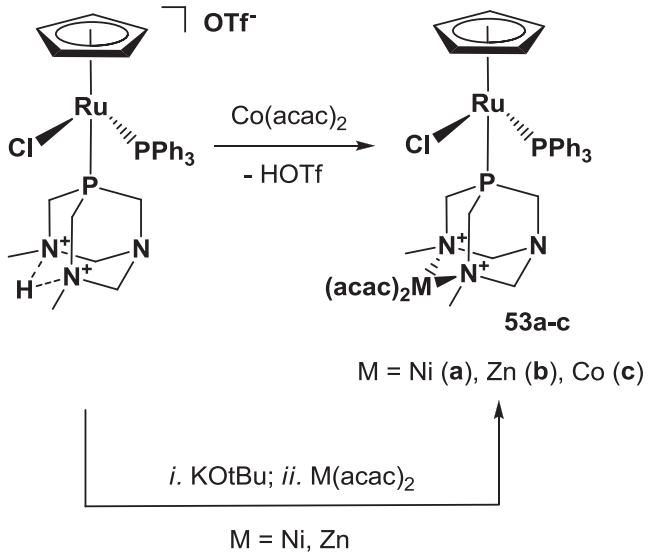

Scheme 10. Synthesis of heterobimetallic complexes **53a–c**.

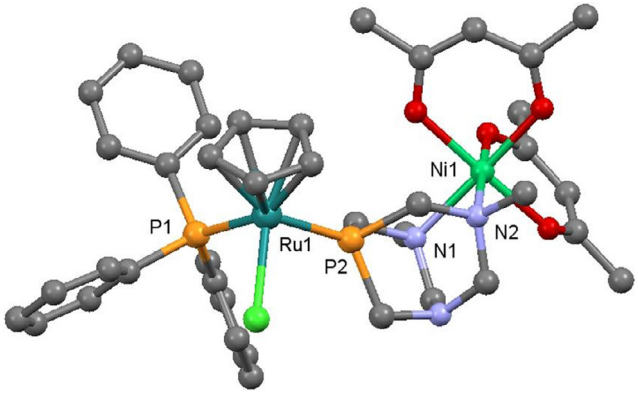

Fig. 5. X-ray crystal structures of **53a**. Adapted from Ref. [37]. Copyright 2011 The Royal Society of Chemistry.

diastereomeric pairs of enantiomers, namely *R*-Ru, *Δ*-Zn; *R*-Ru, *Λ*-Zn; *S*-Ru, *Δ*-Zn; *S*-Ru, *Λ*-Zn. Cyclic voltammetry (CV) studies demonstrated that the redox properties of the complexes depend essentially on the nature of the M atom, with a fully reversible Ru-centred process. The complexes were tested in antiproliferative activity by 48 h exposure SBS assay against human tumour cells HBL-100 (breast cancer), HeLa (cervix carcinoma), SW1573 (lung carcinoma) and WiDR (colorectal adenocarcinoma). GI_{50} values showed higher activities than cisplatin and a small but evident difference in activity in favour of **53a** and **53c** compared to **53b**, confirming that although the main active part of the molecule is the Ru (II) moiety, the introduction of other metals can have an effect on the overall cancer cell growth inhibition [38].

A novel highly water soluble ($S(H_2O)_{25°C}$ = 320 g L^{-1}) homobimetallic CpRu–PTA type complex was described and characterised by neutron diffraction. Complex [$(PTA)_2$CpRu-μ-CN-1κ*C*:2κ*N*-RuCp$(PTA)_2$](OTf) (**54**) was obtained by reaction of previously described [RuCp$(PTA)_2$(κC-CN)] with [RuCpCl$(PTA)_2$] in water, where the two CpRu moieties are bridged by a CN— group acting as bidentate C,N ligand. Measurement of the radial atom–atom correlation functions $g(r)$ confirmed that in water solution the shortest and better-defined correlation for water protons (H_w) resides around the N atoms of PTA, pointing to an almost linear N_{PTA}–H_w–O_w configuration (O_w = water oxygen atoms; d_{N-Hw} = 1.85 Å; d_{N-Ow} = 2.8 Å). The study was complemented by DFT and TD-DFT (time-dependent density functional theory) calculations both in gas phase and using explicit water molecules [39].

Expanding on the synthetic scope starting from complex **54**, the same authors reported on the synthesis of the heterobimetallic water soluble organometallic polymer [{$(PTA)_2$CpRu-μ-CN-1κ*C*:2κ*N*-RuCp$(PTA)_2$}-μ-$NiCl_3$]$_n$ (**55**), which was found to be stable in the solid state for several days in air. The two piano-stool [RuCp$(PTA)_2$]$^+$ moieties are linked by a crystallographically disordered CN^- ligand and connected by N atoms of two different PTA molecules to a $NiCl_3^-$ unit (Scheme 11). NMR studies indicated that **55** is reverted to **54** in water solution. Further proof of this behaviour was obtained by hydrodynamic radius measurements at different concentrations. For both **54** and **55** the same values were measured, namely r (5.2 mg mL^{-1}) = 8.23 Å, r (25 mg mL^{-1}) = 9.09 Å, confirming the observation made by NMR spectroscopy [40].

The new water soluble complexes [RuCpCl$(HPTA)_2$]Cl_2·$2H_2O$ (**56**), [RuCp(κ*S*-DMSO)$(PTA)_2$]Cl (**57**), [RuCp(κ*S*-DMSO)$(PTA)_2$](OTf) (**58**) and [RuCp(κ*S*-DMSO)$(HPTA)_2$]Cl_3·$2H_2O$ (**59**) were synthesised from [RuCpCl_2(PTA)] by ligand N-protonation with HCl and exchange (either in the presence or in absence of AgOTf as chloride scavenger) and fully characterised by NMR, IR and elemental analysis. The solid-state structures of complexes **56·2H$_2$O** and **59·2H$_2$O** were also obtained by single crystal X-ray diffraction [41].

An overview of synthetic routes to complexes of general formulas [RuCpXL^{1}L^2]$^{n+}$ (X = Cl, Br; L^1 = PPh_3, *m*TPPMS; L^2 = mPTA, PTA; L^1 = L^2 = PTA, mPTA) was recently reported, showing a large scope for different synthetic derivatives with tunable water solubilities [42].

Complex [RuCp*$(PTA)_3$]PF_6 (**60**, Cp* = η^5-C_5Me_5) was easily obtained by naphthalene ligand exchange from precursor [RuCp*(η^6-$C_{10}Me_8$)](PF_6) upon irradiation with near-UV (365 nm) or visible light. Relevant bond lengths in the corresponding X-ray crystal structure were measured as Ru—Cp* centroid = 1.915; Ru(1)—P(1) = 2.2997(11); Ru(1)—P(2) = 2.2973(11); Ru(1)—P(3) = 2.2926(11) Å. The $^{31}P\{^1H\}$ NMR spectrum showed a singlet at −37.2 for PTA [43]. Similarly, complex [Ru(η^5-$C_6H_3Me_4$)$(PTA)_3$]PF_6 (**61**) was obtained starting from [Ru(η^5-$C_6H_3Me_4$)(η^6-$C_{10}Me_8$)](PF_6) by PTA–naphthalene exchange reaction in acetone at 60 °C after 10 h and workup. The $^{31}P\{^1H\}$ NMR spectrum showed a singlet at −42.99 for PTA [44].

Water-mediated hydrogen activation by complexes [RuCpCl$(PTA)_2$] and [RuCp*Cl$(PTA)_2$] was re-investigated by DFT calculations using a discrete + continuum model involving a four-water-molecule cluster [45]. It was shown that starting from [RuCp′Cl$(PTA)_2$] (Cp′ = Cp, Cp*), H_2 activation initially gave the dihydrogen species [RuCp′(η^2-H_2)$(PTA)_2$]$^+$. Two different mechanisms involving both PTA- and water-assisted heterolytic or homolytic η^2-H_2 splitting gave the monohydride [RuCpH(PTA)(HPTA)]$^+$ (**62**) and the dihydride [RuCp*$(H)_2(PTA)_2$]$^+$ (**63**), respectively, in agreement with the experimental observations.

The reactivity of [RuCpCl(PTA)(PPh_3)] with HC≡CPh and HC≡CC(OH)PPh_2 has been studied [46]. As previously observed, [46] reaction of [RuCpCl(PTA)(PPh_3)] with phenylacetylene in the presence of AgOTf in DMSO did not afford the expected acetylene complex, instead giving [RuCp(κ*S*-DMSO)(PTA)(PPh_3)](OTf). On the other hand, reaction of [RuCpCl(PTA)(PPh_3)] with HC≡CC(OH)PPh_2 gave the expected diphenylallenylidene complex [RuCp(C=C=CPh_2)(PTA)(PPh_3)](OTf) (**64**). The reactivity of **64** towards water, O_2, *n*-propylamine, cyclohexylamine and ethanethiol was then studied. Addition of amines and thiols was demonstrated to occur on the α–β carbons of the allenylidene moiety, giving in both cases two isomers (**65a–d** and **66a,b**, Scheme 12). Protonation of

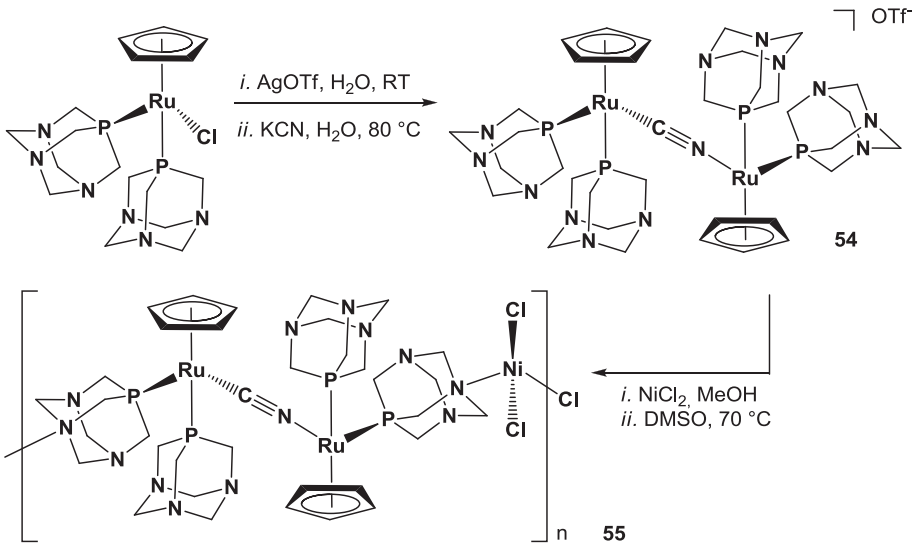

Scheme 11. Synthesis of homobimetallic Ru_2-complex **54** and polymer **55** having a trinuclear Ru_2Ni repeating unit.

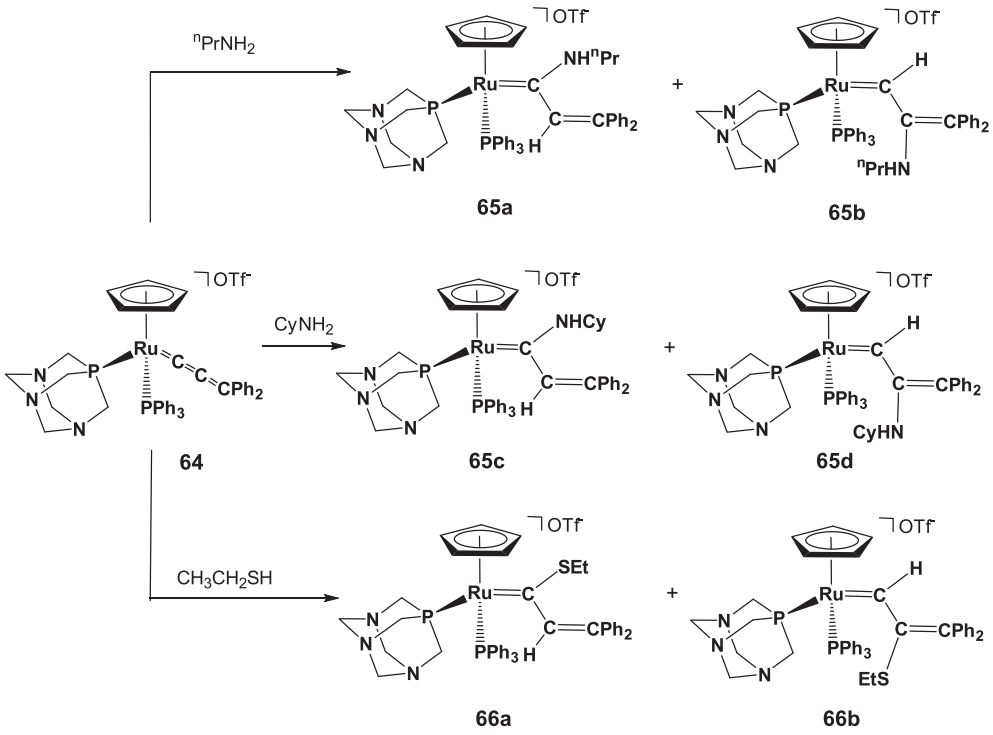

Scheme 12. Reactivity of allenylidene complex **64** towards amines and thiols.

64 with HBF_4 did not afford the desired carbyne derivative expected for selective reactivity on the allenylidene moiety. N-protonation of PTA in **64** occurred instead, and this was attributed to the higher basicity of the N atoms of PTA compared to the allenylidene.

The reactivities of hydrotris(pyrazol-1-yl)borate (Tp) Ru–PTA complexes were investigated by various authors. Reaction of the previously described complex [Ru(κ^3*N*-Tp)Cl(PTA)(PPh_3)] with phenylacetylene gave either the alkynyl complex [Ru(κ^3*N*-Tp)(C≡CPh)(PTA)(PPh_3)] (**67**) or the neutral vinylidene complex [Ru(κ^3*N*-Tp)Cl{C=C(H)Ph}(PTA)] (**68**), depending on the solvent and the reaction conditions. Protonation of **67** with HOTf in CH_2Cl_2 resulted in N-protonation at PTA and a vinylidene moiety in complex [Ru(κ^3*N*-Tp){C=C(H)Ph}(PPh_3)(HPTA)](OTf)$_2$ (**69**). The reactivity of the parent compound was also tested with 1,1-diphenyl-2-propyn-1-ol. The cationic [Ru(κ^3*N*-Tp)(C=C=CPh_2)(PTA)(PPh_3)]PF_6 (**70**) and the neutral [Ru(κ^3*N*-Tp)Cl(C=C=CPh_2)(PTA)] (**71**), were obtained by carrying out the reactions either in MeOH in the presence of $NaPF_6$ or in toluene without other additives, respectively. Then, the reactivity of complexes **70** and **71** toward tertiary phosphines such as PTA and PPh_2Me was investigated. For both compounds, these reactions resulted in the regioselective nucleophilic attack at the allenylidene C-α position yielding the σ-allenyl-phosphonium complexes [Ru(κ^3*N*-Tp){C(L)=C=CPh_2}(PTA)(PPh_3)]PF_6 (**72**, L = PPh_2Me, **a**; PTA, **b**) and [Ru(κ^3*N*-Tp)Cl{C(L)=C=CPh_2}(PTA)] (**73**, L = PPh_2Me, **a**;

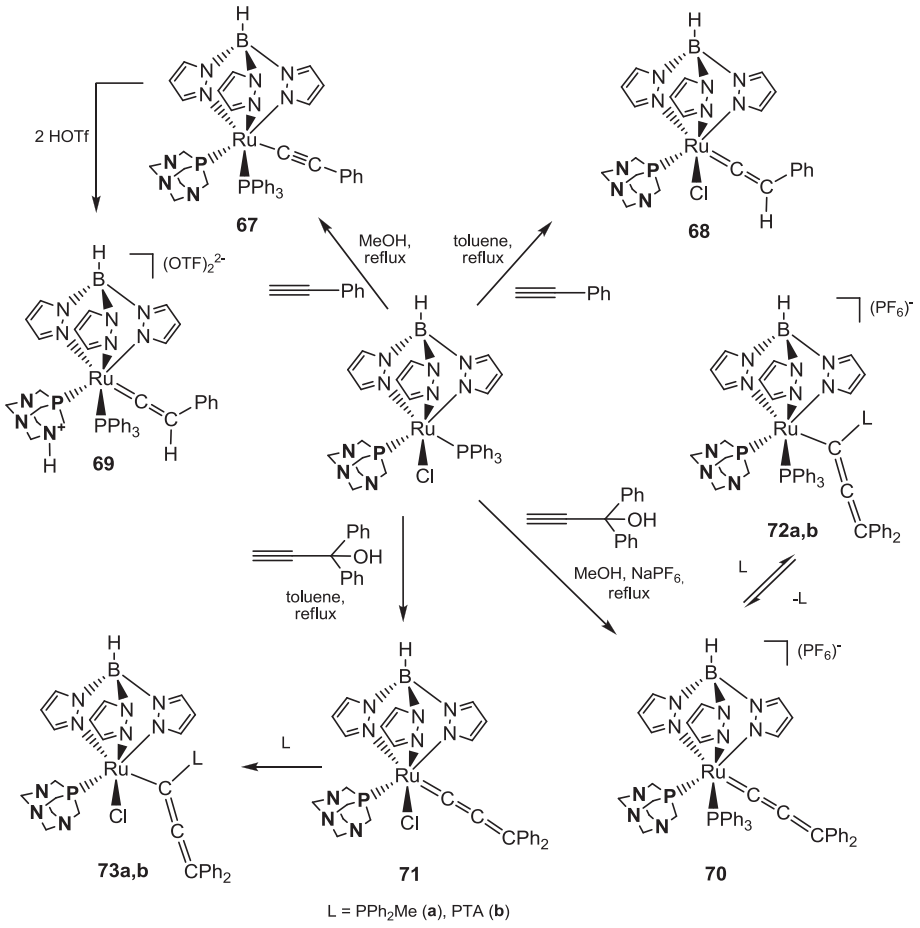

Scheme 13. Reactivity of complex [Ru(κ^3*N*-Tp)Cl(PTA)(PPh_3)] towards phenylacetylene and 1,1-diphenyl-2-propyn-1-ol, followed by C=C unsaturated bond activation by tertiary phosphines L (L = PPh_2Me, PTA).

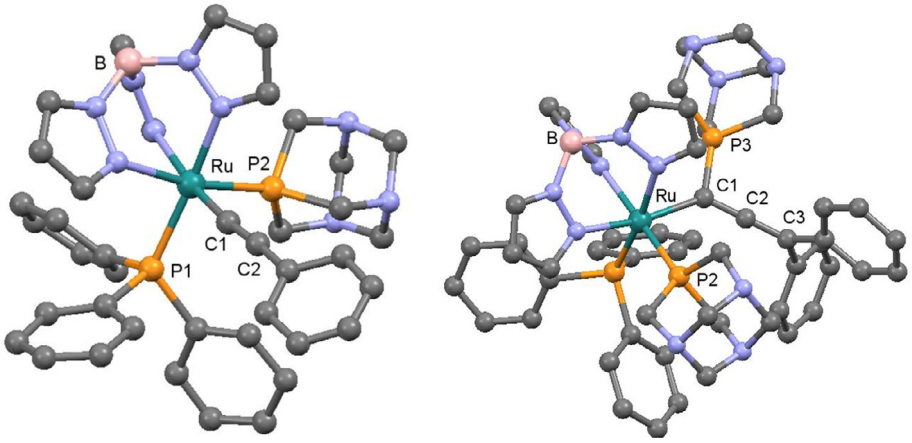

Fig. 6. X-ray crystal structures of **67** (left) and **73b** (right). Adapted from Ref. [47]. Copyright 2009 American Chemical Society.

PTA, **b**), respectively, as shown in Scheme 13. The X-ray crystal structures of **67** and **73b** were also obtained and are shown in Fig. 6 [47].

A similar study was proposed almost at the same time by other authors [48]. In addition to the results described above [47], the reactivity of [Ru(κ^3*N*-Tp)Cl(PTA)(PPh_3)] with other terminal alkynes was tested. The neutral alkynyl complexes [Ru(κ^3*N*-Tp)(C≡R)(PTA)(PPh_3)] (**67**, R = Ph; **74**, R = ^{n}Bu, **a**; 1-cyclopentenyl, **b**; p-methoxypnehyl, **c**; 6-methoxynaphth-2-yl, **d**) were obtained and characterised by NMR techniques. Reaction with propargyl alcohols (1,1-diphenyl-2-propyn-1-ol, 9-ethynyl-9H-fluoren-9-ol) gave as expected complex **70** (either as PF_6^- or OTf^- salt) and the new allenylidene complex [Ru(κ^3*N*-Tp)(C=C=CH—$C_{12}H_8$)(PTA)(PPh_3)]PF_6 (**75**), respectively. Electrophilic attack on **67**, **74** and **75** with MeOTf or HPF_6 (with **75** only) in CH_2Cl_2 at −30 °C gave invariably either N-methylation or N-protonation of PTA.

The synthesis of other [Ru(κ^3*N*-Tp)Cl(L)(PTA)] complexes with different ancillary ligands (**76**, L = PMe_2Ph, **a**; PMe_3, **b**; $P(OMe)_3$,

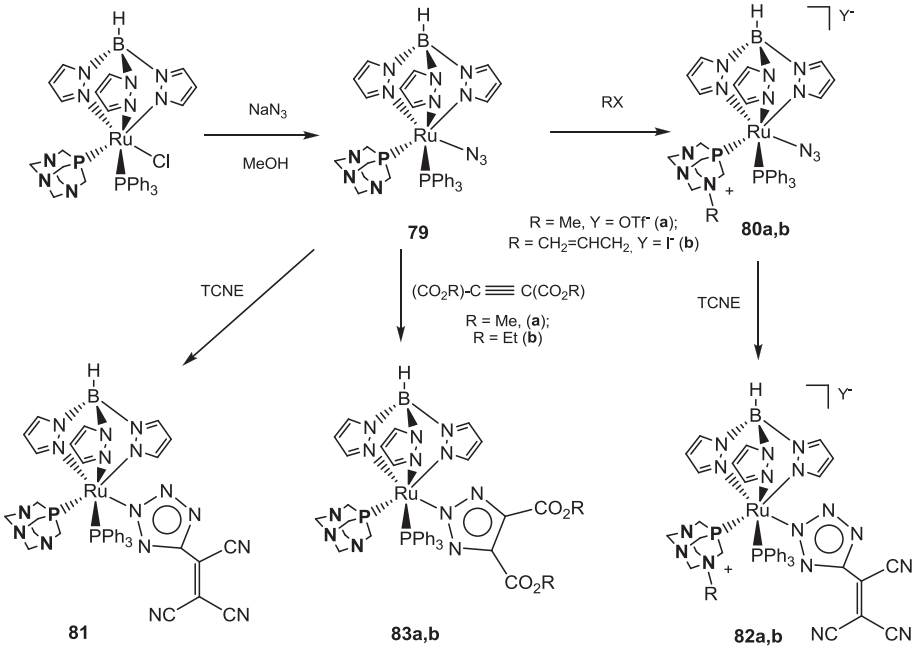

Scheme 14. Reactivity of complex [Ru(κ^3*N*-Tp)Cl(PTA)(PPh_3)] with NaN_3 and further reactions centred on the azide moiety.

c; $P(OPh)_3$, **d**) and the corresponding [Ru(κ^3*N*-Tp)Cl(L)(mPTA)](OTf) complexes (**77a**–**d**) derived from **76** by PTA N-methylation, was also carried out. The hydrido complexes [Ru(κ^3*N*-Tp)H(PPh_3)(L′)](OTf)$_x$ (**78**, L′ = PTA, x = 0, **a**; mPTA, x = 1, **b**) and the cationic complexes [Ru(κ^3*N*-Tp)(MeCN)(PPh_3)(L′)](OTf)$_x$ (**78**, L′ = PTA, x = 1, **a**; mPTA, x = 2, **b**) were also obtained [49]. The study was complemented by electrochemical studies by CV techniques. The antitumour activity of the complexes against three tumour cell lines (NCI-H460, lung cancer; SF-268, brain cancer; MCF-7, breast cancer) and non-tumour cells (HUVEC, Human Umbilical Vein Endothelial Cells) was assessed by a combination of mobility shift assay and DNA binding studies using MALDI-TOF analysis, showing the coordination of the fragments [Ru(κ^3*N*-Tp)(PTA)]$^+$ or [Ru(κ^3*N*-Tp)(mPTA)]$^{2+}$ to a single strand of DNA. High antitumour activity was also observed in some cases, with IC_{50} values comparable to drugs used in clinical practice.

More synthetic reactions were reported starting from [Ru(κ^3*N*-Tp)Cl(PPh_3)(PTA)]. Complex [Ru(κ^3*N*-Tp)(N_3)(PPh_3)(PTA)] (**79**) was obtained reacting the title compound with NaN_3 in MeOH. N-alkylation of **79** with either MeOTf or CH_2=$CHCH_2I$ gave complexes [Ru(κ^3*N*-Tp)(N_3)(PPh_3)(PTA-R)]Y (**80**, R = Me, Y = OTf^-, **a**; R = CH_2=$CHCH_2$, Y = I^-, **b**) [50]. Both **79** and **80** underwent "click" reaction on the azide ligand by reaction with TCNE (tetracyanoethylene) to afford [Ru(κ^3*N*-Tp)(N_4C{C(CN)=C(CN)$_2$})(PPh_3)(L)]$^{n+}Y^{n-}$ (**81**, L = PTA, n = 0, Y = null) and **82** (L = mPTA, n = 1, Y = OTf^-, **a**; L = PTA–CH_2=$CHCH_2$, n = 1, Y = I^-, **b**). Reaction of **79** with alkynes DMAD (dimethylacetylenedicarboxylate) and DEAD (diethylacetylenedicarboxylate) gave instead the triazolato complexes [Ru(κ^3*N*-Tp){$N_3C_2(CO_2R)_2$}(PPh_3)(PTA)] (**83**, R = Me, **a**; Et, **b**), respectively, as shown in Scheme 14.

Other scorpionate-type Ru–PTA complexes were described using Tpms [Tpms = κ^3*N*-tris(pyrazol-1-yl)methanesulfonate lithium salt] and Tpm [Tpm = κ^3*N*-tris(pyrazol-1-yl)methane] instead of Tp. Stepwise reaction of [Ru(κ^3*N*-Tpms)Cl(PPh_3)$_2$] with 1.0 equiv. of PTA in toluene under reflux conditions for 4 h gave complex [Ru(κ^3*N*-Tpms)Cl(PTA)(PPh_3)] (**84**), which was then reacted with another equiv. of PTA to give [Ru(κ^3*N*-Tpms)Cl(PTA)$_2$] (**85**). Complex **85** was also obtained directly from the metal precursor by reaction with 2.3 equiv. of PTA in toluene under reflux conditions for 5 h. A similar reactivity was observed starting from [RuCl(κ^3*N*-Tpm)(PPh_3)$_2$]Cl, which gave [RuCl(κ^3*N*-Tpm)(PTA)(PPh_3)]Cl (**86**) and [RuCl(κ^3*N*-Tpm)(PTA)$_2$]Cl (**87**). Electrophilic attacks on **84**–**87** using BH_3, acids and alkyl halides gave invariably PTA–N-substituted derivatives [51].

Further elaborating on this motif, the same authors described the synthesis of the hydrido complex [Ru(κ^3*N*-Tpms)H(PTA)$_2$] (**88**) by ligand exchange from the PPh_3 analogue [Ru(κ^3*N*-Tpms)H(PPh_3)$_2$], the latter obtained from the reaction of [Ru(κ^3*N*-Tpms)Cl(PPh_3)$_2$] with NaOMe in MeOH [52]. Complex **88** was characterised in solution by a $^{31}P\{^1H\}$ NMR singlet at −20.7 ppm and a ^1H NMR triplet at −15.36 ppm ($^2J_{HP}$ = 28 Hz). In the solid state, a characteristic Ru—H stretching band at 1889 cm^{-1} was observed in the corresponding IR spectrum (KBr pellets). An X-ray crystal structure of **88** was also obtained, showing a Ru(1)—H(1) bond distance of 1.58(4) Å. The reaction of [Ru(κ^3*N*-Tpms)H(PPh_3)$_2$] with 3 equiv. of PTA in refluxing toluene gave complex [Ru(κ^2*N*-Tpms)H(PTA)$_3$] (**89**) with an open arm from the Tpms ligand. The reactivity of **88** with alkynes was then explored and compared to that observed for [Ru(κ^3*N*-Tp)H(PPh_3)(PTA)]. In the case of the Tpms complex, harsher conditions were required (refluxing toluene) to obtain the insertion products [Ru(κ^3*N*-Tpms){(*E*)-C(CO_2Me)=CH(CO_2Me)}(PTA)$_2$] (**90**), [Ru(κ^3*N*-Tpms){(*E*)-CH=CHPh}(PTA)$_2$] (**91**) and [Ru(κ^3*N*-Tpms){(*E*)-CH=CH_2OH}(PTA)$_2$] (**92**), by reactions of **88** with DMAD, phenylacetylene and prop-2-yn-1-ol, respectively. Using alkynes such as but-1-yn-3-ol, 1-ethynylcyclopentanol and 1-ethynylcyclohexanol, the corresponding α,β-unsaturated Ru-alkenyl *E*-complexes were regioselectively obtained, by facile dehydration of the hydroxyalkenyl complexes formed in the insertion reaction involving the Ru—H bond. Finally, hydride ligand protonation in [Ru(κ^3*N*-Tp)H(PPh_3)(PTA)] was reinvestigated. Using HBF_4, selective reaction with the hydrido ligand and hydrogen elimination occurred giving as product complex [Ru(κ^3*N*-Tp)(F-BF_3)(PPh_3)(PTA)] (**93**) bearing a coordinated BF_4 ligand. Monitoring the reaction by VT NMR techniques, it was possible to observe signals corresponding to [Ru(κ^3*N*-Tp)(η^2-H_2)(PPh_3)(PTA)]$^+$ (**94**) at 233 K, with a broad ^1H NMR signal at ca. −9 ppm due to the non-classical dihydrogen ligand. The presence of the η^2-H_2 ligand was further confirmed by T_1 measurement, giving a short T_1 = 62

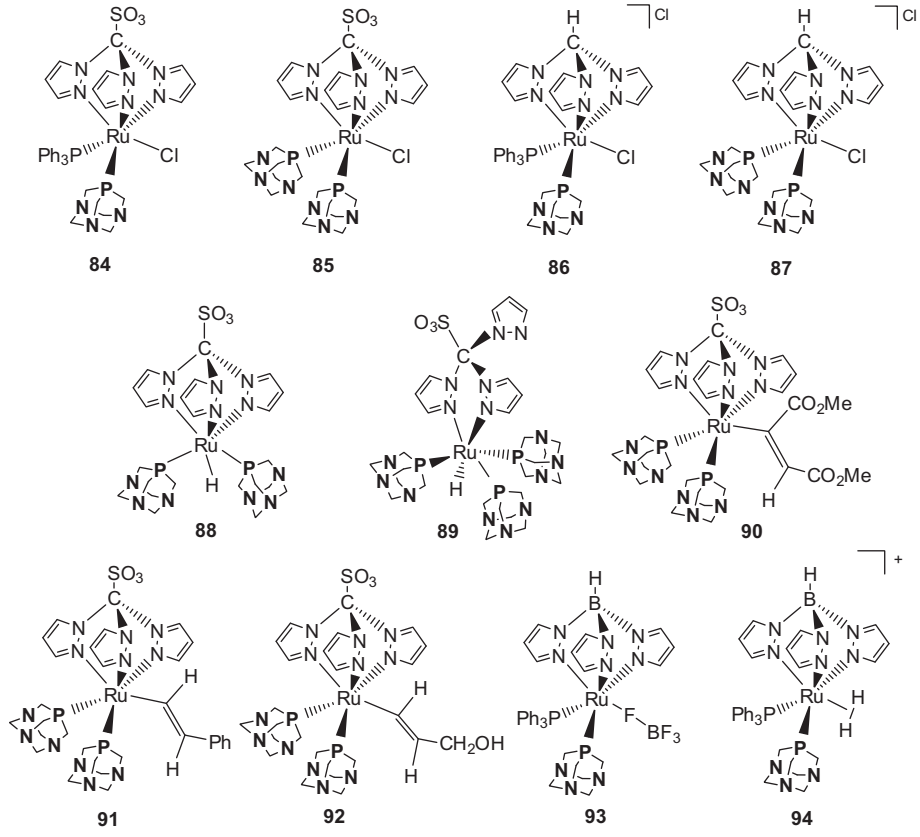

Chart 5. Ruthenium complexes **84**–**94**.

ms, in the expected range for this class of complexes (T_1 = spin–lattice relaxation time). Drawings of complexes **84**–**94** are shown in Chart 5.

A class of Ru–PTA complexes containing 8-thiotheophylline derivatives was recently described and studied for its antiproliferative properties towards cisplatin sensitive (T2) and resistant (SKOV3) ovarian cancer cells. Monometallic complexes including [RuCpX(L)(PTA)] (X = 8-thio-theophyllinate (TTH^-), L = PTA (**95a**), L = PPh_3 (**95b**); X = 8-methylthio-theophyllinate ($8\text{-}MTT^-$), L = PTA (**96a**), L = PPh_3 (**96b**); X = 8-benzylthiotheophyllinate ($8\text{-}BzTT^-$), L = PTA (**97a**), L = PPh_3 (**97b**)) and binuclear complexes [{RuCp(PTA)(L)}$_2$-μ-(Y-κ*N7*,*N′7*)] (Y = bis(S-8-thiotheophyllinate) methane ($MBTT^{2-}$), L = PTA (**98a**), L = PPh_3 (**98b**); Y = 1,2-bis(S-8-thiotheophyllinate)ethane ($EBTT^{2-}$), L = PTA (**99a**), L = PPh_3 (**99b**); Y = 1,3-bis(S-8-thiotheophyllinate)propane ($PBTT^{2-}$); L = PTA (**100a**), L = PPh_3 (**100b**)) have been synthesised and characterised by NMR, IR spectroscopy and elemental analysis [53]. The synthetic pathway usually involved reaction of [RuCpCl(PTA)$_2$] with mono- and bis-thiopurines in water in the presence of KOH. Tests showed that only complex **97b** had an activity comparable to cisplatin on T2 and no activity on SKOV3 cells, and the authors attributed this effect to the favourable lipophilicity/hydrophylicity balance obtained with this combination of ligands around Ru. In the case of the mPTA analogues, the corresponding binuclear complexes with thiopurines $MBTTH_2$, $EBTTH_2$, $PBTTH_2$ were obtained. They were studied by cyclic voltammetry showing two one-electron oxidative responses (Ru^{II}–Ru^{II}/Ru^{III}–Ru^{II}; Ru^{III}–Ru^{II}/Ru^{III}–Ru^{III}) that increase their redox potential when the bis(8-thiotheophylline)-alkyl-bridge grows in length [54].

This chemistry was recently revisited by the same authors, extending the choice of phosphine ligands to combinations of PTA, mPTA and PPh_3 in the presence of 8-MTT. The stability of complexes [RuCp(κ*S*-8MTT)(L)(L′)] (**101**) and [RuCp(κ*N*-8MTT)(L)(L′)] (**102**; L, L′ = PTA, mPTA; L = mPTA, L′ = PPh_3) have been investigated by DFT theoretical methods at B3LYP/DZVP level of theory, both in gas phase and in explicit polar solvents. It was shown that, in the gas phase, complex [RuCp(κ*S*-8MTT)(PPh_3)(mPTA)]$^+$ was slightly more stable than [RuCp(κ*N*-8MTT)(PTA)$_2$] and [RuCp(κ*N*-8MTT)(PPh_3)(mPTA)]$^+$. In water and ethanol, calculations showed that, in general, the κ*S*-8MTT complexes were more stable than the corresponding κ*N*-8MTT complexes [55].

Ru complexes bearing "upper rim" PTA derivatives were also described. The imidazolyl-PTA ligands **6** and **7** were reacted with [RuCl$_2$(p-cymene)]$_2$ in refluxing $CHCl_3$ to form [RuCl(p-cymene)(κ*P*,*N*-L)]Cl (**103**, L = 1-methylimidazolyl-(1,3,5-triaza-7-phosphatricyclo[3.3.1.13,7]dec-6-yl)methanol, **a**; L = bis(1-methylimidazolyl)(1,3,5-triaza-7-phosphatricyclo[3.3.1.13,7]dec-6-yl) methanol, **b**). Similarly, ligands phenyl(1,3,5-triaza-7-phosphatricyclo[3.3.1.1^{3,7}]dec-6-yl)methanol (PZA) and the single diastereoisomer (*SR*, *RS*)-4′-dimethylaminophenyl(1,3,5-triaza-7-phosphatricyclo[3.3.1.1^{3,7}]dec-6-yl)methanol (*SR*,*RS*-PZA-NMe_2) gave complexes [RuCl$_2$(p-cymene)(κ*P*-L)] (**104**, L = PZA, **a**; L = *SR*,*RS*-PZA-NMe_2, **b**). The ligands could bind to Ru either in κ*P* or κ*P*,*N* fashion, but not as κ*P*,*O* chelates, as shown in Scheme 15, as clarified by NMR experiments and DFT calculations [8]. The $^{31}P\{^1H\}$ NMR spectra were generally characterised by one or two singlets, reflecting the diastereomeric nature of some of the ligands. Chemical shift values of −40.23 and −28.71 ppm (**104a**), −40.35 ppm (**104b**), −26.37 and −22.88 ppm (**103a**) and −19.77 ppm (**103b**) were recorded, respectively.

In the case of the potentially κ*P*,*N* bidentate β-aminophosphines **10**–**12**, a solvent-dependent coordination preference κ*P* vs. κ*P*,*N* was observed, depending on the nature of substituents R_1 and R_2 (Scheme 16). In polar solvents, such as water or methanol, com-

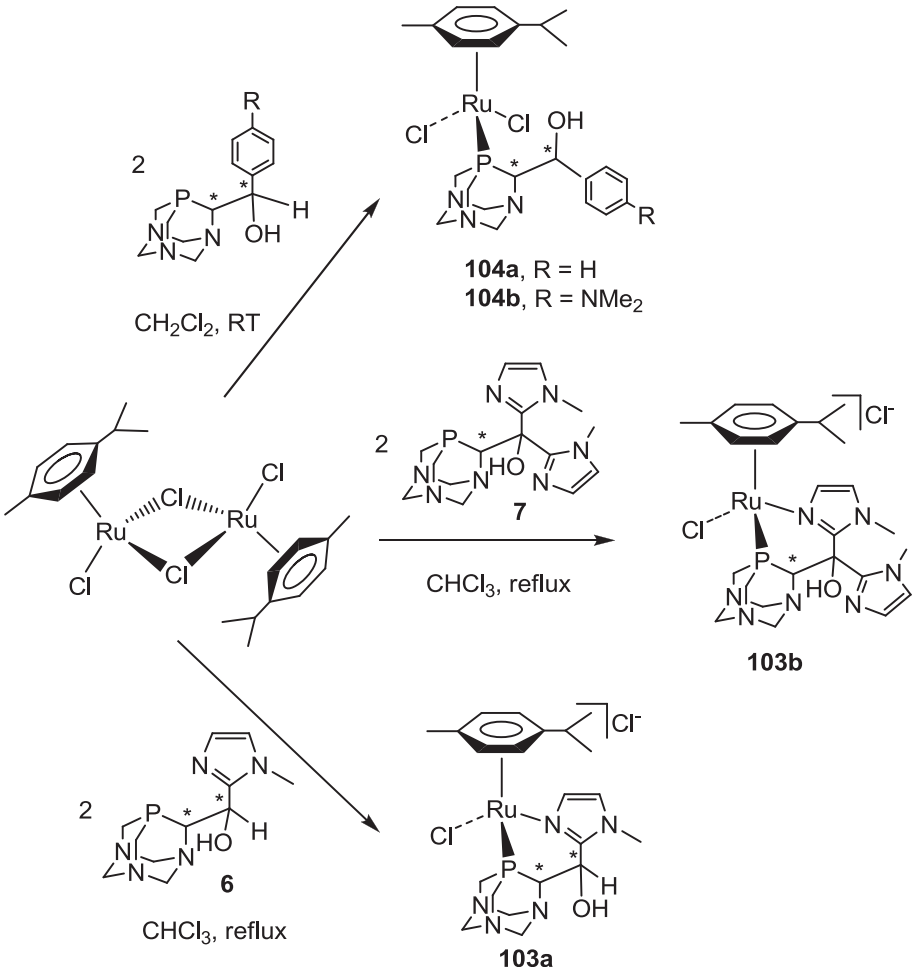

Scheme 15. Synthesis of κ*P* and κ*P*,*N* complexes bearing "upper rim" imidazolyl and benzyl alcohol PTA derivatives.

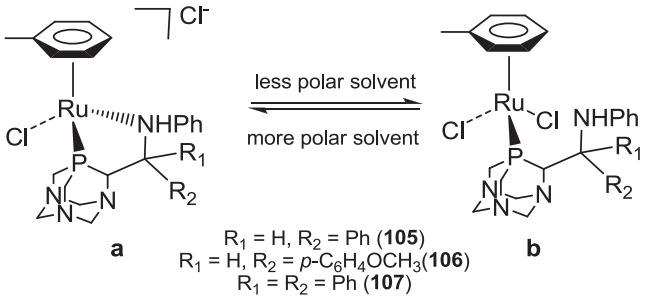

Scheme 16. Solvent-dependent equilibrium between κ*P*,*N* and κ*P* complexes bearing "upper rim" benzylamine PTA derivatives.

plexes [RuCl(η^6-toluene){κ*P*,*N*-(PTA-CR^{1}R^{2}NHPh)}]Cl (R^1 = H, R^2 = Ph, **105a**; R^1 = H, R^2 = *p*-C$_6$H$_4$OMe, **106a**; R^1 = R^2 = Ph, **107a**) were obtained, albeit in methanol **105** showed ca. 15% of κ*P* isomer (**105b**). In less polar solvents, such as CH_2Cl_2 or $CHCl_3$, **105**–**107** exist as equilibrium mixtures of monodentate and bidentate coordination modes, whereas in CD_3CN **105** and **106** exist mainly as the κ*P*,*N* species while **107** is found principally as the κ*P* isomer [9].

The same authors investigated the coordination chemistry of ligand PTA–P^{i}Pr$_2$ (**16**) to Ru(II) and W(0). Starting from [RuCl$_2$(η^6-toluene)]$_2$, addition of 2 equiv. of **16** in benzene at room temperature gave complex [RuCl$_2$(η^6-toluene){κ*P*-(PTA–P^{i}Pr$_2$)}] (**108**), with ^{31}P{^{1}H} NMR signals at 11.17 (d, $^2J_{PP}$ = 65 Hz, P^{i}Pr$_2$) and −27.40 ppm (d, $^2J_{PP}$ = 65 Hz, PTA). On the other hand, addition of 2 equiv. of **16** to the metal precursor in CH_2Cl_2 led, over the course of a few days, to a mixture of **108** and complex [RuCl(η^6-toluene){κ^2*P*-(PTA–P^{i}Pr$_2$)}]Cl (**109**) as a couple of diastereoisomers, with ^{31}P{^{1}H} NMR signals at 62.95 (d, $^2J_{PP}$ = 64 Hz, P^{i}Pr$_2$), −54.97 ppm (d, $^2J_{PP}$ = 64 Hz, PTA) and 51.30 (d, $^2J_{PP}$ = 65 Hz, P^{i}Pr$_2$), −46.41 ppm (d, $^2J_{PP}$ = 65 Hz, PTA). Complex **109** could be also obtained in 94% yield by leaving **108** in CH_2Cl_2 for ca. 3 days. Ligands **16** and **17** were also used to coordinate W(0) using precursor [W(CO)$_4$(pip)] (pip = piperidine). In both cases, the ligands adopted a κ^2*P* binding mode in the corresponding products [W(CO)$_4$(L)] [**110a**, L = κ^2*P*-{PTA–P^{i}Pr$_2$} (**16**); **110b**, L = κ^2*P*-{PTA–(N^{i}Pr)$_2$(CH$_2$)$_2$} (**17**)] [10].

Other ancillary ligands were used to stabilise Ru–PTA complexes. Bis(allyl)ruthenium(IV) complexes containing PTA, PTA–Bn and DAPTA were obtained from the dimeric precursor [{RuCl(μ-Cl)(η^3:η^3-C$_{10}$H$_{16}$)}$_2$] (C$_{10}$H$_{16}$ = 2,7-dimethylocta-2,6-diene-1,8-diyl) by reaction with two equiv. of the water soluble ligands in CH_2Cl_2 [56]. Complexes [RuCl$_2$(η^3:η^3-C$_{10}$H$_{16}$)(L)] [**111**, L = PTA, **a**; (PTA–Bn)Cl, **b**; DAPTA, **c**) were obtained and fully characterised in solution by NMR and IR spectroscopies and in the solid state by single-crystal X-ray diffraction. As an example, the X-ray crystal structure of complex **111c** is shown in Fig. 7.

Complex [RuCp(PTA)(CH$_3$CN){PH$_2$(OH)}]PF$_6$ (**112**), bearing a Ru-coordinated phosphinous acid molecule PH$_2$(OH), the tautomer of elusive phosphine oxide, O=PH$_3$, was obtained by trapping the electrochemically-generated phosphine oxide in water/ethanol mixtures containing white phosphorus (P$_4$), in a water solution containing [RuCp(PTA)(CH$_3$CN)$_2$]PF$_6$. Complex **112** was charac-

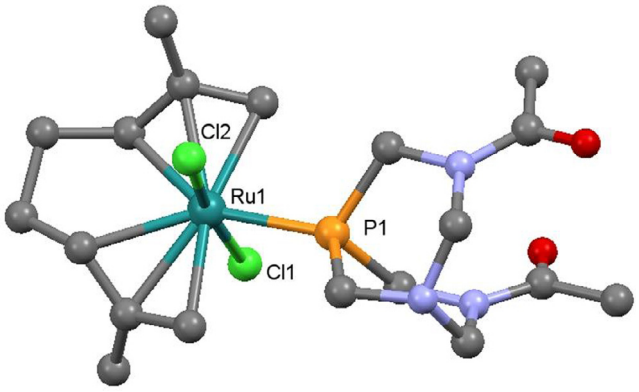

Fig. 7. X-ray crystal structures of **111c**. Adapted from Ref. [56]. Copyright 2010 John Wiley and Sons.

terised by $^{31}P\{^{1}H\}$ NMR spectroscopy, with signals at 74.1 (td, $^{1}J_{PH}$ = 366.2 Hz, $^{2}J_{PP}$ = 63.0 Hz, PH_2OH), −11.6 (d, $^{2}J_{PP}$ = 63.0 Hz, PTA), −145.1 (septet, $^{1}J_{PF}$ = 706.1 Hz, PF_6) [57].

A series of ruthenium–arene complexes of formula [Ru(DBM)(η^6-arene)(PTA)]X (**113a–d**, arene = p-cymene, C_6Me_6; DBM = deprotonated DBMH, dibenzoylmethane; X = PF_6^- or OTf^-) were synthesised and fully characterised in solution by NMR spectroscopy. For five of them, the solid-state structures were determined by single-crystal X-ray diffraction, confirming κ^2O-coordination of DBM to Ru. These complexes show intense photoluminescence emission at room temperature in the solid state and proved efficient in binding to calf thymus DNA through intercalative/electrostatic interactions. Moreover, the antitumour activity of free DBMH ligand and complexes was evaluated against U266 and RPMI human multiple myeloma cell lines. Some of them showed a higher cytotoxic effect for the OTf^- complexes than for the PF_6^- analogues, likely due to solubility reasons [58].

Complexes $[RuCl_2(HL)(HPTA)_2]Cl_2$ (**114a–d**), where HL = bioactive 5-nitrofuryl thiosemicarbazones, have been synthesised and fully characterised in solution by NMR spectroscopy. They were obtained from reaction of $[RuCl_2(DMSO)_4]$ with PTA in refluxing EtOH in the presence of four different thiosemicarbazones, with different substituents R = H, Me, Et, Ph on the NHC(=S)NHR group. Their properties against protozoan parasites such as *Trypanosoma cruzi* and *Entamoeba histolytica* were assessed *in vitro*, and complex **114** containing HL where R = Ph was found to be the most active. The study was complemented with evaluation of cytotoxicity on RAW 246.7 murine macrophages and DNA intercalation [59].

Complex [RuCl{κ^4N-tris(benzimidazole-2-yl-methyl)amine}(PTA)]Cl (**115**) was obtained by ligand exchange from the corresponding PPh_3 precursor. The complex features an octahedral geometry around Ru, with Cl ligand *trans* to the alkyl N atom of the N_4 ligand (Chart 4). The corresponding $^{31}P\{^{1}H\}$ NMR spectrum showed a singlet at −20.88 ppm, consistent with a P atom trans to N. A modest degree of water solubility was measured, with a value of $S(H_2O)_{25°C}$ = 10 g L^{-1} [60]. Drawings of complexes **113–115** are shown in Chart 6.

Ruthenium carbonyl cluster compounds of different nuclearities bearing PTA were obtained and characterised by IR, NMR and HRMS (high resolution mass spectrometry), and some of them in the solid state by single-crystal X-ray diffraction [61]. Starting from $[Ru_3(CO)_{12}]$ by addition of PTA in either CH_2Cl_2 or MeOH, a mixture of three different complexes was obtained and separated by column chromatography, namely $[Ru_3(CO)_{12-x}(PTA)_x]$ (**116a–c**, x = 1–3). $^{31}P\{^{1}H\}$ NMR data showed signals due to a single isomer for **116a** (s, −43.5 ppm) and **116c** (−44.6 ppm) and for two isomers for **116b** (s, −45.96 and −44.02 ppm in 1:4 ratio). Starting from the Ru–carbido carbonyl precursor $[Ru_5C(CO)_{15}]$, addition of 1–5 equiv. of PTA afforded compounds $[Ru_5C(CO)_{15-x}(PTA)_x]$ (**117a–f**, x = 1–6). $^{31}P\{^{1}H\}$ NMR spectra varied from simple singlets for **117a** (−23.7 ppm) and **117b** (−32.5 ppm) to rather complicated patterns with up to 4 signals for **117e** (−52.63, −47.54, −44.11 and −32.31 ppm, in 20/46/20/14 ratio), depending on the number of coordinated PTA ligands and on the symmetry of the molecule. Finally, using $[Ru_6C(CO)_{17}]$ and PTA, compounds $[Ru_6C(CO)_{17-x}(PTA)_x]$ (**118a–f**, x = 1–6) were obtained. For the $[Ru_3(CO)_{12}]$ derivatives, water solubility was observed at acidic pH only in the case of complex **116c**. For higher nuclearity clusters, derived from $[Ru_5C(CO)_{15}]$ and $[Ru_6C(CO)_{17}]$, this property was instead obtained with less than one phosphine per ruthenium atom. According to the authors, in the latter case "PTA has to form a solubility envelope around the metal core", bringing about water solubility even at Ru:PTA ratios lower than 1 (Fig. 8).

Another class of Ru–PTA complexes that is receiving growing interest includes complexes having bipyridine (bipy) as co-ligand. Treatment of $[RuCl_2(bipy)_2]\cdot 2H_2O$ with PTA in the presence of $NaBH_4$ and NH_4PF_6 gave the ruthenium hydrido complex *cis*-$[RuH(bipy)_2(PTA)](PF_6)$ (**119**), with a $^{31}P\{^{1}H\}$ NMR singlet at −29.7 ppm and a ^{1}H NMR doublet at −12.6 ($^{2}J_{PH}$ = 32 Hz) for the hydrido ligand, respectively. Complex **119** was reacted with CO_2 and CS_2 to give the corresponding formato and dithioformato complexes *cis*-[Ru{η^1-EC(E)H}(bipy)$_2$(PTA)](PF$_6$) (**120**, E = O, **a**; E = S, **b**). Reaction of **119** with HOTf in CH_3CN gave *cis*-[Ru(MeCN)(bipy)$_2$(PTA)](PF$_6$)$_2$ (**121**) by coordination of one molecule of acetonitrile to Ru on the vacant coordination site obtained upon loss of hydrogen [62]. Both insertion reactions followed second-order

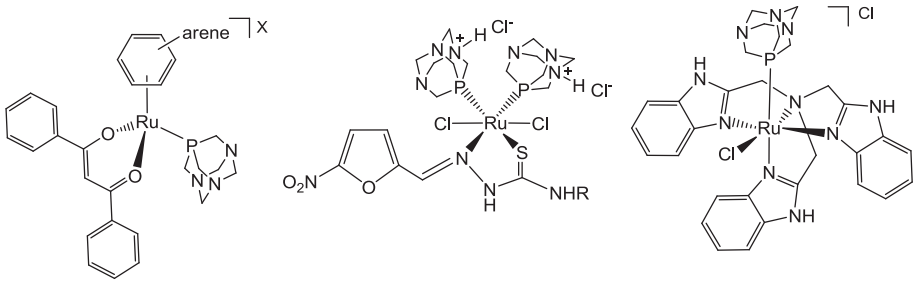

113a (arene= p-cymene; X= PF_6, **a**; arene= p-cymene; X= OTf, **b**; arene= C_6Me_6; X= PF_6, **c**; arene= C_6Me_6; X=OTf, **d**)

114 (R= H, **a**; R = Me, **b**: R= Et, **c**; R = Ph, **d**

115

Chart 6. Ruthenium complexes **113–115**.

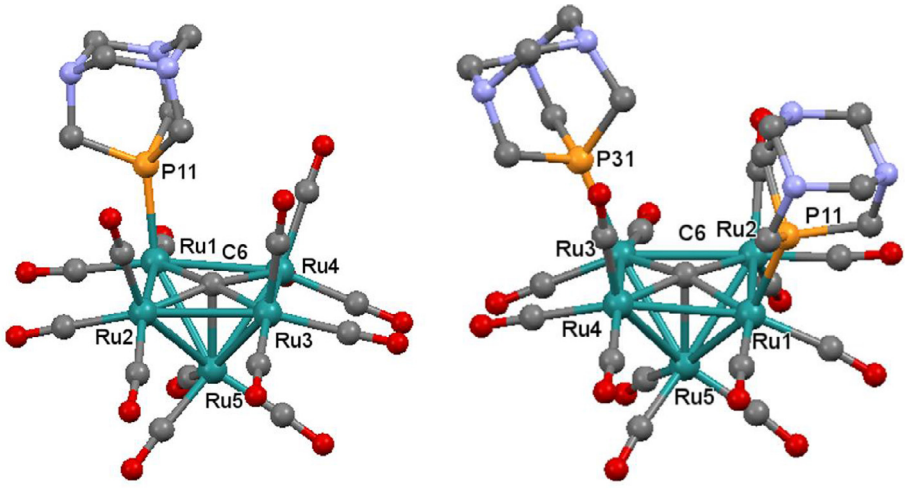

Fig. 8. X-ray crystal structures of **118a** (x = 1, left) and **118b** (x = 2, right). Adapted from Ref. [61]. Copyright 2015 Elsevier Science B.V.

kinetics, with second-order rate constants (k_2) ranging from $(9.40 \pm 0.41) \times 10^{-4}$ M^{-1} s^{-1} in acetone to $(1.13 \pm 0.08) \times 10^{-1}$ M^{-1} s^{-1} in MeOH for CO_2 and from (3.43 ± 0.10) M^{-1} s^{-1} in MeOH to (24.0 ± 0.5) M^{-1} s^{-1} in DMF for CS_2. By electrochemical methods, using a Ag/AgCl reference electrode (Ag/AgCl *vs* NHE = 197 mV), it was observed that in MeCN the anodic oxidation of **119** irreversibly occurred at 0.5 V to give **121**, which in turn was oxidised irreversibly at a potential exceeding 1.5 V. It was proposed that the electrochemical formation of **121** should proceed *via* a sequential loss of two electrons and a proton from **119** followed by the coordination of a solvent molecule (MeCN).

A detailed study on synthetic modifications, interconversion and ligand release upon irradiation under acidic conditions of a series of Ru(bipy)–PTA complexes was reported [63]. Complex *cis*-$[Ru(bipy)_2(PTA)_2]Cl_2$ (**122a**) was obtained from $[RuCl_2(bipy)_2]$ by reaction with 10 equiv. of PTA in H_2O under reflux conditions, whereas the *trans*-isomer *trans*-$[Ru(bipy)_2(PTA)_2](OTf)_2$ (**122b**) was instead obtained from *trans*-$[Ru(bipy)_2(H_2O)_2](OTf)_2$ under identical reaction conditions. Both complexes showed fluorescence properties in water at room temperature, both in air and under nitrogen atmosphere. Under strongly acidic conditions (pH = 0, using HOTf 1.0 M), irradiation of **122a** (λ = 360 nm) and **122b** (λ = 402 nm) caused the decoordination of one PTA molecule and protonation of the Ru-bound PTA, with formation of *cis*-$[Ru(bipy)_2(HPTA)](OTf)_3{\cdot}H_2O$ (**123a**) and *trans*-$[Ru(bipy)_2(HPTA)](OTf)_3{\cdot}H_2O$ (**123b**), respectively. This reaction was followed by *trans–cis* isomerisation and water coordination to yield the final common product *cis*-$[Ru(bipy)_2(H_2O)(HPTA)](OTf)_3$ (**124**). The electrochemical behaviour of **122a** and **122b** was then studied in water and DMF, using a standard Ag/AgCl reference electrode. Irreversible anodic oxidation in water, corresponding to the Ru^{II}/Ru^{III} redox process, occurs at 1.47 V (E_{ox}) with reduction at 0.39 V (E_{red}) (ΔE_P = 1.08 V) for **122a**, whereas for **122b** the process is quasi-reversible (E = 0.89 V; ΔE_P = 0.79 V). In DMF, both complexes showed irreversible anodic oxidations at lower potential than in water (E_{ox} = 1.00 V, **122a**; 0.98 V, **122b**). The X-ray crystal structures of **122a** and **122b** were also obtained.

The controversial *trans–cis* isomerisation mechanism for the known complex $[RuCl_2(PTA)_4]$ (**125**) was further investigated, and it was concluded that the best synthetic procedure to get the thermodynamic product *cis*-$[RuCl_2(PTA)_4]$ was the irradiation of an aqueous solution of *trans*-$[RuCl_2(PTA)_4]$ with blue light (λ = 470 nm) for 1 h [64]. In the same article, the authors employed *trans*-**125** and *cis*-**125** as precursors for further syntheses. Reaction of *trans*-**125** with bipy in refluxing water gave *mer*-$[RuCl(bipy)(PTA)_3](PF_6)$ (**126a**), while a mixture of **126a** (minor) and *fac*-$[RuCl(bipy)(PTA)_3](PF_6)$ (**126b**, major) was obtained starting from *cis*-**125** in the presence of Ag^+ salts. Moreover, complex *cis,cis*-$[RuCl_2(bipy)(PTA)_2]$ (**127**) was obtained by ligand substitution from *cis,cis,trans*-$[RuCl_2(\kappa S\text{-DMSO})_2(PTA)_2]$ with bipy in EtOH under reflux conditions. In water complex **127** slowly released a chloride and coordinated H_2O to give the ionic *cis*-$[RuCl(bipy)$

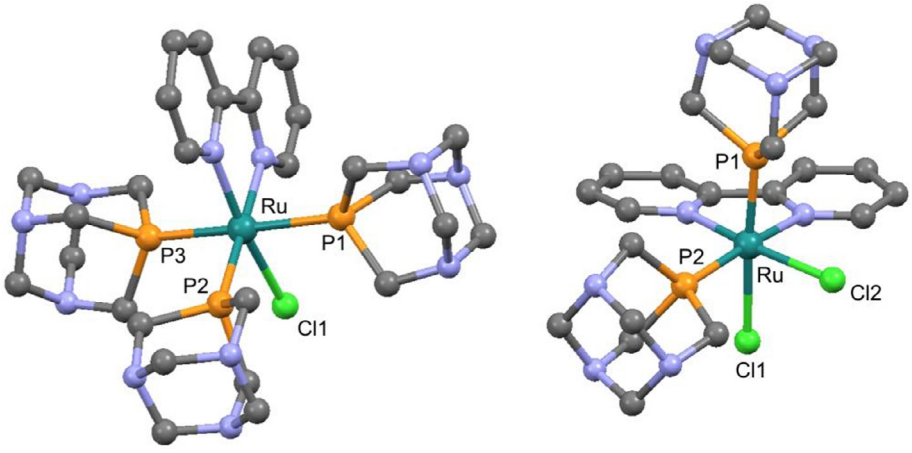

Fig. 9. X-ray crystal structures of **126a** cation (left) and **127** (right). Adapted from Ref. [64]. Copyright 2016 John Wiley and Sons.

$(H_2O)(PTA)_2]Cl$ (**128**). The X-ray crystal structures of **126a** (cation) and **127** are shown in Fig. 9. On the other hand, reaction of *cis,cis,-trans*-$[RuCl_2(\kappa S\text{-DMSO})_2(PTA)_2]$ with 4-methyl-2,2′-bipyridine-4-carboxylic acid (bipyAc) gave *cis,cis*-$[RuCl_2(bipyAc)(PTA)_2]$ (**129**) as a 50:50 mixture of two isomers with 4-carboxylic acid either *trans* or *cis* to PTA, respectively.

Fe–hydrogenase-inspired Fe–Fe carbonyl complexes bearing PTA where synthesised in an attempt to increase basicity of the metal core by CO substitution, and increase the electrocatalytic activity in hydrogen release from acetic acid (HOAc) in polar media. Thus, complexes $[Fe_2(\mu\text{-}C_6H_4S_2)(CO)_5(PTA)]$ (**130a**) and $[Fe_2(\mu\text{-}C_6H_4S_2)(CO)_4(PTA)_2]$ (**130b**) were obtained from the carbonyl precursor $[Fe_2(\mu\text{-}C_6H_4S_2)(CO)_6]$ by reaction with 1 or 2 equiv. of PTA in either MeOH or THF, respectively [65]. The electrocatalytic reduction of HOAc took place at −2.15 V (**130a**) and −2.35 V (**130b**), however only moderate activities were observed at overpotentials near 0.7–0.9 V ($E°_{HOAc}$ = −1.46 V).

Cluster carbonyl complexes $[Os_3(CO)_{12-x}(PTA)_x]$ (**131a–d**, x = 1–4) were obtained by different synthetic routes and in different yields, and their water solubility as a function of pH was measured. It was found that complex **131d** (x = 4) was soluble in water at ca. neutral pH. In acidic media, **131c** (x = 3) undergoes protonation at PTA, resulting in $[Os_3(CO)_9(HPTA)_3]Cl_3$ (**131e**). The X-ray crystal structures of **131a** and **131c**, both obtained as MeOH adducts, are shown in Fig. 10 [66].

Complex *trans*-$[OsCl_2\{(S,S)$-^{i}Pr-pybox$\}(PTA)]$ (**132**, (*S,S*)-^{i}Pr-pybox = 2,6-bis[4′(*S*)-isopropyloxazolin-2′-yl]pyridine) was obtained from the corresponding η^2-C_2H_4 precursor by reaction with PTA in toluene at reflux in 63% yield, and characterised in solution by a $^{31}P\{^1H\}$ NMR singlet at −93.5 ppm for PTA *trans* to pyridine [67]. Further reaction of **132** with $HCl{\cdot}OEt_2$ gave as expected the N-PTA-protonated *trans*-$[OsCl_2\{(S,S)$-^{i}Pr-pybox$\}(HPTA)]Cl$ (**133**), whereas alkylation with RX (R = methyl, **a**; allyl, **b**; propargyl, **c**; benzyl, **d**; X = I^-, Br^-) gave complexes *trans*-$[OsCl_2\{(S,S)$-^{i}Pr-pybox$\}$(PTA-R)]X (**134a–d**). All complexes were found to be water soluble, in the range 1.98 (for **133**) to 10.10 g L^{-1} (for **134d**) at 20 °C and were tested for plasmid DNA mobility shift assay for DNA intercalation studies, as *in vitro* antitumour drugs against cell lines of human cervical cancer (HeLa) and colon cancer (HT29), and as antimicrobial agents against bacteria such as *Micrococcus luteus, Bacillus subtilis, Escherichia coli, Streptomyces coelicolor, Streptomyces antibioticus, Pseudomonas aeruginosa* and yeasts (*Candida albicans* and *Candida parapsilosis*). Complex **134d** showed the highest activity in all tests and largest intercalation with DNA.

The first Ru–arene complexes bearing CAP as ligand were recently described [19]. The RAPTA-C analog $[RuCl_2$(p-cymene)(CAP)] (**135**) was obtained in 87% yield reacting $[RuCl_2$(p-cymene)$]_2$ with 2 equiv. of CAP in CH_2Cl_2 at room temperature. Complex **135** was used as precursor for the synthesis of $[RuCl$(p-cymene)$(CAP)_2](PF_6)$ (**136**) by reaction with one equiv. of CAP and a stoichiometric amount of $TlPF_6$, and to obtain complex [RuCl(p-cymene)(MeCN)(CAP)](PF_6) (**137**) by a similar reaction in the presence of MeCN. The $^{31}P\{^1H\}$ NMR spectra showed singlets at 52.83 (**135**, $CDCl_3$), 51.60 (**136**, acetone-d_6) and 48.17 ppm (**137**, acetone-d_6), respectively. The X-ray crystal structures of **135** and **136** were also obtained. Compared to RAPTA-C, the compounds tested are considerably more cytotoxic toward A2780 (IC_{50} = ca. 48–65 vs. 230 μM, RAPTA-C) and A2780cisR (IC_{50} = ca. 70–108 vs. 270 μM, RAPTA-C) ovarian cancer cell lines. However, only complex **135** showed equal cytotoxicity toward both types of cells. Noteworthy, all complexes maintain their cancer cell selectivity by a 2-fold stronger growth inhibition effect on A2780 cancer cells compared to noncancerous HEK293 cells (IC_{50} = ca. 80–163 μM vs. >1000, RAPTA-C).

3.3. Group 9 complexes

The Co(II) compounds $[CoCl(bipy)_2(\kappa S\text{-PTA=S})]X$ (**138**, X = BF_4, PF_6) $[CoCl(bipy)_2(\kappa O\text{-PTA=O})]X$ (**139**, X = BF_4, PF_6) and $[CoCl(bipy)_2(\kappa N\text{-PTA})]BF_4$ (**140**) were obtained by reacting anhydrous $CoCl_2$ with PTA=S, PTA=O and PTA, respectively, in EtOH at room temperature, and in the presence of bipy and $NaBF_4$ or $NaPF_6$. When the reaction with PTA is carried out in EtOH under nitrogen atmosphere, complex **140** is formed, showing a $^{31}P\{^1H\}$ NMR singlet at −95.4 ppm. Upon dissolution in water and standing in air, **140** evolves to **139** by PTA oxidation followed by κ*O*-coordination to Co [68].

On the other hand, attempted coordination of (mPTA)I to Co(II) by reaction with $CoCl_2$ in MeOH or EtOH resulted in Co oxidation giving the salt $[mPTA][CoCl_4]$ [69].

The rhodium(I) complex *trans*-$[RhCl_2(PTA)(HPTA)]$ (**141**) was obtained either by reaction of known *trans*-$[RhCl(CO)(PTA)_2]$ with aqueous HCl or N-chlorosuccinimide, or by room temperature reduction of $RhCl_3$ and coordination by PTA in EtOH [70]. It was characterised in solution by IR, ^1H and $^{31}P\{^1H\}$ NMR spectroscopies and ESI-MS spectrometry, and in the solid state by single crystal X-ray diffraction, showing as expected a square planar $RhCl_2P_2$ geometry. Monitoring the stepwise addition of diluted HCl to an aqueous solution of *trans*-$[RhCl(CO)(PTA)_2]$ by $^{31}P\{^1H\}$ NMR and ESI-MS techniques, the authors proposed a rationale for the formation of **141**, namely passing through steps involving $[RhCl(PTA)_4]_2$, then a mixture of $[RhCl(H_2O)(PTA)_2]$ and $[RhCl(H)(PTA)(HPTA)]$, converting into *cis*-$[RhCl_2(PTA)(HPTA)]$ and finally isomerising to **141**.

The Rh(I) complex $[Rh(CO)(PTA)_4]Cl$ (**142**) and the Rh(III) complex $[RhCl_2(PTA)_4]Cl$ (**143**) were synthesised by reaction of $[RhCl(CO)_2]_2$ or $RhCl_3{\cdot}3H_2O$ with stoichiometric amounts of PTA, respectively [71]. Reduction of **143** to **142** was also obtained under

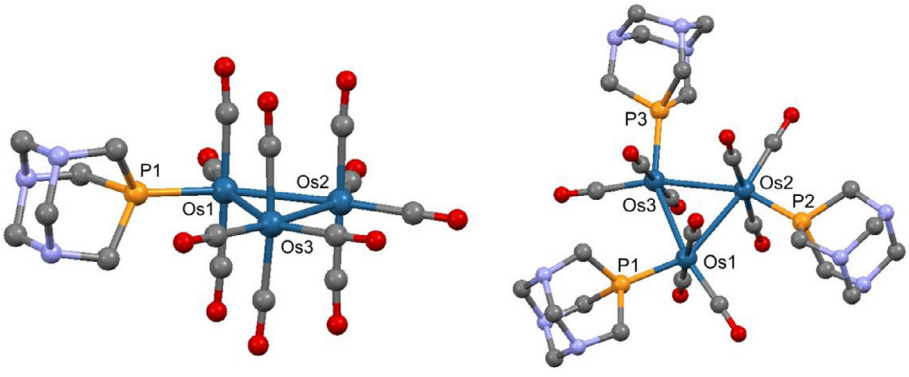

Fig. 10. X-ray crystal structures of **131a** (left) and **131c** (right). Adapted from Ref. [66]. Copyright 2016 Elsevier Science B.V.

Please cite this article in press as: A. Guerriero et al., Coordination chemistry of 1,3,5-triaza-7-phosphatricyclo[3.3.1.1]decane (PTA) and derivatives. Part III. Variations on a theme: Novel architectures, materials and applications, Coord. Chem. Rev. (2017), https://doi.org/10.1016/j.ccr.2017.09.024

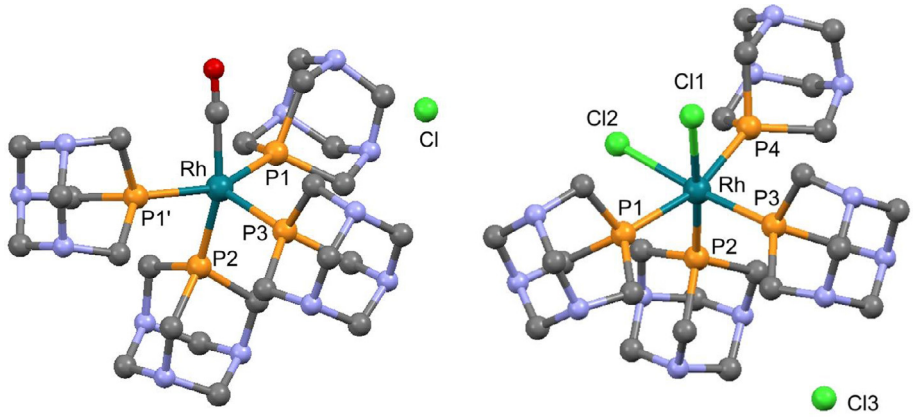

Fig. 11. X-ray crystal structures of **142** (left) and **143** (right). Adapted from Ref. [71]. Copyright 2013 The Royal Society of Chemistry.

syngas (H_2/CO = 1:1). Upon addition of $NaBH_4$ to either **142** or **143**, the hydrido species [RhH(PTA)$_4$] (**144**) was obtained. The authors reported $^{31}P\{^1H\}$ NMR patterns as unresolved broad singlets in D_2O at −56.6 ppm for **142** and at −46.0 for **143**. Complex **144** instead showed a more complex pattern with signals at −39.50 ppm (dtd, $^1J_{PRh}$ = 94.1 Hz; $^2J_{PP}$ = 23.7 Hz), −53.55 ppm (dt, $^1J_{PRh}$ = 85.2 Hz) and −53.65 ppm (dt, $^1J_{PRh}$ = 85.2 Hz). The hydrido ligand showed a ^1H NMR resonance at −11.2 ppm (ddtd, $^2J_{PH}$ = 123.0 and 25.6 Hz; $^1J_{RhH}$ = 13.6 Hz). The X-ray crystal structures of **142** and **143** are shown in Fig. 11.

Complex [RhCl(cod)(PTA-R)]PF_6 (**145**, cod = η^4-1,5-C_8H_{12}; R = *p*-^{t}Bu-$C_6H_4CH_2$) was obtained from the reaction of the Rh(I) dimer [RhCl(cod)$_2$]$_2$ with the PF_6^- analogue of ligand **21a**. The complex showed a $^{31}P\{^1H\}$ NMR doublet at −33.1 ppm ($^1J_{PRh}$ = 160 Hz) [72].

The chemistry of cyclopentadienyl rhodium(III) derivatives bearing PTA was revisited. For example, the known complexes [RhCp*Cl(PTA)$_2$]X (**146**, X = I^-, Cl^-, OTf^-, PF_6^-, BF_4^-) were shown to undergo an H/D exchange process between the methyl groups of Cp* and D_2O and that the rate depended on the coordinating ability of the counterion X^-. Kinetic studies and DFT calculations indicated that deuteration proceeds by abstraction of a proton from the methyl group of the pentamethylcyclopentadienyl ligand by a coordinated OH^- and that this process is mediated by the basic N atoms of PTA [73].

The novel water-soluble rhodium complexes [RhCp*(PTA)$_3$]Cl_2 (**147**) and [RhCp*Cl(PTA)(THP)]Cl [**148**, THP = tris(hydroxymethyl) phosphine] have been synthesised, by addition of either PTA or THP to **146**, respectively. Very high water solubilities were measured, with values of $S(H_2O)_{20°C}$ = 650 and 533 g L^{-1}, respectively [74]. Cp*M-PTA (M = Rh, Ir) type complexes bearing the *O,O*-chelating ligands curcumin (curcH) and bis-demethoxycurcumin (bdcurcH) in their deprotonated forms were obtained as [MCp*(L)(PTA)](OTf) (**149a–d**, M = Rh, Ir, L = curc, bdcurc) and tested as anticancer agents towards A2780, A2780cisR ovarian cancer cells and non-tumourigenic HEK293 hembrionic kidney cell lines, after evaluation of stability to aquation and ligand exchange under pseudo-physiological conditions. Only moderate cytotoxicity and cell selectivity were observed in all cases [75].

Examples of "upper rim" PTA derivatives coordination to Ir(I) were described [7]. Reaction of [IrCl(cod)]$_2$ with two equiv. of either PZA (PZA = phenyl-(1,3,5,-triaza-7-phosphatricyclo[3.3.1.1] dec-6-yl)methanol) or PZA–NMe_2 (**3**) in CH_2Cl_2 at room temperature gave the corresponding [IrCl(cod)(κ*P*-PZA)] (**150**) and [IrCl (cod)(κ*P*-PZA–NMe_2)] (**151**). Complex **151** was then reacted with $TlPF_6$ to give complex [IrCl(cod)(κ*P,O*-L′)] [**152**, L′ = 1-H-4-(dimethy lamino)phenyl-(1,3,5,-triaza-7-phosphatricyclo[3.3.1.1]dec-6-yl)m ethanolate]. In this compound, κ*P,O*-coordination was accompanied by deprotonation of the ligand alcohol pendant arm and protonation of one N atoms of the lower rim, as demonstrated by a combination of NMR studies and DFT calculations.

Starting from precursor [Ir(cod)$_2$](PF_6), by addition of 2 equiv. of PTA, complex [Ir(cod)(PTA)$_2$](PF_6) (**153**) was obtained. Complex **153** was anchored on two sulfonated gel-type Dowex resins, differing from the nature of the cation (Li^+ or H^+). In the first case, anchoring was obtained by electrostatic interactions through exchange of **153** with Li^+, whereas in the second case this was obtained by prior protonation of the N atoms of PTA on the Ir complex, as shown in Scheme 17 [76].

3.4. Group 10 complexes

A few novel Pd and Pt complexes bearing PTA and derivatives were reported. Pd(II) imidate complexes *trans*-[Pd(imidate)$_2$(PTA)$_2$] (**154**, imidate = succinimidate, **a**; maleidimidate, **b**; phthalimidate, **c**; saccharinate, **d**) were synthesised from reactions of PTA with the precursors *trans*-[Pd(imidate)$_2$(SMe_2)$_2$]. The products were characterised by spectroscopic techniques, showing $^{31}P\{^1H\}$ NMR singlets in the range −51.4 to −41.8 ppm and IR ν_{asym} CO stretching frequencies for the imidate ligands in the range 1675–1609 cm^{-1} [77].

Other water-soluble cyclometalated Pd–imidate complexes were obtained starting from precursors [Pd(μ-imidate)(C^N)]$_2$ where C^N are κ*C,N*-coordinated coligands such as 2-phenylpyridine and 2-benzoylpyridine and imidate are phthalimidate and saccharinate. The corresponding complexes of general formula [Pd(C^N)(imidate)(PTA)] (**155**) showed as expected a square-planar geometry around Pd with a chelate C,N ligand, a N-coordinated imidinate and PTA in mutually *cis* position, also shown in the solid-state structures obtained by single-crystal X-ray diffraction with imidate = phthalimidate [78].

Another class of palladacycle complexes bearing PTA is represented by compounds [PdCl(C^E)(PTA)] (**156**, E = N = N,N-dimethyl-1-phenylmethanamine, **a**; 1-methyl-5-phenyl-1H-benzo[e][1,4]diazepin-2(3H)-one, **b**; E = S = benzyl(methyl)sulfane, **c**). The complexes were characterised in solution and in the solid state by single-crystal X-ray diffraction. They were tested as *in vitro* cytotoxic agents on A2780/S ovarian cancer cells and evaluated as cathepsin B (cat B) inhibitors, showing however lower activities (IC_{50} cat B = 70 vs. 9.5 μM; IC_{50} A2780/S = >50 vs. <2 μM) than counterparts containing diphosphine ligands such as dppe (dppe = bis(diphenylphosphino)ethane) [79].

Mononuclear platinum-hypoxanthine complexes of the type [Pt(dmba)(PTA)(9-mhypH-N7)]ClO_4 [**157**, dmba = κ*N,C*-2-(dimethyl-

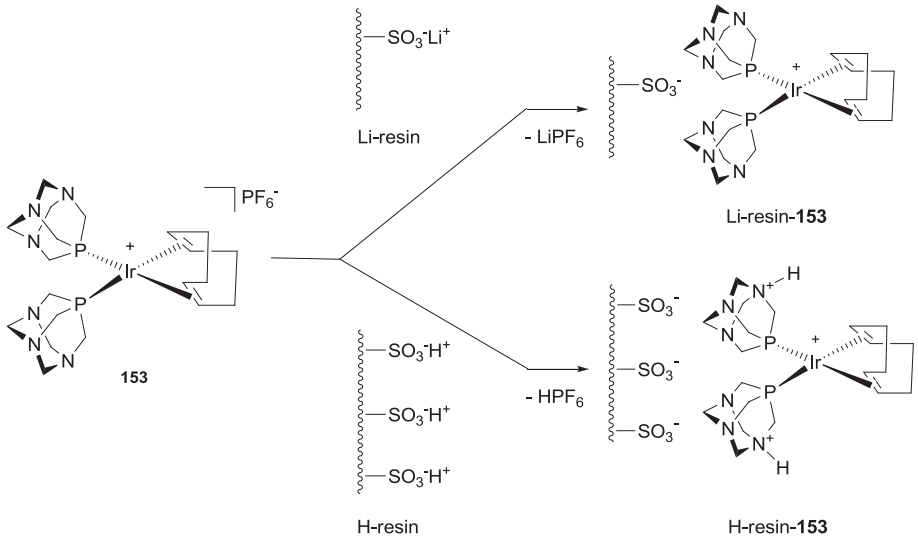

Scheme 17. Heterogenisation of **153** by ion-exchange (above) and by ion-exchange plus acid–base interaction (below).

aminomethyl)phenyl; 9-mhypH-N7 = 9-methylhypoxanthine, coordinating by N7 atom to Pt] and [Pt(dmba)(PTA)(9-mhyp-N1)] [**158**, 9-mhyp-N1 = deprotonated 9-methylhypoxanthine, coordinating by N1 atom to Pt] were obtained from precursor [Pt(dmba)(PTA)Cl]. After chloride abstraction by addition of $AgClO_4$ in acetone, the solvent complexes [M(dmba)(L)(Me_2CO)](ClO_4) (M = Pd or Pt), generated *in situ*, reacted with 1 equiv of 9-mhypH to give the cationic complexes [Pt(dmba)(PTA)(9-mhypH)](ClO_4), which gave the desired products upon deprotonation with base. Preferential hypoxanthine binding to metal, either by N1 or N7 atoms, was confirmed by DFT calculations, which results agreed with the experimentally obtained X-ray crystal structures [80]. Drawings of complexes **154**–**158** are shown in Chart 7.

Among Pd complexes bearing novel lower rim PTA derivatives, *cis*-[$PdCl_2$(PTA–Bn)$_2$]Cl_2 [**159**] was prepared reacting a suspension of *cis*-[$PdCl_2$(cod)] with 2 equiv. of (PTA–Bn)Cl in methanol overnight at room temperature. The complex showed a $^{31}P\{^1H\}$ NMR singlet at −16.98 ppm [81]. More recently, reactions of [NH_4]$_2$[$PdCl_4$] with HPTA or N-alkylated PTA salts (PTA–R)I (R = Me, **a**; Et, **b**; ^{n}Pr, **c**; ^{n}Bu, **d**) in the presence of excess KI were shown to afford the water-soluble palladium(II) complexes of type [PdI_3(PTA–R)] (**160a**–**d**) in isolated yields of 62–81% [82].

The lower rim open version of PTA, originally named PTN–Me (PTN–Me = 7-methylphospha-3-methyl-1,3,5-triazabicyclo[3.3.1]nonane), was used to coordinate in a κ*P,N* fashion to $PdCl_2$, by reaction with *cis*-[$PdCl_2$(cod)], obtaining the [$PdCl_2$(κ*P,N*-PTN–Me)] complex (**161**), showing a $^{31}P\{^1H\}$ NMR singlet at −26.6 ppm [83]. The corresponding X-ray crystal structure was also obtained. In the same article, the authors described the synthesis of the *p*-^{t}Bu analogue of a previously described lower rim PTA derivative, namely 2,4,6-tri(phenyl)-1,3,5-phosphatricyclo[3.3.1.1]decane (PTA_{R3}) and its tert-butyl analogue $PTA_{R3'}$, *i.e.* 2,4,6-tri(p-tert-butyl phenyl)-1,3,5-phosphatricyclo[3.3.1.1]decane. Both PTA_{R3} and $PTA_{R3'}$ were used as κ*P* ligands to $PdCl_2$, obtaining the novel *trans*-[$PdCl_2$(κ*P*-L)$_2$] complexes (**162**, L = PTA_{R3}, **a**; L = $PTA_{R3'}$, **b**). The $^{31}P\{^1H\}$ NMR spectrum of **162b** contained as expected a singlet resonance at −51.4 ppm in $CDCl_3$. Compound **162a** was obtained as a mixture of *cis*- and *trans*-isomers with singlets at −51.5 (*trans*-**162a**) and at −34.0 ppm (*cis*-**162a**) in $CDCl_3$. The X-ray crystal structure of **162b** is shown in Fig. 12.

Salicylaldiminato thiosemicarbazone (saltsc-R, R = H, **a**; 3-OMe, **b**; 3-^{t}Bu, **c**; 5-Cl, **d**), dianionic tridentate ligands with different substituents on 3- or 5-position, were used to coordinate Pd(II) from precursors *cis*-[$PdCl_2L_2$] (L = PPh_3, PTA, 4-picoline) in the presence of base. The resulting water-soluble complexes [Pd(saltsc-R)(PTA)] (**163a**–**d**) showed PTA coordination *trans* to the N atom of the N,S,O tridentate ligands, as demonstrated by NMR spectra and single-crystal X-ray diffraction analysis for **163c**. The complexes were tested as antimicrobial agents against *Trichomonas vaginalis*, and complex **163d** gave the best inhibition with IC_{50} = 17 μM, ca. 95% of the activity observed with FDA approved drug metronidazole [84a]. The study was extended to multimeric salicylaldimine di- and trithiosemicarbazones, showing again N,S,O tridentate ligand behaviour. In spite of the low water solubilities, especially for the dithiosemicarbazone derivatives, some activity was observed during *in vitro* tests against WHCO1 oesophageal cancer cells [84b].

Cyclometalated Pd complexes of ligand PTA═N—C(O)—2-BrC_6H_4 (**1c**) were obtained, starting from the dimeric [Pd(μ-Br){C_6H_4(C(O)N═PTA-κ*C,N*)-2}]$_2$ (**164**) obtained by oxidative addition of **1c** to [Pd_2(dba)$_3$]. Small libraries of complexes of type [Pd(L–L){C_6H_4(C(O)N═PTA-κ*C,N*)-2}] (**165**, L—L = acac, **a**; S_2CNMe_2, **b**; 4,7-diphenyl-1,10-phenanthrolinedisulfonic acid disodium salt, $C_{12}H_6N_2$($C_6H_4SO_3Na$)$_2$, **c**) and [PdBr(L){C_6H_4(C(O)N═PTA-κ*C,N*)-2}] (**166**, L = *m*TPPTS, **a**; P(3-pyridyl)$_3$, **b**; PTA, **c**) were obtained from **164** by ligand addition and cleavage of the μ-Br bridged dimer [4]. All new complexes were tested as potential anticancer agents, and their cytotoxicity properties were evaluated *in vitro* against human *Jurkat-T* acute lymphoblastic leukaemia cells, normal T-lymphocytes (PBMC), and DU-145 human prostate cancer cells. Best results were obtained with **164** and **165a**, with IC_{50} values in the range of other promising cyclopalladated compounds, and lower toxicity towards normal T-lymphocytes (PBMC).

Complex *trans*-[Pd(PTA)$_2$(N_3)$_2$] (**167**) was obtained by ligand exchange from *trans*-[Pd(PPh_3)$_2$(N_3)$_2$] in CH_2Cl_2 at room temperature. The obtained product was used as scaffold for the synthesis of tetrazolato complexes *trans*-[Pd(PTA)$_2$(N_4CR)$_2$] (**168**, R = Ph, **a**; 2-NC_5H_4, **b**; 3-NC_5H_4, **c**; 4-NC_5H_4, **d**) by reaction with the corresponding RCN organonitriles under reflux for 12 h or by microwave irradiation at 125 °C for 1 h. The reaction of **168a** with diluted HCl (0.5 M) under reflux for 1 h gave *trans*-[Pd(HPTA)$_2$$Cl_2$]$Cl_2$ (**169**) with liberation of 5-phenyl-1*H*-tetrazole, showing that this can be a convenient tool for the synthesis of substituted tetrazoles [85].

Please cite this article in press as: A. Guerriero et al., Coordination chemistry of 1,3,5-triaza-7-phosphatricyclo[3.3.1.1]decane (PTA) and derivatives. Part III. Variations on a theme: Novel architectures, materials and applications, Coord. Chem. Rev. (2017), https://doi.org/10.1016/j.ccr.2017.09.024

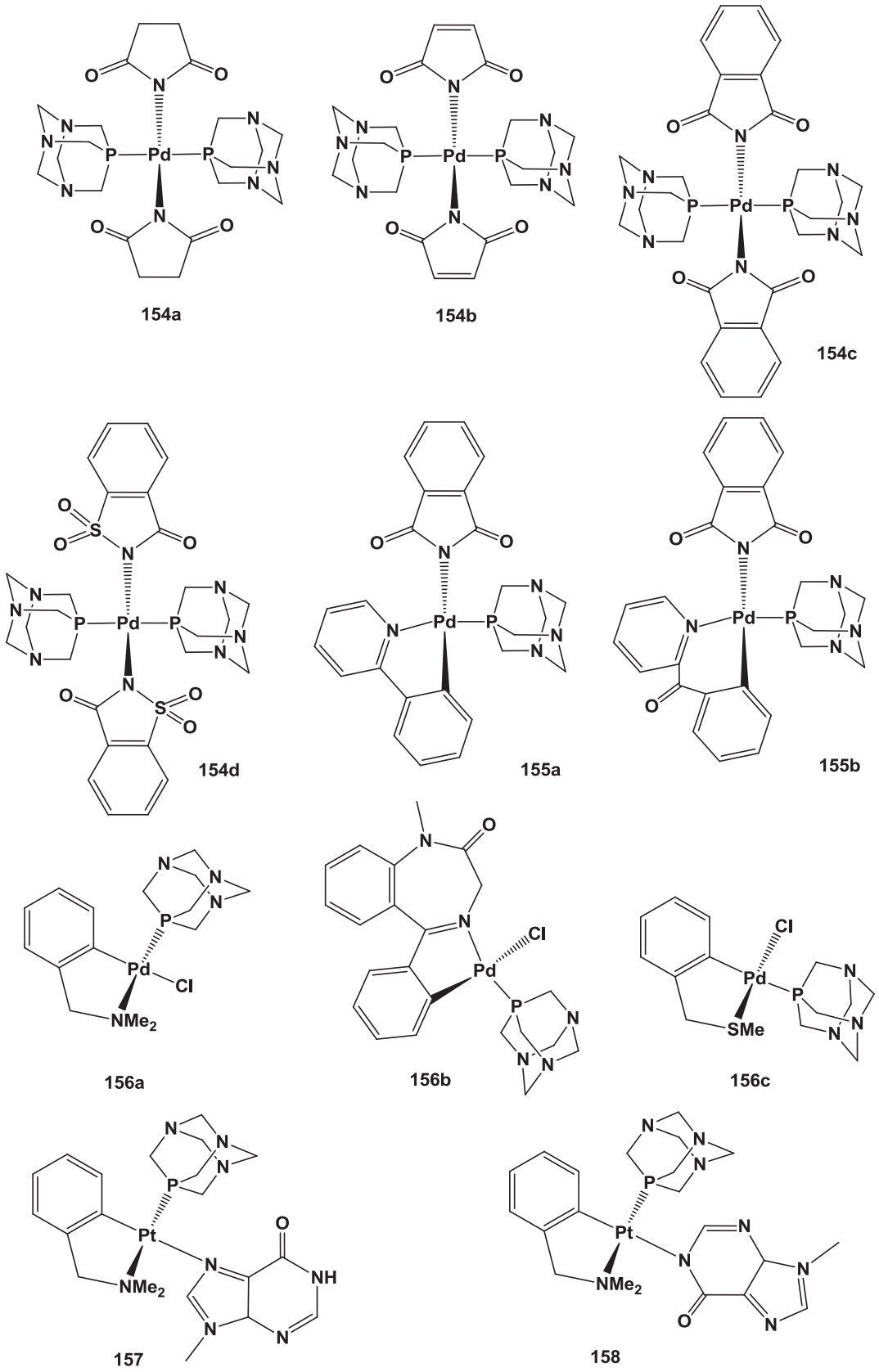

Chart 7. Pd and Pt-PTA complexes **154**–**158**.

The water soluble *cis*- and *trans*-Pt(II) and Pd(II) complexes $[MR_2(PTA)_2]$ (**170**), $[M(Me)X(PTA)_2]$ (**171**), $[Pt(Et)X(PTA)_2]$ (**172**), $[MR_2(DAPTA)_2]$ (**173**), $[MX_2(DAPTA)_2]$ (**174**) and $[M(Me)X(DAPTA)_2]$ (**175**), with M = Pt or Pd; R = Me, Et, C≡CR (R = Ph, $SiMe_3$); X = Cl, Br, I, were obtained either by ligand exchange starting from $[M(R)_2(cod)]$ or $[M(R)(X)(cod)]$, or by metathesis reactions

Please cite this article in press as: A. Guerriero et al., Coordination chemistry of 1,3,5-triaza-7-phosphatricyclo[3.3.1.1]decane (PTA) and derivatives. Part III. Variations on a theme: Novel architectures, materials and applications, Coord. Chem. Rev. (2017), https://doi.org/10.1016/j.ccr.2017.09.024

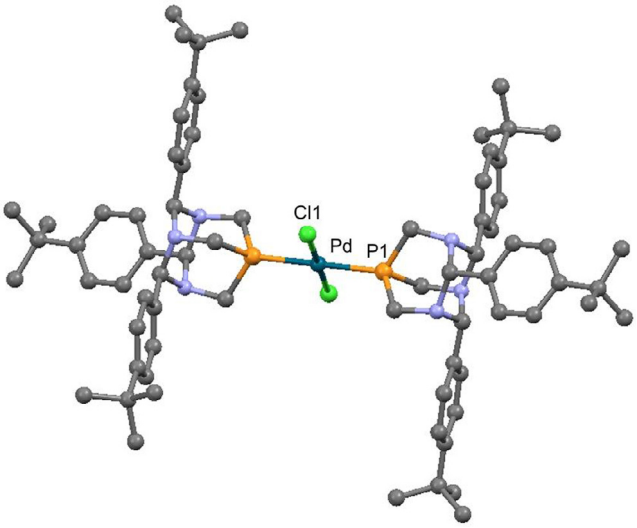

Fig. 12. X-ray crystal structure of Pd complex **162b**. Adapted from Ref. [83].

from $[MCl_2L_2]$ (L = PTA, DAPTA) in good yields (63–90%) [86]. All complexes were characterised by NMR, IR and ESI-MS techniques and for some of them the corresponding X-ray crystal structures were obtained. All of them showed lower water solubilities compared to the free water-soluble ligands, in the range 0.35–3.5 mol L^{-1} vs. 1.5 (PTA) and 7.4 mol L^{-1} (DAPTA). Later on, the same authors expanded on the scope of these synthetic reactions, to get bis-alkynyl Pt(II) and Pd(II) complexes of general formula *cis*- or *trans*-$[M(C{\equiv}CR)_2L_2]$ (**176a–p**, L = PTA or DAPTA; R = *p*-tolyl, *o*-pyridyl, *m*-pyridyl, *m*-$C_6H_4NH_2$, and CH_2Ph, see NMR data and full nomenclature in Table S1). The complexes were prepared either from $[M(C{\equiv}CR)_2(cod)]$ or $[MCl_2L_2]$ precursors by reaction either with the water soluble ligands or with the alkynes, respectively [87]. Alternative syntheses of known *cis*-$[PtCl_2(PTA)_2]$ and $[PtCl(PTA)_3]Cl$ were also proposed, by room-temperature reaction of *trans*-$[PtCl_2(\kappa S\text{-DMSO})_2]$ with 2 equiv of PTA in $MeNO_2$ and by reaction of $K_2[PtCl_4]$ with 3 equiv. of PTA in aqueous EtOH, respectively [88].

Heteroleptic complexes *cis*-$[M([9]aneS_3)(PTA)_2](PF_6)_2$ (**177**) or $[MCl([9]aneS_3)(PTA)](PF_6)$ (**178**) (M = Pt(II), **a**; Pd(II), **b**; [9]$aneS_3$ = 1,4,7-trithiacyclononane) were synthesised by reaction of $[MCl_2([9]aneS_3)]$ with either 2 or 1 equiv. of PTA and NH_4PF_6 in $MeNO_2$, respectively [89].

Complexes *cis*-$[Pt(L)(PTA)_2]$ (**179**, L = ethane-1,2-dithiolato, **a**; 3-hydroxypropane-1,2-dithiolato, **b**) and *cis*-$[Pt(L)(PPh_3)(PTA)]$ (**180**, L = 2-hydroxypropane-1,3-dithiolato) were obtained by ligand exchange from *cis*-$[PtCl_2(PTA)_2]$. The $^{31}P\{^1H\}$ NMR spectra showed a singlet at −55.3 ppm with Pt satellites ($^1J_{PPt}$ = 2554 Hz) for **179a**, and more complex AB spin systems with signals at −55.6 ($^1J_{PPt}$ = 2546 Hz, $^2J_{PP}$ = 59 Hz) and −56.3 ppm ($^1J_{PPt}$ = 2568 - Hz, $^2J_{PP}$ = 59 Hz) for **179b**, and signals at 21.5 ($^1J_{PPt}$ = 2872 Hz, $^2J_{PP}$ = 27 Hz) and −63.6 ppm ($^1J_{PPt}$ = 2442 Hz, $^2J_{PP}$ = 27 Hz) for **180**, respectively. No antiproliferative activity was observed against A2780 ovarian cancer cells [90].

The same reaction pathway and precursor were used to obtain thiocarbamato complexes *cis*-$[Pt\{SC(NR'_2){=}NC_6H_4R\}(PTA)_2](PF_6)$ (**181**, R = H, R′ = Me: **a**; R = Cl, R′ = Me: **b**; R = Cl, R′ = Et: **c**) and *cis*-$[Pt\{SC(NR){=}NC_6H_4Cl\}(PTA)_2](PF_6)$ (**182**, R = 2-pyridylpiperazine).

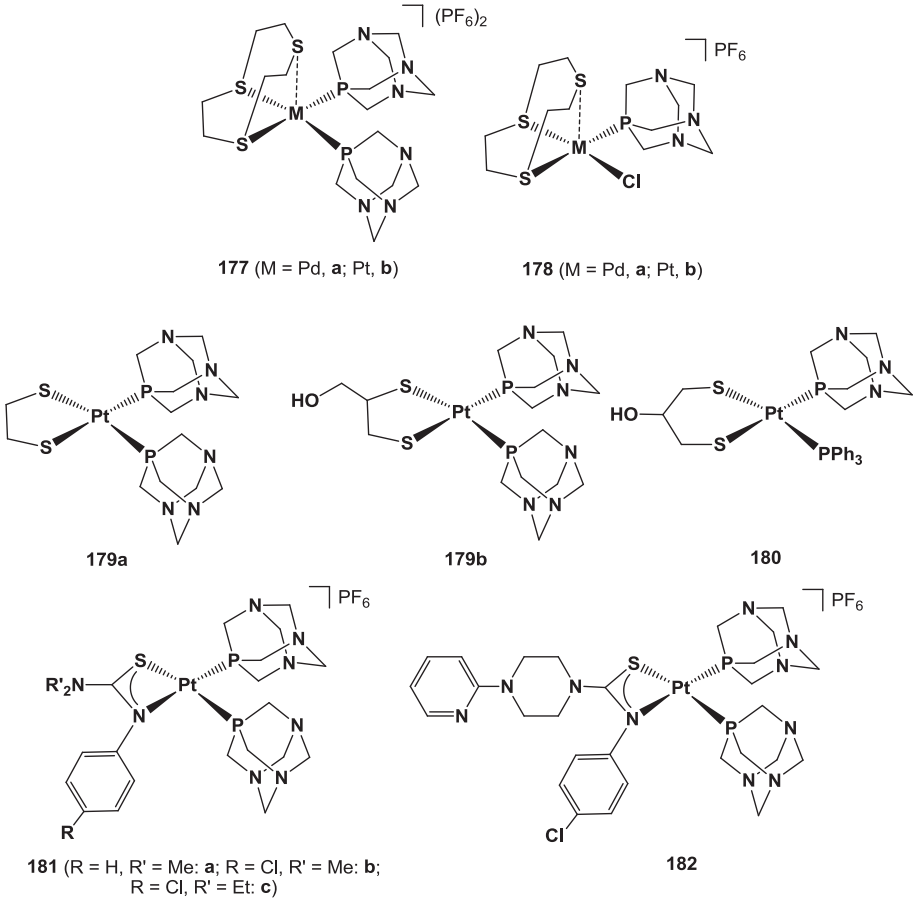

Chart 8. Pd(II) and Pt(II)-PTA complexes **177–182**.

The complexes were evaluated as *in vitro* antitumour agents in three human cancer cell lines (non-small cells lung A549, ovarian CH1, colon SW480), using the MTT assay to assess cytotoxicity. IC_{50} values showed that these complexes are by one to two orders of magnitude less active than cisplatin in A549 and SW480 cells, but have a remarkably high activity in the cisplatin-sensitive CH1 cells (IC_{50} = 0.66 μM) [91]. Drawings of complexes **177**–**182** are shown in Chart 8.

Cyclometalated analogues of the salicylaldiminato thiosemicarbazones [84] were prepared by reacting at first $K_2[PtCl_4]$ with ligand 3,4-dichloroacetophenone thiosemicarbazone, obtaining the tetranuclear species [Pt(κ*C*,*N*,*S*-3,4-dichloroacetophenone thiosemicarbazone)]$_4$ that, upon further reaction with PTA, gave the monometallic complex [Pt(κ*C*,*N*,*S*-3,4-dichloroacetophenone thiosemicarbazone)(PTA)] (**183**), with PTA trans to the N atom of the tridentate ligand. Poor antiparasitic activity of **183** was observed against *Plasmodium falciparum* strains and *T. vaginalis*, whereas good activity as antitumour agent was observed against ovarian cancer cell lines A2780 and cisplatin resistant A2780cisR (IC_{50} = 21.2 and 32 μM, respectively) [92].

Pd and Pt–PTA complexes [MCl(κ*N*,*S*-L)(PTA)] (**184a**–**h**, see Table S1 in Supporting Information) where L = 5-nitrofuryl thiosemicarbazones were synthesised from $[MCl_4]^{2-}$ salts in the presence of PTA and L. They were studied by cyclic voltammetry, ESR (electron spin resonance) spectroscopy, lipophilicity assessment and tested against *Trypanosoma cruzi*, showing in all cases activities similar to the free thiosemicarbazones, without significant differences between Pd and Pt [93].

A small library of PTA and DAPTA-type Pt(II) and Pd(II) thionate complexes *trans*-[M(SN)$_2$P$_2$] (**185**) were prepared from *cis*-[MCl$_2$P$_2$] (M = Pt, Pd; P = PTA, DAPTA) with deprotonated heterocyclic thiones *S*-*m*-methylpyrimidine-2-thione, *S*-4,6-dimethylpyrimidine-2-thione, *S*-4,6-dihydroxypyrimidine-2-thione, benzothiazole-2-thione, benzoxazole-2-thione, *S*-1,3,4,-thiadiazole-2-thione, S-4,5-H-thiazolan-2-thione, and S-pyrimidine-4(1H)-one-2-thione. Complexes **185** were tested *in vitro* against ovarian cancer cell lines A2780 and A2780cisR. All showed high inhibition of cellular growth comparable to cisplatin, up to 7-fold higher activity in cisplatin-resistant A2780cisR cell lines. X-ray crystal structures were obtained for six different complexes, all showing *trans*-geometry. In the case of bimetallic [Pd$_2$-Cl$_2$(*S*-pyrimidine-4(1*H*)-one-2-thionate)$_2$(PTA)$_2$], a Pd–Pd distance of 3.0265(14) Å was measured (Fig. 13) [94].

Natural and synthetic oestrogens have been attached to a range of different organometallic and coordination units with the aim of targeting the oestrogen receptors (ER) and achieve more efficient

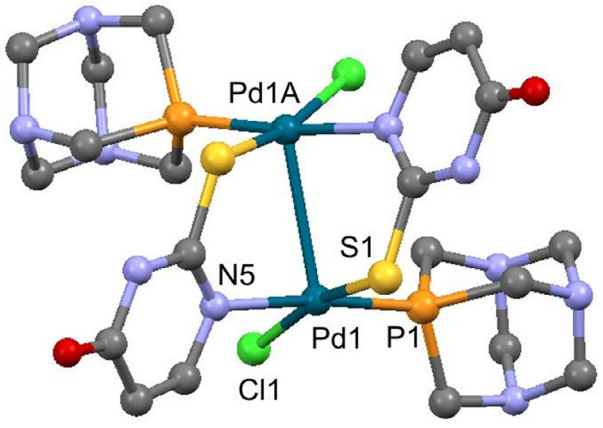

Fig. 13. X-ray crystal structure of [Pd$_2$Cl$_2$(*S*-pyrimidine-4(1*H*)-one-2-thionate)$_2$(-PTA)$_2$]. Adapted from Ref. [94]. Copyright 2013 American Chemical Society.

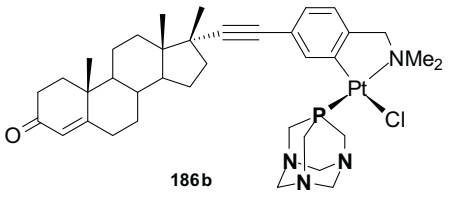

Chart 9. Complex [PtCl(ET-dmba)(PTA)] (**186b**).

Pt-based drug delivery with decreased general toxicity. Novel 17-α-[4′-ethynyldimethylbenzylamine]-17-β-testosterone (ET-dmbaH) was used to coordinate to Pt(II) precursors by C,N-chelation giving complexes [PtCl(ET-dmba) (L)] (**186**, L = DMSO, **a**; PTA, **b**). Complex **186b** was synthesised from reaction of [PtCl$_2$(DMSO)$_2$] with ET-dmbaH giving **186a**, followed by dimethyl sulfoxide exchange with PTA (Chart 9). IC_{50} values were measured for **186a**,**b** against a panel of human tumour cell lines representative of ovarian (A2780 and A2780cisR) and breast cancers (T47D). Very low resistance factors (RF) were measured at 48 h (RF = 0.9–1.5) against an A2780 cell line which has acquired resistance to cisplatin, thus proving that efficient circumvention of cisplatin resistance was obtained [95].

Pt(II) complexes bearing ligands PTA–C_2H_4OCOMe (**25**) and of PTA–CH_2COOEt were obtained as *cis*-[PtCl$_2$L$_2$]X$_2$ (**187**, X = Cl^-, PF_6^-) [14]. They showed low activity on ovarian cisplatin-resistant SKOV3 and appreciable activity towards ovarian A2780 cell lines (IC_{50} = 17–36 vs. 0.91 μM for cisplatin).

3.5. Group 11 complexes

The coordination chemistry of coinage metals to PTA was further developed, and some of the corresponding Cu, Ag and Au complexes were used as antitumour and antimicrobial agents.

Starting from [Cu(CH$_3$CN)$_4$](BF$_4$) or [Cu(CH$_3$CN)$_4$](PF$_6$) precursors, a series of Cu(I) complexes bearing PTA, HPTA and (mPTA)X (X = OTf^-, I^-) were obtained, namely [Cu(PTA)$_4$](BF$_4$) (**188**·**BF$_4$**), [Cu(HPTA)$_4$][Cl$_4$(BF$_4$)] (**189**), [Cu(mPTA)$_4$][(OTf)$_4$(BF$_4$)] (**190a**), [Cu(mPTA)$_4$][(OTf)$_2$(BF$_4$)$_3$] (**190b**), [Cu(mPTA)$_4$][(OTf)$_4$(PF$_6$)] (**190c**) and [CuI(mPTA)$_3$]I$_3$ (**191**). $^{31}P\{^1H\}$ NMR spectra showed singlets in the range −78.0 to −81.5 ppm. For some of the complexes the corresponding X-ray crystal structures were obtained, showing as expected a tetrahedral geometry around Cu(I). Tests performed with **188**, **189**, **190a**, **190c** on cisplatin-sensitive and resistant cell lines showed that against human ovarian 2008/C13 tumour cell line pair, the resistance factor was ca. 7-fold lower than that of cisplatin, whereas against human cervix cancer A431/A431-Pt cell line pair it was about 2.5-fold lower, confirming the circumvention of cisplatin resistance [96]. The study was extended to DAPTA and PTA–SO_2 (PTA–SO_2 = 2-thia-1,3,5-triaza-7-phosphatricyclo[3.3.1.1] decane-2,2-dioxide) obtaining the corresponding [CuL$_4$](BF$_4$) complexes (**192**, L = DAPTA, **a**; PTA–SO_2, **b**). The complexes showed *in vitro* antiproliferative activity against several human cancer cell lines derived from solid tumours and an anti-angiogenic activity at sub-cytotoxic concentrations. The compounds were further assessed by *in vivo* experiments in C57BL mice, on a murine model of solid tumour and on an established *in vivo* bioassay of physiological angiogenesis, showing a higher performance and lower toxicity for **192a** [97]. More recently, the same authors studied the effect of different ionic media on **188** and the related Ag analogue [Ag(PTA)$_4$]X (**193**, X = BF_4^-, PF_6^-) to establish a relationship between their stability in solution, formation equilibria and cytotoxicity, by a series of thermodynamic studies and DFT calculations. It was demonstrated that cations [Cu(PTA)$_2$]$^+$ and [Ag(PTA)]$^+$ are

the most stable species under pseudo-physiological conditions [98].

A series of heteroleptic PTA–Cu complexes bearing bidentate κ^2N-dihydrobis(pyrazolyl)borate, $[H_2B(pz)_2]^-$; dihydrobis(triazolyl)borate, $[H_2B(tz)_2]^-$; dihydrobis(3-nitro-1,2,4-triazolyl)borate, $[H_2B(tzNO_2)_2]^-$; bis(pyrazol-1-yl)methane, $CH_2(pz)_2$; tridentate $\kappa N,N,O$-bis(3,5-dimethylpyrazol-1-yl)acetate, [bdmpza]$^-$; κ^3N-tris (pyrazol-1-yl)methane, Tpm, were obtained either from CuCl or from $[Cu(CH_3CN)_4](BF_4)$ and tested against a range of tumour cell lines such as breast MCF-7, cervical A431, colon HCT-15 and LoVo, lung A549 cancer, leukaemia HL60 and melanoma A375, comparing the results of IC_{50} values with those of cisplatin. Results showed that, in general, the most efficient antitumour agents could be found among complexes having pyrazolyl ligands binding with only two out of three N atoms. The most active complex was found to be [Cu($\kappa N,N,O$-bdmpza)(PTA)] (**194**), whereas the cationic κ^3N-complexes were the least effective [99].

The reactivity of Cu(I)/Cu(II) salts with PTA and some of its derivatives brought about unexpected structural features, of importance for crystal engineering, coordination polymers syntheses and supramolecular self-assembly reactions. This was demonstrated for instance in the reaction of $Cu(NO_3)_2$ with PTA which, in the presence of either sodium azide or iodide as auxiliary ligands, gave either the coordination polymer $[Cu(\mu\text{-}N_3)(\mu{:}\kappa P,N\text{-PTA})]_n$ (**195**) or the monomeric species $[CuI(PTA)(HPTA)_2]I_2{\cdot}H_2O$ (**196**), respectively. In the absence of auxiliary ligands, complex $[Cu(PTA)_4](NO_3){\cdot}6H_2O$ (**188·NO$_3$**) was obtained. X-ray crystal structure analyses showed that in the solid state **195** is composed of a unique 1D coordination network with a $[Cu_2(\mu\text{-}N_3)_2]$ core. In the case of **196**, extensive interlikage of $[CuI(PTA)(HPTA)_2]^{2+}$ cations is brought about by intermolecular H-bonding yielding a 1D supramolecular cationic chain. Finally, **188·NO$_3$** showed a more common 3D network due to extensive O—H···N hydrogen bonding with the solvent molecules [100]. In the case of N-alkyl PTA derivatives, reaction of (PTA-R)I (R = Me, Et, ^{n}Pr) gave as expected complex **191**, the ethyl analogue $[CuI(PTA\text{–}Et)_3]I_3$ (**197**) and, rather surprisingly, a trinuclear species $[Cu_3I_2(\mu\text{-}I)(\mu_3\text{-}I)_2(PTA\text{–}{}^nPr)_2]$ (**198**), featuring the unprecedented copper iodide cluster $\{Cu_3I_2(\mu\text{-}I)(\mu_3\text{-}I)_2\}$, all endowed with tunable luminescence properties depending on the solvent, the nature of PTA ligand and the nuclearity [101]. The reaction between $Cu(NO_3)_2$, sodium azide and (mPTA)I was then investigated by the same authors, achieving the self-assembled, mixed valence tetranuclear Cu(I)/Cu(II) complex $[Cu_4I_4(\mu\text{-}N_3)_2(N_3)_4(\mu\text{-mPTA})_2(mPTA)_2]{\cdot}2H_2O$ (**199**), featuring a hexaazido dicopper(II) core $\{Cu_2(\mu\text{-}N_3)_2(N_3)_4\}^{2-}$ and two copper (I) $\{CuI_2(\mu\text{-mPTA})(mPTA)\}^+$ units (Fig. 14). Magnetic susceptibility and EPR studies showed the presence of a ferromagnetic interaction between the Cu(II) atoms through μ-azido ligands [102].

On the other hand, the unusual combination of $Cu(HCO_2)_2$ and Cu powder with PTA in MeCN gave the unexpected 1D mixed valence Cu(II)/Cu(I) coordination polymer $[Cu_3(\mu\text{-}HCO_2)_2(HCO_2)_3(\mu\text{-PTA})_3(PTA)]_n{\cdot}nH_2O$ (**200**). This polymer has bitubular 1D chains made of tetracopper $\{Cu_4(\mu\text{-}HCO_2)_4(HCO_2)_6\}^{2-}$ anions, in turn kept together by ionic interactions through the $\{\mu_3\text{-}Cu(PTA)_4\}^+$ units. Compound **200** also showed magnetic properties, in details a global antiferromagnetic exchange between the "outer" and "inner" pairs of copper atoms [103].

Even more spectacular variations on coordination typologies were observed switching from Cu to Ag. The reaction of $AgNO_3$ with PTA in the presence of a base and various arylcarboxylic acids (benzoic, Hba; 4-cyanobenzoic, Hcba; 2-aminobenzoic, Haba; terephthalic, H_2tpa) as auxiliary ligands, gave an array of different *P,N*-PTA coordination polymers such as the 1D zigzag $[Ag(ba)(\mu\text{-PTA})]_n$ (**201**), the ladder-like $[Ag(\mu\text{-cba})(\mu\text{-PTA})]_n{\cdot}5nH_2O$ (**202**), the tubular-like $[Ag(\mu\text{-aba})(\mu\text{-PTA})]_n{\cdot}3nH_2O$ (**203**) and the 2D grid-like undulating nets in $[Ag_2(\mu_4\text{-tpa})(\mu\text{-PTA})_2]_n{\cdot}2nH_2O$ (**204**). The polymers **202** and **203** act as supramolecular hosts for water molecules, which are associated by H-bonding interactions either into 2D $\{(H_2O)_{11}\}_n$ wavelike layers or discrete $(H_2O)_3$ clusters, respectively [104]. Furthermore, the first PTA-based luminescent 3D-MOFs (metal organic frameworks) of formula $[Ag_2(\mu_2\text{-bpca})(\mu_3\text{-PTA})_2]_n{\cdot}2nH_2O$ (**205**, H_2bpca = biphenyl-4,4′-dicarboxylic acid) and $[Ag_4(\mu_4\text{-pma})(\mu_2\text{-PTA})_2(\mu_3\text{-PTA})_2]_n{\cdot}8nH_2O$ (**206**, H_2-pma = pyromellitic acid) were obtained by simple change of auxiliary carboxylic acids. An interesting structural feature in **206** (Fig. 15) is the presence of PTA binding the metal in both μ_2 and μ_3-coordination modes, never observed before [105].

Further variations included the use of alkyl instead of aryl carboxylic acids. For instance, reacting Ag_2O with PTA and acids such as succinic (H_2suc), adipic (H_2adip) or malonic (H_2mal) acids gave unconventional $\kappa N,P$ or $\kappa^3N{:}\kappa P$-coordinations modes at PTA, depending on the flexibility of the ancillary ligands, resulting in the silver–organic networks $[Ag_2(\mu\text{-PTA})_2(\mu\text{-suc})]_n{\cdot}2nH_2O$ (**207**, 1D polymer), $[Ag_2(\mu\text{-PTA})_2(\mu_4\text{-adip})]_n{\cdot}2nH_2O$ (**208**, 2D polymer), and $[Ag_2(\mu_4\text{-PTA})(\mu_4\text{-mal})]_n$ (**209**, 3D polymer). All compounds showed a certain degree of activity as antimicrobial and antifungal agents against Gram-negative (*E. coli*, *P. aeruginosa*) and Gram-positive (*Staphylococcus aureus*) bacteria and yeast (*C. albicans*) [106]. Similarly, the use of substituted cyclohexanecarboxylate building blocks such as cyclohexanecarboxylic (Hchc), 1,4-cyclohexanedicarboxylic (H_2chdc), and 1,2,4,5-cyclohexanetetra carboxylic (H_4chtc) acid, gave the silver–organic 1D network $[Ag(\mu_3\text{-PTA})(chc)]_n{\cdot}n(Hchc){\cdot}2nH_2O$ (**210**), the 3D MOF $[Ag_2(\mu_3\text{-PTA})_2(\mu_2\text{-chdc})]_n{\cdot}5nH_2O$ (**211**), and the 2D polymer $[Ag_2(\mu_2\text{-PTA})_2(\mu_4\text{-}H_2chtc)]_n{\cdot}6nH_2O$ (**212**), active against the bacteria

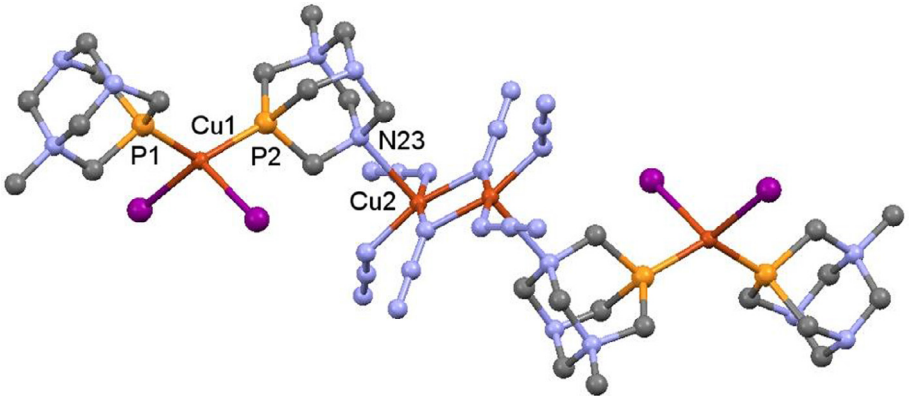

Fig. 14. X-ray crystal structure of mixed valence tetracopper complex **199**. Adapted from Ref. [102]. Copyright 2012 American Chemical Society.

Please cite this article in press as: A. Guerriero et al., Coordination chemistry of 1,3,5-triaza-7-phosphatricyclo[3.3.1.1]decane (PTA) and derivatives. Part III. Variations on a theme: Novel architectures, materials and applications, Coord. Chem. Rev. (2017), https://doi.org/10.1016/j.ccr.2017.09.024

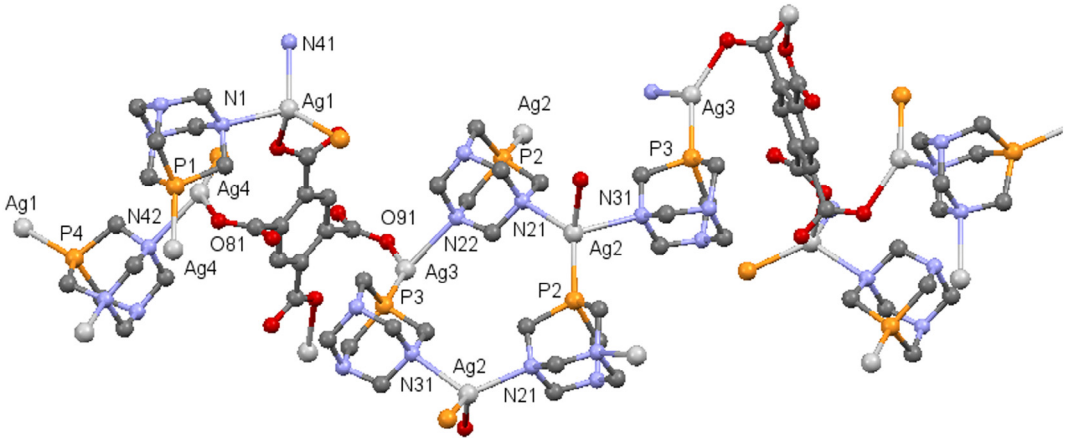

Fig. 15. X-ray crystal structure of 3D-MOF **206** core. Adapted from Ref. [105]. Copyright 2011 The Royal Society of Chemistry.

(10–18 nmol L^{-1}) and yeast (57 nmol L^{-1}) listed above [107]. Replacing these acids with substituted glutarates (3-phenylglutaric acid, H_2pga; 3,3-dimethylglutaric acid, H_2dmga) and malonate (phenylmalonic acid, H_2pma) gave $[Ag_2(\mu_2\text{-PTA})(\mu_3\text{-PTA})(\mu_2\text{-pga})(H_2O)]_n{\cdot}6H_2O$ (**213**), $[Ag_2(\mu_2\text{-PTA})(\mu_3\text{-PTA})(Hpmal)_2]_n{\cdot}2H_2O$ (**214**), and $[Ag(\mu_3\text{-PTA})(Hdmga)]_n$ (**215**), endowed with biological activities, similar to the parent compounds [108]. Other variations included the use of Ag(I) acetate or trifluoroacetate giving 1-D coordination polymers $[Ag(\mu_2{:}\kappa P,N\text{-PTA})(\mu_2{:}\kappa^2O\text{-}O_2CCH_3)]_n{\cdot}2nH_2O$ (**216**) and $[Ag(\mu_2{:}\kappa P,N\text{-PTA})(\mu_2{:}\kappa^2O\text{-}O_2CCF_3)]_n{\cdot}nH_2O$ (**217**), and reaction of Ag(I) trifluoroacetate with mPTA to achieve the coordination polymer $[Ag(mPTA)(\mu_3\text{-}O_2CCF_3{:}\kappa^2O\text{-}O_2CCF_3)(\mu_2\text{-}O_2CCF_3{:}\kappa^2O\text{-}O_2CCF_3]_n$ (**218**) [109].

Ancillary ligands other than carboxylic acids were tested for their properties in building coordinations polymers *vs.* monomeric discrete structures. Chelating diimines (N—N) such as 2,2′-bipyridine (bipy, **a**), 4,4′-di-tert-butyl-2,2′-bipyridine (dtbpy, **b**), 1,10-phenanthroline (phen, **c**), 2,9-dimethyl-1,10-phenanthroline (neocup, **d**) and 1,10-phenanthroline-5,6-dione (dione, **e**) were reacted with $AgNO_3$ and PTA to yield coordination polymers $[Ag(N\text{—}N)(\mu\text{-PTA})]_nX_n$ (**219**) and monomers $[Ag(N\text{—}N)(PTA)_2]X$ (**220**, $X = NO_3^-$, PF_6^-) endowed with antimicrobial and antiproliferative activities [110]. Tris(pyrazolyl)methanesulfonate (Tpms) was also used with Ag salts in combination with PTA and mPTA to obtain complexes active as antibacterial and antifungal agents. The pyrazolyl ligand showed different coordination modes in various cases. For instance, in complex [Ag(Tpms)(PTA)] (**221**) the Tpms ligand adopts a κ*N,N,O*-coordination mode [111], whereas κ^3N-coordination was observed for $[Ag(\kappa^3N\text{-Tpms})(mPTA)](BF_4)$ (**222**). An unusual behaviour was instead observed for the highly water-soluble $[S(H_2O)_{25°C} = 30\ g\ L^{-1}]$ complex $[Ag(mPTA)_4](Tpms)_4(BF_4)$ (**223**), where Tpms acts for the first time as non-coordinating anion [112]. Complexes **222** and **223** were studied for intercalation with calf thymus DNA by fluorescence studies. Moreover, the interaction with BSA (bovine serum albumin) was tested to assess the affinities of the complexes to proteins and the corresponding binding constants were determined. Their antimicrobial and antifungal activities towards *S. aureus*, *Enterococcus faecalis*, *P. aeruginosa*, *E. coli*, and *C. albicans* were also assessed.

Among PTA derivatives, interesting properties were observed for PTA=O and PTA=S in combination with Ag(I) salts. In the former case, self-assembly reactions with $AgNO_3$ or Ag_2SO_4 gave two distinct silver–organic frameworks $[Ag(NO_3)(\mu_3\text{-PTA=O})]_n$ (**224**) and $[Ag_2(\mu_2\text{-}SO_4)(\mu_5\text{-PTA=O})(H_2O)]_n$ (**225**), respectively. Single-crystal X-ray diffraction data showed the formation of infinite 3D non-interpenetrating networks driven by multiply bridging PTA=O spacers that adopt unprecedented N_2O- or N_3O-coordination modes (Fig. 16) [113]. Both compounds exhibited high antibacterial and antifungal activities against Gram-negative *E. coli* and *P. aeruginosa*, and Gram-positive *S. aureus* bacteria, as well as *C. albicans* fungi.

In the case of PTA=S, silver–organic frameworks $[Ag(\mu_3\text{-PTA=S})]_n(NO_3)_n{\cdot}nH_2O$ (**226**) and $[Ag_4(\mu_4\text{-PTA=S})(\mu_5\text{-PTA=S})(\mu_2\text{-}SO_4)_2(H_2O)_2]_n{\cdot}2nH_2O$ (**227**) were obtained, and X-ray crystal structure analysis revealed unprecedented N_2S-coordination modes of PTA=S [114].

The number of articles describing the synthesis of novel Au–PTA complexes and their use in medicinal inorganic chemistry has

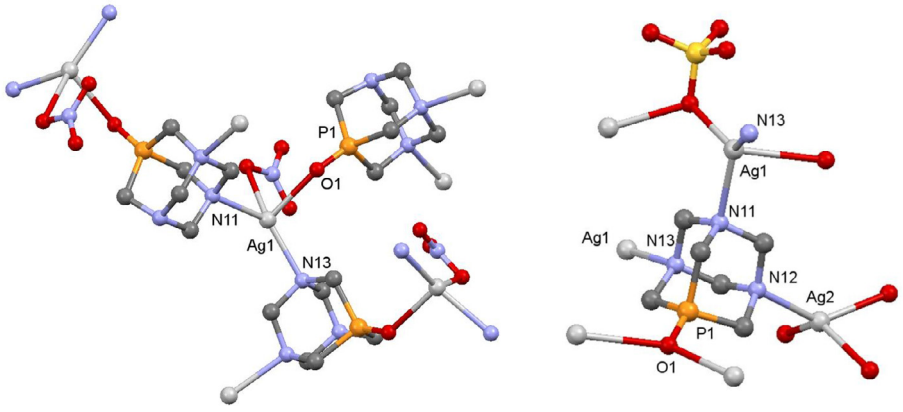

Fig. 16. X-ray crystal structures of **224** and **225** cores. Adapted from Ref. [113]. Copyright 2011 American Chemical Society.

grown in recent years and has been already reviewed [115]. Apart from other reports on this specific application [116], a few more examples will be summarised here.

Ligand exchange from [AuCl(tht)] (tht = tetrahydrothiophene) in the presence of PTA N-derivatives **20** and **22a**,**b** gave the corresponding κ*P*–Au(I) complexes [AuCl(L)]X (**228**, L = **20**, **22a**, **22b**; X = Br^-, OTf^-), characterised by $^{31}P\{^1H\}$ NMR singlets at ca. −31.5 ppm [11]. The synthetic scope was further expanded by the same authors, for instance by halide metathesis to obtain the corresponding [AuBr(L)]Br (**229**), by use of Au precursor [Au(C_6F_5)(tht)] giving [Au(C_6F_5)(L)]Br (**230**), or by addition of another equivalent of ligand L to **228** to obtain the bis(phosphine) derivatives [$AuClL_2$]Br_2 (**231**). X-ray crystal structure analysis of [AuBr(PTA–Bn)]Br showed that the asymmetric unit consisted of two symmetry-related Au molecules, leading to a crossed structure with a short Au…Au interaction of 2.8439(11) Å [117]. The complexes were tested for luminescence and antiproliferative properties against ovarian cancer cell lines A2780 and A2780cisR. All Au complexes showed better activities than cisplatin and, in particular, complex [AuCl(PTA–Bn)]Cl (**228a**–**Cl**) showed IC_{50} values 11 times lower than cisplatin for cell line A2780. Further developments were disclosed later on by the same group, with the synthesis of thiolato derivatives [Au(SR)(PTA–R)]Br (**232**, PTA–R = PTA–Bn, PTA–CH_2CO_2Me; SR = pyridine-2-thiolate, Spy; pyrimidine-2-thiolate, Spyrim; 4-methylpyrimidine-2-thiolate, Smepyrim; 4,6-dimethylpyrimidine-2-thiolate, SMe_2pyrim) by ligand exchange from the corresponding bromide precursors. The complexes were tested for their cytotoxicity properties against human colon cancer cell lines Caco-2 and Caco-2/TC7 and compared to cisplatin and auranofin. It was observed that complexes bearing (PTA–Bn)Br as ligand were the most effective in inducing cell apoptosis, in particular the one with Spyrim as ancillary ligand [118].

The luminesce properties of Au(PTA)-type systems have been investigated by various research groups. Polymer [Au(C≡C–C_5H_4N)(κ*P*-PTA)]$_n$ (**233**) belongs to the class of low molecular weight gelators (LMWGs) and showed a gel structure composed of very long fibres. It is characterised by head-to-head 1D chains based on π–π interactions between the Au–C≡C-py units, which in turn favoured aurophilic interactions in water. The compound displayed luminescence by excitation at 280 nm at room temperature, yielding an emission band at 420 nm, or excitation at 320 nm at 77 K, in turn giving a new broad emission band at ca. 500 nm [119]. The study was then extended to DAPTA gold complexes bearing coumarin-based coligand, namely [Au(7-prop-2-in-1-yloxy)-1-benzopyran-2-one)(DAPTA)] (**234**), shown in Chart 10. In this case, the fibres showed strong blue luminescence with a broad emission band centred at 350–380 nm due to the coumarin emission. Fluorescence microscopy revealed the presence of luminescent fibre-like structures at millimolar concentrations. While strong blue emission (bandpass filter at 300–400 nm, corresponding to the fluorescence of the coumarin) was only observed in isolated fibres, green emission (bandpass filter at 450–490 nm, derived from coumarin phosphorescence) was observed throughout the bulk of the reticulated network of fibres. The authors suggest that this phenomenon may be related to increased intersystem crossing at high concentrations in water solution [120]. In aqueous media, aurophilic, π–π interactions and hydrogen bonding all contribute to fibre formation, as shown by single-crystal X-ray diffraction.

A rather striking difference in the morphologies resulting from supramolecular assemblies was observed upon subtle changes in the pyridyl structure and using positively charged $(mPTA)^+$. Complexes [Au(C≡C–C_5H_4N)(mPTA)]X (**235**, X = I, **a**; X = OTf, **b**), [Au(C≡C–$C_5H_4NCH_3$)(PTA)]X (**236**, X = I, **a**; X = OTf, **b**) and [Au(C≡C–$C_5H_4NCH_3$)(DAPTA)]X (**237**, X = I, **a**; X = OTf, **b**) showed structures ranging from rod-like (**235a**) to vesicles (**236a** and **237a**) and square-like assemblies (**236b** and **237b**). Solvent effects were also observed to influence aggregation and luminescence properties [121].

Finally, a rather spectacular behaviour of CAP and derivatives toward gold was observed. $(CAP\text{-}H_3)Cl_3$ was able to reduce $AuCl_4^-$ to Au(0) giving in turn CAP=O. CAP was observed to promote oxidation of nanocrystalline gold(0) with formation of [Au(CAP–H_2)$_3$]Cl_7 (**238**), and finally to displace cyanide from K[Au($CN)_2$] to give the $[Au(CAP)_3]^+$ cation [18].

3.6. Group 12 complexes

A few examples of Group 12 coordination compounds bearing PTA and derivatives were reported. Reaction of $ZnCl_2$ with PTA=O and 1,10-phenathrolin-5,6-dione (dione) in the presence of $NaBF_4$ gave [ZnCl(dione)(κ*O*-PTA=O)](BF_4) (**239**) which was endowed with high cytotoxic activity against human colorectal (HCT116) hepatocellular (HepG2) and breast (MCF-7) cancer cell lines [69]. PTA=O and PTA=S were used to obtain monomeric and polymeric species [$ZnCl_2$(κ*O*-PTA=O)(H_2O)] (**240**), [$ZnCl_2$(μ-PTA=O)]$_n$ (**241**), [$CdCl_2$(κ*O*-PTA=O)(H_2O)] (**242**), [$CdBr_2$(κ*O*-PTA=O)(H_2O)] (**243**), [CdI_2(κ*O*-PTA=O)(μ-PTA=O)] (**244**), [$HgCl_2$(μ-PTA=O)]$_n$ (**245**), [$CdCl_2$(κ*S*-PTA=S)(CH_3OH)]$_n$ (**246**) and the unusual [$ZnCl_2$(-HPTA=S){(PTA=S)$ZnCl_3$}] (**247**, Fig. 17), depending on reaction conditions, starting from the corresponding metal dichloride precursors. X-ray analysis could elucidate the different coordination modes of the water-soluble ligands in each case, often involving both O (or S) and N atoms of the PTA lower rim [122].

A library of self-assembled Zn(salphen)-type supramolecular complexes bearing PTA was obtained by reacting a series of differently substituted Zn(R-salphen)$_2$ complexes (R-salphen = substituted *N*,*N*′-bis(salilcylidene)imine-1,2-phenylene diamine, Chart 11) with PTA. It was observed that 2 up to 3 Zn units were kept together by PTA by available N-coordination to the metal, giving namely [{Zn(R-salphen)$_2$}$_2$(κ^2*N*-PTA)] (**248a**,

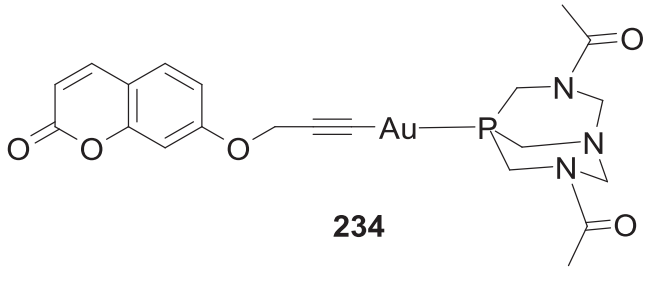

Chart 10. Complex [Au(7-prop-2-in-1-yloxy)-1-benzopyran-2-one)(DAPTA)] (**234**).

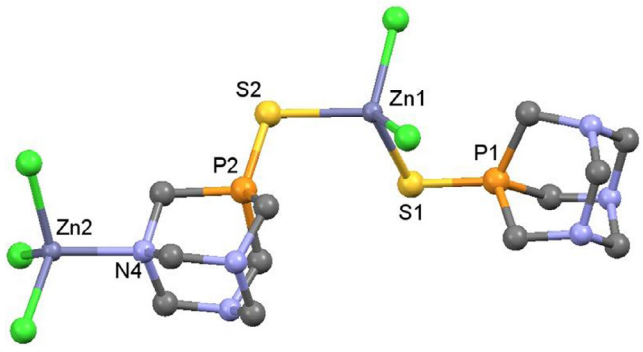

Fig. 17. X-ray crystal structure of **247**. Adapted from Ref. [122]. Copyright 2010 Elsevier Science B.V.

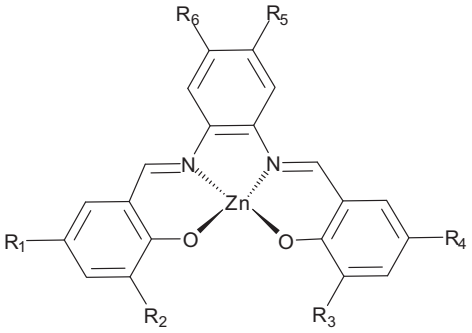

$R_1 = R_2 = R_3 = R_4 = tBu$; $R_5 = R_6 = H$
$R_1 = R_4 = R_5 = R_6 = H$; $R_2 = R_3 = tBu$
$R_2 = R_3 = R_5 = tBu$; $R_1 = R_4 = R_6 = H$
$R_2 = R_3 = tBu$; $R_1 = R_4 = H$; $R_5 = R_6 = Cl$
$R_1 = R_2 = R_3 = tBu$; $R_4 = R_5 = R_6 = H$
$R_1 = R_2 = F$; $R_3 = tBu$; $R_4 = R_5 = R_6 = H$
$R_2 = NO_2$; $R_3 = tBu$; $R_1 = R_4 = R_5 = R_6 = H$

Chart 11. Zn complexes bearing substituted salphen-type ligands [123].

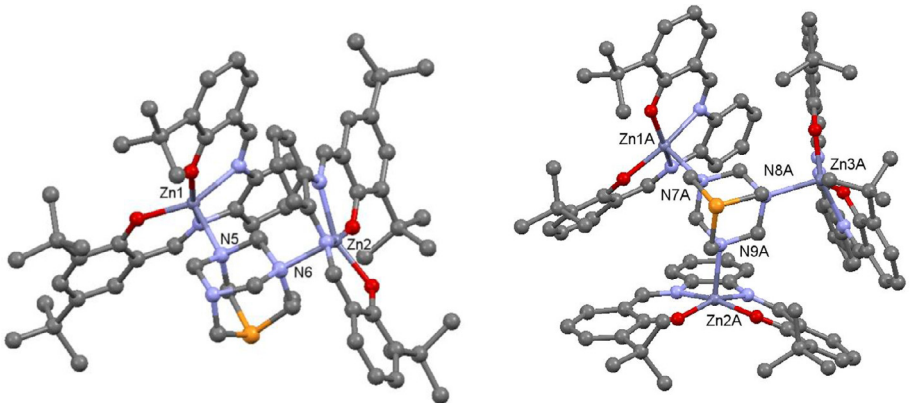

Fig. 18. X-ray crystal structures of **248a** and **248b**. Adapted from Ref. [123]. Copyright 2013 The Royal Society of Chemistry.

R = 3,4-^{t}Bu$_2$) or [{Zn(R-salphen)$_2$}$_3$(κ^3*N*-PTA)] (**248b**, R = 3,4-^{t}Bu$_2$). The nature of substituents on the salphen-type ligand influenced the bulkiness and flexibility of the Zn(R-salphen)$_2$ moieties (Fig. 18), and in general, a preference was observed for a Zn:PTA = 2:1 stoichiometry [123].

Reaction of the cluster complex [Re$_6$(μ_3-Se)$_8$(PEt$_3$)$_5$(PTA)](SbF$_6$)$_2$ with HgI$_2$ in MeCN/MeOH gave two distinct products depending on the reaction time and conditions. At room temperature after 5 min, complex [{Re$_6$(μ_3-Se)$_8$(PEt$_3$)$_5$(PTA)}$_2$(Hg$_4$I$_9$)](SbF$_6$)$_3$·2MeCN (**249**) was obtained. On the other hand, running the reaction for 30 min under reflux, gave instead the chain-like product [{Re$_6$(μ_3-Se)$_8$(PEt$_3$)$_5$(PTA)}$_2$(Hg$_3$I$_7$)(SbF$_6$)]$_n$·(MeCN)$_n$ (**250**), where the Re atom is κ*P*-coordinated and three HgI$_3$ units are coordinated to PTA in a κ:μ_3-*N*$_3$ fashion [124].

4. Selected applications of complexes of PTA and derivatives in catalysis

4.1. Organonitrile hydration reactions

Catalytic nitrile hydration to amides (Eq. (1)) is an atom-efficient process of potential interest as amides are versatile intermediates in synthetic chemistry including pharmaceuticals, polymers, detergents, lubricants etc.

$$R\text{-}C{\equiv}N + H_2O \rightarrow R\text{-}C(O)NH_2 \quad (1)$$

Metal-mediated nitrile activation and addition of H$_2$O to the C≡N bond obviates the need for strong bases or acids and harsh conditions that reduce the scope of the reactions due to functional group sensitivity. Some Ru–PTA complexes were demonstrated to be active catalysts for this class of reactions in water phase or biphasic conditions. Complexes [RuCl$_2$(η^3:η^3-C$_{10}$H$_{16}$)(L)] (**111**, L = PTA, **a**; (PTA–Bn)Cl, **b**; DAPTA, **c**, Fig. 7) were used (5 mol%) for the hydration of benzonitrile to benzamide at 100 °C, reaching 94–97% yields and 100% selectivities after 24 h, a lower activity if compared to the corresponding RAPTA-type complexes [56].

Nano-RAPTA complexes were obtained by tethering [PTA—(CH$_2$)$_3$—Si(OMe)$_3$]I to Fe$_3$O$_4$ magnetic nanoparticles, then using this material to coordinate to [RuCl$_2$(p-cymene)] moiety. The so-obtained heterogeneous catalysts, which could be recovered from the reaction solution at the end of the runs by application of an external magnetic field, gave excellent results in the hydration of a large family of variously substituted aryl and alkyl nitriles using 1.58 mol% Ru in neat water at 150 °C under microwave irradiation, with the possibility to recycle the catalyst for consecutive runs. Yields ranging from 75% to 99% were obtained, with reaction time from 0.5 to 16 h. The dicyano-derivatives were also tested with good results, yielding either the corresponding monoamides or diamides depending on reaction time [125].

The long-known air-stable complex [RuCl$_2$(PTA)$_4$] (**125**) was applied as catalyst for nitrile hydration, with a good substrate scope. All nitriles were converted with 67–99% conversions after 7 h and >99% after 24 h, using 5 mol% of catalyst at 100 °C in neat water, with best efficiency observed for aryl substrates containing electron-withdrawing groups. Catalyst loadings as low as 0.001 mol% could be used in the hydration of benzonitrile, reaching TON >22,000 (TON = turnover number). However, under these conditions the reactions were low-yielding (max 22%) and extremely sluggish (ca. 2300 h, TOF = 9.5 h^{-1}). Excellent recyclability was observed, with quantitative benzonitrile conversions after 7 consecutive runs. Biphasic water/t-amyl alcohol conditions were also successfully tested, with good activity and recyclability [126]. Ligand variations were explored, showing that with catalysts obtained *in situ* either from [RuCl$_2$(κ*S*-DMSO)$_4$] and (PTA–Bn)Cl in 3:1 ratio, or using [RuCl$_2$(p-cymene)]$_2$ and (PTA–Bn)Cl in 6:1

ratio, 16 aromatic and aliphatic nitriles were hydrated to the corresponding amides in 92–99% conversions in refluxing water after only 1 h [127]. The $[RuCl_2(\kappa S\text{-DMSO})_4]$/(PTA–Bn)Cl system was also able to bring about the hydration of glycosyl cyanides to C-glycosyl formamides in water or water/N-methylpyrrolidone with good functional group tolerance and conversions [128].

Complexes $[RuCl_2(\eta^6\text{-toluene})(\kappa P\text{-PTA—P}^i\text{Pr}_2)]$ **108** [10] and $[RuCl(\eta^6\text{-toluene})(\kappa P,N\text{-PTA—CR}^1\text{R}^2\text{NHPh})]Cl$ (R^1 = H, R^2 = Ph, **105a**; R^1 = H, R^2 = *p*-C_6H_4OMe, **106a**; R^1 = R^2 = Ph, **107a**, Scheme 16) [9] also showed activity in nitrile hydration. The former (5 mol%) brought about the catalytic hydration of various nitriles to amides at 43–99% conversions in the air at 100 °C. A slightly higher efficiency than for the κ^2P-derivative **109** was observed, suggesting that chelation did not allow for the (reversible) hemilabile behaviour needed to free a coordination site on the metal for substrate activation. Complexes **105**–**107** showed to be active in catalysis, with benzonitrile conversions ranging from 53% to 95%, respectively. Complex **107** proved to be the most active, with the best performance (TON = 97,000, TOF = 285 h^{-1}) achieved using 0.001 mol% of catalyst. A catalyst scope study was also performed and a small library of aryl and alkyl nitriles was converted to the corresponding amides in yields in the range 51–85% using 5 mol % of **107**.

Ag-PTA nanoparticles (AgNPs) of average diameter of 3.5 nm were synthesised and tested as catalysts for aryl nitrile hydrations, however it was established that their role was merely of precursors for the catalytically active molecular species, which the authors suggest to be $[Ag(CN)_2]^-$ [129].

4.2. Hydrogenation and transfer hydrogenation reactions

Hydrogenation of unsaturated C=C, C=O and C=N groups in a variety of organic substrates were reported using novel PTA-based complexes, both under a hydrogen pressure and using transfer hydrogenation conditions. The iridium complexes [IrCl(cod)(κP-L)] (**150**, L = PZA; **151**, L = PZA-NMe_2) bearing upper rim PTA derivatives were used as catalysts for the reduction of α,β-unsaturated substrates such as cinnamaldehyde (CNA), benzylidene acetone (BZA), 2-cyclohexen-1-one and for acetophenone. For CNA, high conversions and selectivities to cinnamol (C=O bond reduction) were observed using HCO_2Na/H_2O/MeOH as transfer hydrogenation protocol ([H] in Eq. (2)) at 40 °C, however further studies demonstrated that the catalytic activity was partially due to colloidal or nanosized Ir particles formed during the reactions.

$$Ph(CH{=}CH)CHO + [H] \rightarrow Ph(CH{=}CH)CH_2OH + Ph(CH_2CH_2)CHO + Ph(CH_2CH_2)CH_2OH \quad (2)$$

As an example of cyclic substrates, 2-cyclohexen-1-one was reduced essentially at the C=C double bond under the same conditions to give cyclohexanone, whereas more forcing reductants (KOH/^{i}PrOH) gave higher selectivity to the fully hydrogenated product (cyclohexanol) after 24 h at 80 °C. Acetophenone was reduced efficiently to 2-phenylethanol with the latter method, with yields in the range 84–94%. Using instead ^{t}BuOK/^{i}PrOH and H_2 (30 bar), acetophenone was reduced in up to 94.1% yield after 6 h at room temperature [7]. At higher temperature and shorter reaction times (60 °C, 4 h), the same substrate was quantitatively reduced using the latter protocol, in the presence of the ruthenium imidazolyl–PTA complex [RuCl(p-cymene)($\kappa P,N$-L)]Cl (**103a**, L = 1-methylimidazolyl-(1,3,5-triaza-7-phosphatricyclo[3.3.1.$1^{3,7}$]dec-6-yl)methanol, Scheme 15) [8].

The heterogeneous Ir catalyst **H-resin-153**, obtained by immobilisation of $[Ir(cod)(HPTA)_2]^{3+}$ on a Dowex resin (Scheme 17), was particularly effective for C=N bond reduction for a small library of aromatic imines in neat water at 80 °C under H_2 pressure (20 bar), with negligible metal leaching and good recyclability (Scheme 18) [76].

Water-phase hydrogenation of a small library of allylic alcohols was achieved under H_2 pressure (20 bar) and mild temperature (30 °C) using a self-assembled supramolecular Rh(I) catalyst obtained from the interaction of [RhCl(cod)(PTA—R)](PF_6) (**145**, R = *p*-^{t}Bu-$C_6H_4CH_2$) with mono-amino-β-cyclodextrin, and the importance of first and second sphere ligands for this target reaction was demonstrated [72]. Catalytic hydrogenation-dehydration of levulinic acid to γ-valerolactone was demonstrated, albeit at low conversion (34%) and selectivity (14%), using a combination of $[Ru(acac)_3]$ and PTA in water at 140 °C and 50 bar of H_2. The poor performance was attributed to the lack of proper steric and electronic properties in PTA, if compared to higher performances obtained using the more bulky, less basic TPPTS ligand [130].

PTA-stabilised Ru and Pt nanoparticles were obtained by established reduction methods from the corresponding organometallic precursors in the presence of PTA. Under hydrogen at 70 °C in THF, stable and very small MNPs (1.3 nm, Ru; 0.9 nm, Pt) were obtained [131]. These were tested as aqueous biphasic hydrogenation catalysts for simple olefins and aromatic substrates, under hydrogen pressures in the range 1–10 bar and at room temperature. Very high conversions to alkanes were observed using catalysts with 1.0 mol% of metal content, but long reaction times (up to 16 h) were usually needed to fully reduce aromatic rings in substrates such as toluene and *m*-methylanisole [132].

PTA and (mPTA)I were also used to stabilise Pd nanoparticles of size 2.8–3.5 nm obtained from Pd@TOAB precursors (TOAB = tetraoctylammonium bromide) by exchange with the

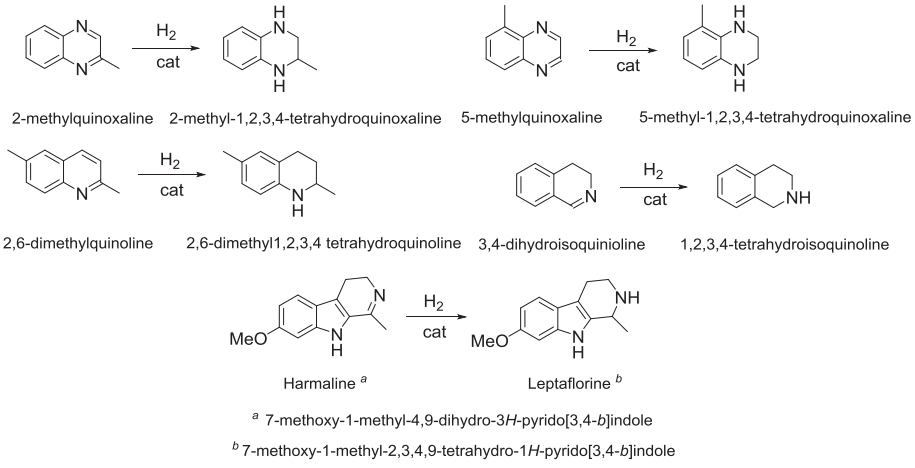

[a] 7-methoxy-1-methyl-4,9-dihydro-3*H*-pyrido[3,4-*b*]indole

[b] 7-methoxy-1-methyl-2,3,4,9-tetrahydro-1*H*-pyrido[3,4-*b*]indole

Scheme 18. Imines to amines hydrogenation using the immobilised Ir(I) catalyst **H-resin–153** [76].

water-soluble ligands. The Pd@PTA nanoparticles obtained were tested as catalysts for selective C=C and C≡C bond reduction under biphasic conditions at room temperature, using hydrogen pressures in the range 1–10 bar. Excellent recyclability of the catalyst confined in the water phase was demonstrated, with up to 9 consecutive runs for the hydrogenation of 1-dodecene, virtually without any loss of activity [133].

C=C double bond reductions of allylic substrates were also accomplished using Re-catalysed (complex **35**, Chart 3) transfer hydrogenation by alcoholysis of amine–borane adducts, obtaining excellent yields at 70 °C in ^{i}PrOH and in the presence of ^{t}BuOK as base (TOFs up to 396 h^{-1} for the reduction of allylcyclohexane) [25a].

Complex $[RuCl_2(PTA)_4]$ (**125**) recently found application as catalyst for the direct hydrogenation of CO_2 to HCOOH using hydrogen, an important reaction for CO_2 utilisation and hydrogen storage, in aqueous phase and in DMSO without any additives. In water, at 40 °C, 0.2 M formic acid solutions were obtained using a total pressure of 200 bar. Further optimisation showed that a maximum TON = 159 was obtained at 60 °C using a pressure of 100 bar of CO_2/H_2 mixture (1:1). Other solvents were tested, and in pure DMSO at 50 °C, a 1.93 M formic acid solution was obtained using a pressure of 100 bar of CO_2/H_2 mixture (1:1), with TON = 635 after 120 h [134].

4.3. Hydroformylation and hydrosilylation reactions

A thermocontrolled long-chain terminal alkene hydroformylation catalytic system was obtained by supramolecular interaction of β-cyclodextrins with $[Rh(acac)(CO)_2]$ and ligands (PTA–Bn)Cl and **21a** (Scheme 7). Both ligands gave high conversions and chemoselectivities to aldehydes using 1-decene, 1-dodecene and 1-tetradecene as substrates, with linear to branched (l/b) ratios of ca. 2 at 100–120 °C under H_2/CO = 50 bar in water. The advantage of the cyclodextrin/**21a** couple was the rapid decantation of the biphasic system after the reaction, allowing for efficient product separation, catalyst recovery and recycle (Scheme 19) [12].

The Ru–arene complex $[RuCl_2(\eta^6\text{-arene})(PTA)]$ (**251**, arene = $C_6H_5OCH_2CH_2OH$) was tested as catalyst for 1-octene hydroformylation at 125 °C under H_2/CO = 50 bar in water. Although good conversions were reached (83%), high chemoselectivity to isomerised alkene (83.74%) was observed, with 6% selectivity to aldehydes and 10.19% selectivity to alcohol, respectively. This was attributed to the high basicity of the ligand, favouring Ru-catalysed isomerisation–hydrogenation *vs.* hydroformylation [135].

Hydrosilylation of 1-hexene was tested in the presence of the supramolecular self-assembled $Zn(salphen)_2$/PTA complexes **248a**,**b** (Fig. 18) and $[RhCl(C_2H_4)_2]_2$ using $PhMe_2SiH$ at room temperature for 1 h reaction time. The highest conversions and yields were obtained using a ratio $Zn(salphen)_2$/PTA = 3. It was observed that conversions as high as 79% were obtained with ratios Rh/Zn/PTA = 1:2:6 and comparable values (74%) were obtained with ratios Rh/Zn/PTA = 1:4:12, suggesting that even in the presence of an excess of the supramolecular bulky phosphine-based system, active Rh(I) catalysts are formed. The authors concluded that the supramolecular *in situ* formation of bulky phosphines may be useful as an alternative for covalent phosphines for Rh(I)-catalysed olefin hydrosilylation reactions [123].

4.4. Allylic alcohol isomerisation reactions

Catalytic allyl alcohol isomerisation was investigated in the presence of water-soluble complexes, mainly Ru-based, as a useful and atom-efficient reaction to obtain the corresponding ket-2-ones. Reaction of precursor *cis*-$[RuCl_2(\kappa S\text{-DMSO})_3(\kappa O\text{-DMSO})]$ with 2 equiv. of PTA, (mPTA)(OTf) or (PTA–Bn)Cl gave *cis*,*cis*,*trans*-$[RuCl_2(\kappa S\text{-DMSO})_2(L)_2]^{n+}X^{n-}$ complexes (n = 0, L = PTA; n = 2, L = mPTA, PTA–Bn; X = Cl, OTf) which were tested as catalysts for isomerisation of a small library of allylic alcohols CH=CHCH(OH)R (R = CH_3, C_2H_4, C_3H_7, C_4H_9, C_5H_{11}), both under a hydrogen atmosphere and using HCO_2Na (50 equiv. to Ru) as reductant in neat water at 80 °C for 1h. It was observed that for all the Ru–phosphine complexes the activities were lower than for the phosphine-free Ru precursor, although good selectivity to ketone formation was observed in all cases [136].

Deeper insights on pH effects in catalysis were obtained by testing complexes $[RuCpCl(mPTA)_2](OTf)_2$ and $[RuCp(H_2O)(mPTA)_2](OTf)_3\cdot(H_2O)(C_4H_{10}O)_{0.5}$ (**252**) for the conversion of a series of alk-1-en-3-ols to the corresponding ketones in aqueous solutions or in biphasic systems at 80 °C. Conversions at different pH values were monitored over time, showing that in phosphate buffer the highest values were obtained at ca. pH = 4.75. In the case of **252**, at this pH the activity was lower and kept decreasing with increasing pH. By a combination of kinetic and NMR measurements, the authors concluded that $H_2PO_4^-$ and HPO_4^{2-} anions strongly interacted with the cationic complexes, in turn causing a severe drop in activity in the pH range 5–7 [137]. These observations were also confirmed in a following study, comparing the effect of phosphate buffers in alcohol isomerisations in the presence of complexes

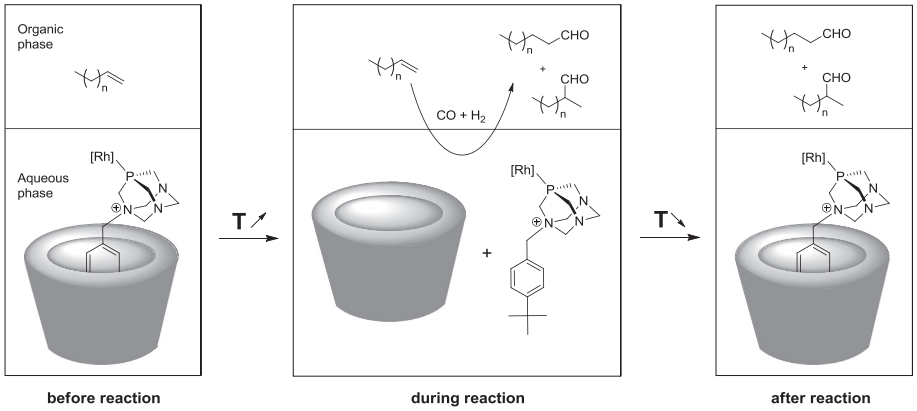

Scheme 19. Thermocontrolled hydroformylation of higher olefins in the presence of cyclodextrin/**21a** and Rh(I). Reproduced from Ref. [12] by permission of The Royal Society of Chemistry.

Please cite this article in press as: A. Guerriero et al., Coordination chemistry of 1,3,5-triaza-7-phosphatricyclo[3.3.1.1]decane (PTA) and derivatives. Part III. Variations on a theme: Novel architectures, materials and applications, Coord. Chem. Rev. (2017), https://doi.org/10.1016/j.ccr.2017.09.024

$[RuCpCl(HPTA)_2]Cl_2{\cdot}2H_2O$ (**56**), $[RuCp(\kappa S\text{-DMSO})(PTA)_2]Cl$ (**57**), $[RuCp(\kappa S\text{-DMSO})(PTA)_2](OTf)$ (**58**) and $[RuCp(\kappa S\text{-DMSO})(HPTA)_2]Cl_3{\cdot}2H_2O$ (**59**) [41].

Complexes $[RuCl_2(\eta^6\text{-arene})(mPTA)]Cl$ (**48**, η^6-arene = C_6H_6, **a**; p-cymene, **b**; 1,3,5-$C_6H_3Me_3$, **c**; C_6Me_6, **d**) were also tested for allylic alcohols isomerisation in combination with K_2CO_3 in refluxing THF, reaching TOF values of ca. 800 h^{-1} with **48a** using $CH_2{=}CH(OH)CH_3$ as substrate. By heterogenisation of **48a** on Montmorillonite K-10 clay, it was possible to obtain a highly efficient and recyclable system (11 consecutive runs) for the isomerisation of 1-octen-3-ol [32].

Complex $[Ru(\eta^2\text{-}O_2CO)(p\text{-cymene})(PTA)]$ (**51**) gave high activity in oct-1-en-3-ol isomerisation to 2-octanone in pH >10 buffer solutions or in the presence of alkali metal carbonates, reaching for example ca. 95% conversion after 1 h at 75 °C. The catalyst formed *in situ* by $[RuCl_2(p\text{-cymene})(PTA)]$ and 2 equiv. of Na_2CO_3 could be reused for up to 5 times under biphasic conditions without loss of activity [35].

Very recently, the new complex $[RuCp(H_2O)(PTA)_2](OTf)$ (**253**) was obtained from the parent chloride complex in water by halide abstraction with AgOTf. The catalytic properties of **253** in the isomerisation of a small library of allylic alcohols to the corresponding ketones were tested, reaching good to excellent conversions (45–99%) under mild (40 °C) to moderate (85 °C) temperatures, depending on the nature of the substrate. The need of a protecting nitrogen atmosphere was demonstrated, as well as the dependence of the activities on the amount of water present in the catalytic mixture. A proposed mechanism and deactivation pathway were also described [138]. The previously described $[RuCpCl(dmoPTA)(PPh_3)](OTf)$ and the bimetallic derivatives $[RuCp(PPh_3)Cl(\mu\text{-dmoPTA-}1\kappa P{:}2\kappa N,N'\text{-}MCl_2]$ (M = Zn, Co, Ni, Scheme 10) were tested as catalysts for the isomerisation of 1-octen-3-ol, 1-hepten-3-ol and 1-hexen-3-ol with good results under mild conditions, with higher activities observed in phosphate buffer solutions than in neat water. The monometallic compound gave the best results, acting as precursor for the catalytically active species $[RuCp(H_2O)(dmoPTA)(PPh_3)]^{2+}$, whereas the bimetallic complexes decomposed under reaction conditions releasing MCl_2 and in turn chloride anions, whose increased concentration in solution hampered the formation of the active aquo species [139].

Rh-PTA macromolecular catalysts were obtained by tethering PTA on the surface of phosphorhydrazone dendrimers. The complexes were used as catalysts for the isomerisation of 1-octen-3-ol to octen-2-one. It was shown that the best (albeit moderate) catalytic activity could be obtained at 75 °C with the smallest (generation G_1) dendrimer, containing 12 PTA molecules on the external layer of the macromolecule [13].

The catalyst obtained *in situ* from $[Rh(cod)(MeCN)_2](BF_4)$ and PTA showed very fast redox isomerisation of a series of aryl and alkyl allylic secondary and primary alcohols in the temperature range 25–80 °C in water at neutral pH, with catalyst loadings as low as 0.5 mol%. Mechanistic investigations using deuterium labelled substrates or D_2O showed that intramolecular 1,3-hydrogen shift occurs, with formation of Rh–alcohol, –enone and –enol intermediates [140]. The same catalytic system was also used for isomerisation of codeine and morphine into hydrocodeine and hydromorphine, respectively, with high yields using catalyst loadings in the range 0.05–10 mol% and temperatures from 70 to 130 °C in neat water, and the reactions could be scaled up to 100 g [141]. Rhodium complexes $[Rh(CO)(PTA)_4]Cl$ (**142**, Fig. 11) and $[RhH(PTA)_4]$ (**144**) were used as catalyst precursors for isomerisation/condensation of allyl alcohol to 3-hydroxy-2-methylpentanal (HP) and 2-methyl-2-pentenal (MP) in water under ambient conditions in the presence of NaOH, required only

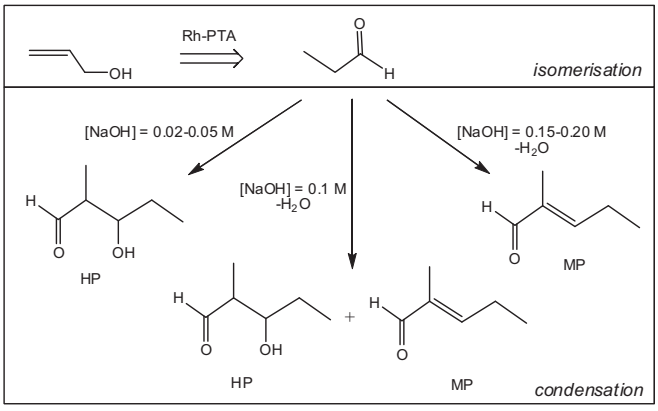

Scheme 20. Isomerisation-condensation reactions catalysed by Rh–PTA complexes **142** and **144** [71].

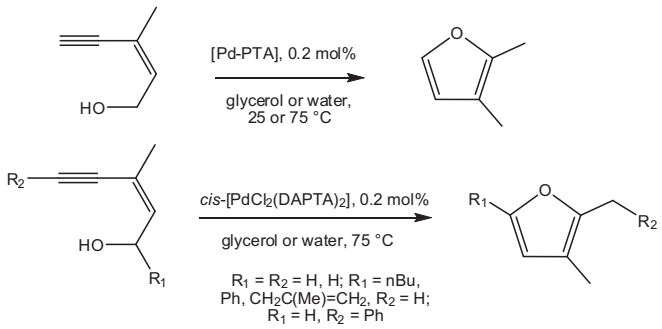

Scheme 21. Cycloisomerisation reactions catalysed by Pd–PTA complexes [81].

Please cite this article in press as: A. Guerriero et al., Coordination chemistry of 1,3,5-triaza-7-phosphatricyclo[3.3.1.1]decane (PTA) and derivatives. Part III. Variations on a theme: Novel architectures, materials and applications, Coord. Chem. Rev. (2017), https://doi.org/10.1016/j.ccr.2017.09.024

for the condensation step (Scheme 20). High yields in the desired products and TOFs as high as 2000 h^{-1} were obtained in the NaOH concentration range 0.05–0.2 M [71].

Finally, efficient Pd-catalysed cycloisomerisation of (Z)-3-methyl-2-penten-4-yl-1-ol into 2,3-dimethylfuran was obtained both in water and glycerol as reaction media using *cis*-[$PdCl_2$(DAPTA)$_2$], *cis*-[$PdCl_2$(PTA)$_2$] and *cis*-[$PdCl_2$(PTA–Bn)$_2$]Cl_2 (**159**) either at room temperature or 75 °C for 3–9 h (Scheme 21). The Pd–DAPTA complex outperformed the others, with TOFs as high as 1980 h^{-1} in water at 75 °C, giving 99% of desired product after 15 min, allowing also for high catalyst recyclability (up to 17 consecutive cycles). The scope of the reaction was extended to substituted Z-enynols, achieving fast reactions and high yields using the Pd–DAPTA catalyst [81].

Acknowledgement

The Italian Ministry for Education and Research (MIUR) is kindly acknowledged for financial support through Project PRIN 2015 (grant number 20154X9ATP).

Appendix A. Supplementary data

Supplementary data associated with this article can be found, in the online version, at https://doi.org/10.1016/j.ccr.2017.09.024.

References

[1] (a) A.D. Phillips, L. Gonsalvi, A. Romerosa, F. Vizza, M. Peruzzini, Coord. Chem. Rev. 248 (2004) 955–993;
(b) J. Bravo, S. Bolaño, L. Gonsalvi, M. Peruzzini, Coord. Chem. Rev. 254 (2010) 555–607.
[2] B.S. Murray, M.V. Bavak, C. Hartinger, P.J. Dyson, Coord. Chem. Rev. 306 (2016) 86–114.
[3] (a) J. Garcia-Alvarez, J. Diaz, J. Gimeno, Green Chem. 12 (2010) 2127–2130;
(b) J. Garcia-Alvarez, J. Diaz, J. Gimeno, F.J. Suarez, C. Vincent, Eur. J. Inorg. Chem. (2012) 5854–5863.
[4] M. Carreira, R. Calvo-Sanjuan, M. Sanau, I. Marzo, M. Contel, Organometallics 31 (2012) 5772–5781.
[5] A. Udvardy, M. Purgel, T. Szarvas, F. Joó, A. Kathó, Struct. Chem. 26 (2015) 1323–1334.
[6] (a) G.W. Wong, J.L. Harkreader, C.A. Mebi, B.J. Frost, Inorg. Chem. 45 (2006) 6748–6755;
(b) M. Erlandsson, L. Gonsalvi, A. Ienco, M. Peruzzini, Inorg. Chem. 47 (2008) 8–10;
(c) G.W. Wong, W.-C. Lee, B.J. Frost, Inorg. Chem. 47 (2008) 612–620.
[7] A. Guerriero, M. Erlandsson, A. Ienco, D.A. Krogstad, M. Peruzzini, G. Reginato, L. Gonsalvi, Organometallics 30 (2011) 1874–1884.
[8] D.A. Krogstad, A. Guerriero, A. Ienco, G. Manca, M. Peruzzini, G. Reginato, L. Gonsalvi, Organometallics 30 (2011) 6292–6302.
[9] W.-C. Lee, J.M. Sears, R.A. Enow, K. Eads, D.A. Krogstad, B.J. Frost, Inorg. Chem. 52 (2013) 1737–1746.
[10] J.M. Sears, W.-C. Lee, B.J. Frost, Inorg. Chim. Acta 431 (2015) 248–257.
[11] S. Schäfer, W. Frey, A.S.K. Hashmi, V. Cmrecki, A. Luquin, M. Laguna, Polyhedron 29 (2010) 1925–1932.
[12] (a) N. Six, A. Guerriero, D. Landy, M. Peruzzini, L. Gonsalvi, F. Hapiot, E. Monflier, Catal. Sci. Technol. 1 (2011) 1347–1353;
(b) L. Gonsalvi, A. Guerriero, F. Hapiot, D.A. Krogstad, E. Monflier, G. Reginato, M. Peruzzini, Pure Appl. Chem. 85 (2013) 385–396.
[13] P. Servin, R. Laurent, H. Dib, L. Gonsalvi, M. Peruzzini, J.-P. Majoral, A.-M. Caminade, Tetrahedron Lett. 53 (2012) 3876–3879.
[14] V. Ferretti, M. Fogagnolo, A. Marchi, L. Marvelli, F. Sforza, P. Bergamini, Inorg. Chem. 53 (2014) 4881–4890.
[15] (a) R. Cortesi, P. Bergamini, L. Ravani, M. Drechsler, A. Costenaro, M. Pinotti, M. Campioni, L. Marvelli, E. Esposito, Int. J. Pharm. 431 (2012) 176–182;
(b) P. Bergamini, L. Marvelli, A. Marchi, F. Vassanelli, M. Fogagnolo, P. Formaglio, T. Bernardi, R. Gavioli, F. Sforza, Inorg. Chim. Acta 391 (2012) 162–170.
[16] P. Bergamini, L. Marvelli, A. Marchi, V. Bertolasi, M. Fogagnolo, P. Formaglio, F. Sforza, Inorg. Chim. Acta 398 (2013) 11–18.
[17] A. Udvardy, A.C. Benyei, P. Juhasz, F. Joó, A. Kathó, Polyhedron 60 (2013) 1–9.
[18] S.N. Britvin, A. Lotnyk, J. Am. Chem. Soc. 137 (2015) 5526–5535.
[19] A. Guerriero, W. Oberhauser, T. Riedel, M. Peruzzini, P.J. Dyson, L. Gonsalvi, Inorg. Chem. 56 (2017) 5514–5518.
[20] S.N. Britvin, A.M. Rumyantsev, A.E. Zobnia, M.V. Padkina, Chem. Eur. J. 22 (2016) 14227–14235.
[21] E. Nicolas, A. Guerriero, V. Lyaskovsky, M. Peruzzini, K. Lammertsma, L. Gonsalvi, J.C. Slootweg, Inorganics 4 (2016) 34–41.
[22] F. Mohr, J. Nielsen, U. Schatzschneider, C.W. Lehrmann, Z. Anorg. Allg. Chem. 638 (2012) 543–546.
[23] I. Chakraborty, S.J. Carrington, G. Roseman, P.K. Mascharak, Inorg. Chem. 56 (2017) 1534–1545.
[24] R.S. Herrick, C.J. Ziegler, S. Sripothongnak, N. Barone, R. Costa, W. Cupelo, A. Gambella, J. Organomet. Chem. 694 (2009) 3929–3934.
[25] (a) E. Maccaroni, H. Dong, O. Blacque, H.W. Schmalle, C.M. Frech, H. Berke, J. Organomet. Chem. 695 (2010) 487–494;
(b) H. Dong, H. Berke, J. Organomet. Chem. 696 (2011) 1803–1808.
[26] X. Tu, G.S. Nichol, Z. Zheng, J. Cluster Sci. 20 (2009) 93–103.
[27] L.M.D.R.S. Martins, E.C.B.A. Alegria, P. Smolenski, M.L. Kuznetsov, A.J.L. Pombeiro, Inorg. Chem. 52 (2013) 4534–4546.
[28] W.-H. Ang, A. Casini, G. Sava, P.J. Dyson, J. Organomet. Chem. 696 (2011) 989–998.
[29] (a) B.M. Blunden, D.S. Thomas, M.H. Stenzel, Polym. Chem. 3 (2012) 2964–2975;
(b) B.M. Blunden, H. Lu, M.H. Stenzel, Biomacromolecules 14 (2013) 4177–4188.
[30] E. Quartapelle Procopio, S. Rojas, N.M. Padial, S. Galli, N. Masciocchi, F. Linares, D. Miguel, J.E. Oltra, J.A.R. Navarro, E. Barea, Chem. Commun. 47 (2011) 11751–11753.
[31] I. Czerwinska, J. Far, C. Kune, C. Larriba-Andaluz, L. Delaude, E. De Pauw, Dalton Trans. 45 (2016) 6361–6370.
[32] L. Menendez-Rodriguez, P. Crochet, V. Cadierno, J. Mol. Catal. A: Chem. 366 (2013) 390–399.
[33] R. Kishan, R. Kumar, S. Baskaran, C. Sivasankar, N. Thirupathi, Eur. J. Inorg. Chem. (2015) 3182–3194.
[34] N. Marozsan, H. Horvath, A. Erdei, F. Joó, J. Mol. Catal. A: Chem. 425 (2016) 103–109.
[35] E. Bolyog-Nagy, A. Udvardy, A. Barczáne-Bertók, F. Joó, A. Kathó, Inorg. Chim. Acta 455 (2017) 514–520.
[36] E.M. Peña-Mendez, B. Gonzalez, P. Lorenzo, A. Romerosa, J. Havel, Rapid Commun. Mass Spectrom. 23 (2009) 3831–3856.
[37] A. Mena-Cruz, P. Lorenzo-Luis, V. Passarelli, A. Romerosa, M. Serrano-Ruiz, Dalton Trans. 40 (2011) 3237–3244.
[38] M. Serrano-Ruiz, L.M. Aguilera-Saez, P. Lorenzo-Luis, J.M. Padron, A. Romerosa, Dalton Trans. 42 (2013) 11212–11219.
[39] M. Serrano-Ruiz, S. Imberti, L. Bernasconi, N. Jadagayeva, F. Scalambra, A. Romerosa, Chem. Commun. 50 (2014) 11587–11590.
[40] F. Scalambra, M. Serrano-Ruiz, A. Romerosa, Macromol. Rapid Commun. 36 (2015) 689–693.
[41] M. Serrano-Ruiz, P. Lorenzo-Luis, A. Romerosa, A. Mena-Cruz, Dalton Trans. 42 (2013) 7622–7630.
[42] M. Serrano-Ruiz, P. Lorenzo-Luis, A. Romerosa, Inorg. Chim. Acta 455 (2017) 528–534.
[43] D.S. Perekalin, N.V. Shvydkiy, Y.V. Nelyubina, A.R. Kudinov, Mendeleev Commun. 25 (2015) 29–31.
[44] E.A. Trifonova, D.S. Perekalin, N.L. Loskutova, Y.V. Nelyubina, A.R. Kudinov, J. Organomet. Chem. 785 (2015) 106–111.
[45] G. Kovacs, A. Rossin, L. Gonsalvi, A. Lledos, M. Peruzzini, Organometallics 29 (2010) 5121–5131.
[46] (a) M. Serrano-Ruiz, C. Lidrissi, S. Mañas, M. Peruzzini, A. Romerosa, J. Organomet. Chem. 751 (2014) 654–661; A similar study was reported earlier by the same groups, see (b) C. Lidrissi, A. Romerosa, M. Saoud, M. Serrano-Ruiz, L. Gonsalvi, M. Peruzzini Angew. Chem. Int. Ed. 44 (2005) 2568–2572.
[47] S. Bolaño, M.M. Rodriguez-Rocha, J. Bravo, J. Castro, E. Oñate, M. Peruzzini, Organometallics 28 (2009) 6020–6030.
[48] A. Garcia-Fernandez, M.P. Gamasa, E. Lastra, J. Organomet. Chem. 695 (2010) 162–169.
[49] A. Garcia-Fernandez, J. Diaz, A. Manteca, J. Sanchez, R. Garcia-Navas, B.G. Sierra, F. Mollinedo, M.P. Gamasa, E. Lastra, Dalton Trans. 39 (2010) 10186–10196.
[50] A. Garcia-Fernandez, J. Diaz, M.P. Gamasa, E. Lastra, Eur. J. Inorg. Chem. (2014) 917–924.
[51] S. Miguel, J. Diaz, M.P. Gamasa, E. Lastra, Eur. J. Inorg. Chem. (2011) 4745–4755.
[52] A. Garcia-Fernandez, S. Miguel, J. Diaz, M.P. Gamasa, E. Lastra, Eur. J. Inorg. Chem. (2016) 2516–2526.
[53] L. Hajji, C. Saraiba-Bello, A. Romerosa, G. Segovia-Torrente, M. Serrano-Ruiz, P. Bergamini, A. Canella, Inorg. Chem. 50 (2011) 873–882.
[54] L. Hajji, C. Saraiba-Bello, M. Serrano-Ruiz, A. Romerosa, J. Coord. Chem. 67 (2014) 2701–2710.
[55] L. Hajji, V. Jara-Perez, C. Saraiba-Bello, G. Segovia-Torrente, M. Serrano-Ruiz, A. Romerosa, Inorg. Chim. Acta 455 (2017) 557–567.
[56] V. Cadierno, J. Diaz, J. Francos, J. Gimeno, Chem. Eur. J. 16 (2010) 9808–9817.
[57] D. Yakhvarov, M. Caporali, L. Gonsalvi, S. Latypov, V. Mirabello, I. Rizvanov, O. Sinyashin, P. Stoppioni, M. Peruzzini, Angew. Chem. Int. Ed. 50 (2011) 5370–5373.
[58] R. Pettinari, F. Marchetti, A. Petrini, C. Pettinari, G. Lupidi, B. Fernandez, A. Rodriguez Dieguez, G. Santoni, M. Nabissi, Inorg. Chim. Acta 454 (2017) 139–148.
[59] C. Sarniguet, J. Toloza, M. Cipriani, M. Lapier, M. Vieites, Y. Toledano-Magaña, J.C. Garcia-Ramos, L. Ruiz-Azuara, V. Moreno, J.D. Maya, C. Olea Azar, D. Gambino, L. Otero, Biol. Trace Elem. Res. 159 (2014) 379–392.

[60] J.G. Hernandez, P. Thangarasu, H. Höpfl, J. Cruz, M. Serrano-Ruiz, A. Romerosa, Inorg. Chim. Acta 431 (2015) 258–265.
[61] (a) R. Mager, K. Robeyns, S. Hermans, J. Organomet. Chem. 794 (2015) 48–58; The preparation and X-ray crystal structure of $Ru_3(CO)_9(PTA)_3$ were already reported, see (b) D.J. Darenbsourg, F.A. Beckford, J.H. Reibenspies, J. Cluster Sci. 11 (2000) 95–108.
[62] J. Huang, J. Chen, H. Gao, L. Chen, Inorg. Chem. 53 (2014) 9570–9580.
[63] F. Scalambra, M. Serrano-Ruiz, S. Nahim-Granados, A. Romerosa, Eur. J. Inorg. Chem. (2016) 1528–1540.
[64] F. Battistin, G. Balducci, E. Iengo, N. Demitri, E. Alessio, Eur. J. Inorg. Chem. (2016) 2850–2860.
[65] A.K. Vannucci, S. Wang, G.S. Nichol, D.L. Lichtenberger, D.H. Evans, R.S. Glass, Dalton Trans. 39 (2010) 3050–3056.
[66] A.C. Dugan, B.S.N. Nolan, K.L. Brehm, J.L. Jackson Jr., N. Gwini, S.D. Floris, D.M. Marolf, J.E. Johnstone, S.H. Yoon, G.L. Powell, V.N. Nesterov, H.M. Johnson, K. N. Green, Polyhedron 114 (2016) 292–298.
[67] E. Menendez-Pedregal, A. Manteca, J. Sanchez, J. Diez, M.P. Gamasa, E. Lastra, Eur. J. Inorg. Chem. (2015) 1424–1432.
[68] P. Smolenski, A. Kochel, Polyhedron 29 (2010) 1561–1566.
[69] T.F.S. Silva, P. Smolenski, L.M.D.R.S. Martins, M.F.C. Guedes da Silva, A.R. Fernandes, D. Luis, A. Silva, S. Santos, P.M. Borralho, C.M.P. Rodrigues, A.J.L. Pombeiro, Eur. J. Inorg. Chem. (2013) 3651–3658.
[70] P. Smolenski, A.M. Kirillov, M.F.C. Guedes da Silva, A.J.L. Pombeiro, Inorg. Chim. Acta 378 (2011) 342–346.
[71] P. Smolenski, M.V. Kirillova, M.F.C. Guedes da Silva, A.J.L. Pombeiro, Dalton Trans. 42 (2013) 10867–10874.
[72] J. Potier, A. Guerriero, S. Menuel, E. Monflier, M. Peruzzini, F. Hapiot, L. Gonsalvi, Catal. Commun. 63 (2015) 74–78.
[73] G. Ciancaleoni, S. Bolaño, J. Bravo, M. Peruzzini, L. Gonsalvi, A. Macchioni, Dalton Trans. 39 (2010) 3366–3368.
[74] S. Bolaño, M. Plaza, J. Bravo, J. Castro, M. Peruzzini, L. Gonsalvi, G. Ciancaleoni, A. Macchioni, Inorg. Chim. Acta 363 (2010) 509–516.
[75] R. Pettinari, F. Marchetti, C. Pettinari, F. Condello, A. Petrini, R. Scopelliti, T. Riedel, P.J. Dyson, Dalton Trans. 44 (2015) 20523–20531.
[76] P. Barbaro, L. Gonsalvi, A. Guerriero, F. Liguori, Green Chem. 14 (2012) 3211–3219.
[77] A. Kapdi, V. Gayakhe, Y.S. Sanghvi, J. Garcia, P. Lozano, I. da Silva, J. Perez, J.L. Serrano, RSC Adv. 4 (2014) 17567–17572.
[78] V. Gayakhe, A. Ardhapure, A. Kapdi, Y.S. Sanghvi, J.L. Serrano, L. Garcia, J. Perez, J. Garcia, G. Sanchez, C. Fischer, C. Schulzke, J. Org. Chem. 81 (2016) 2713–2729.
[79] J. Spencer, A. Casini, O. Zava, R.P. Rathnam, S.K. Velhanda, M. Pfeffer, S.K. Callear, M.B. Hursthouse, P.J. Dyson, Dalton Trans. (2009) 10731–10735.
[80] J. Ruiz, N. Cutillas, M.D. Villa, G. Lopez, A. Espinosa, D. Bautista, Dalton Trans. (2009) 9637–9644.
[81] J. Francos, V. Cadierno, Green Chem. 12 (2010) 1552–1555.
[82] A. Zatajska, M. Siczek, A. Skarzynska, P. Smolenski, Inorg. Chim. Acta 455 (2017) 701–706.
[83] J.A. Weeden, R. Huang, K.D. Galloway, P.W. Ginrich, B.J. Frost, Molecules 16 (2011) 6215–6231.
[84] (a) P. Chellan, T. Stringer, A. Shokar, P.J. Dornbush, G. Vazquez-Anaya, K.M. Land, K. Chiale, G.S. Smith, J. Inorg. Biochem. 105 (2011) 1562–1568;
(b) T. Stringer, D.T. Hendricks, H. Guzgay, G.S. Smith, Polyhedron 31 (2012) 486–493.
[85] J. Lasri, M.J. Fernandez Rodriguez, M.F.C. Guedes da Silva, P. Smolenski, M.N. Kopylovich, J.J.R. Frausto da Silva, A.J.L. Pombeiro, J. Organomet. Chem. 696 (2011) 3513–3520.
[86] J. Braddock-Wilking, S. Acharya, N.P. Rath, Polyhedron 79 (2014) 16–28.
[87] J. Braddock-Wilking, S. Acharya, N.P. Rath, Polyhedron 87 (2015) 55–62.
[88] M.Y. Demakova, K.V. Luzyanin, G.L. Starova, V.Yu. Kukushkin, Inorg. Chem. Commun. 50 (2014) 17–18.
[89] T.P. Latendresse, S.J. Adams, G.J. Grant, J.P. Lee, A.G. Oliver, Polyhedron 114 (2016) 80–87.
[90] C. Mügge, C. Rothenburger, A. Beyer, H. Görls, C. Gabbiani, A. Casini, E. Michelucci, I. Landini, S. Nobili, E. Mini, L. Messori, W. Weigand, Dalton Trans. 40 (2011) 2006–2016.
[91] P. Bippus, M. Skocic, M.A. Jakupec, B.K. Keppler, F. Mohr, J. Inorg. Biochem. 105 (2011) 462–466.
[92] P. Chellan, K.M. Land, A. Shokar, A. Au, S.H. An, C.M. Clavel, P.J. Dyson, C. de Kock, P.J. Smith, K. Chibale, G.S. Smith, Organometallics 31 (2012) 5791–5799.
[93] M. Cipriani, J. Toloza, L. Bradford, E. Putzu, M. Vieites, E. Curbelo, A.I. Tomaz, B. Garat, J. Guerrero, J.S. Gancheff, J.D. Maya, C. Olea Azar, D. Gambino, L. Otero, Eur. J. Inorg. Chem. (2014) 4677–4689.
[94] E. Guerrero, S. Miranda, S. Lüttenberg, N. Frölich, J.-M. Koenen, F. Mohr, E. Cerrada, M. Laguna, A. Mendia, Inorg. Chem. 52 (2013) 6635–6647.
[95] J. Ruiz, V. Rodriguez, N. Cutillas, A. Espinosa, M.J. Hannon, J. Inorg. Biochem. 105 (2011) 525–531.
[96] M. Porchia, F. Benetollo, F. Refosco, F. Tisato, C. Marzano, V. Gandin, J. Inorg. Biochem. 103 (2009) 1644–1651.
[97] V. Gandin, A. Trenti, M. Porchia, F. Tisato, M. Giorgetti, I. Zanusso, L. Trevisi, C. Marzano, Metallomics 7 (2015) 1497–1507.
[98] F. Endrizzi, P. Di Bernardo, P.L. Zanonato, F. Tisato, M. Porchia, A.A. Isse, A. Melchior, M. Tolazzi, Dalton Trans. 46 (2017) 1455–1466.
[99] (a) M. Porchia, A. Dolmella, V. Gandin, C. Marzano, M. Pellei, V. Peruzzo, F. Refosco, C. Santini, F. Tisato, Eur. J. Med. Chem. 59 (2013) 218–226;
(b) V. Gandin, F. Tisato, A. Dolmella, M. Pellei, C. Santini, M. Giorgetti, C. Marzano, M. Porchia, J. Med. Chem. 57 (2014) 4745–4760.
[100] L. Jaremko, A.M. Kirillov, P. Smolenski, A.J.L. Pombeiro, Cryst. Growth Des. 9 (2009) 3006–3010.
[101] A.M. Kirillov, P. Smolenski, Z. Ma, M.F.C. Guedes da Silva, M. Haukka, A.J.L. Pombeiro, Organometallics 28 (2009) 6425–6431.
[102] A.M. Kirillov, M. Filipowicz, M.F.C. Guedes da Silva, J. Klak, P. Smolenski, A.J.L. Pombeiro, Organometallics 31 (2012) 7921–7925.
[103] P. Smolenski, J. Klak, D.S. Nesterov, A.M. Kirillov, Cryst. Growth Des. 12 (2012) 5852–5857.
[104] A. Lis, M.F.C. Guedes da Silva, A.M. Kirillov, P. Smolenski, A.J.L. Pombeiro, Cryst. Growth Des. 10 (2010) 5244–5253.
[105] A.M. Kirillov, S.W. Wieczorek, M.F.C. Guedes da Silva, J. Sokolnicki, P. Smolenski, A.J.L. Pombeiro, CrystEngComm 13 (2011) 6329–6333.
[106] S.W. Jaros, M.F.C. Guedes da Silva, M. Florek, M.C. Oliveira, P. Smolenski, A.J.L. Pombeiro, A.M. Kirillov, Cryst. Growth Des. 14 (2014) 5408–5417.
[107] S.W. Jaros, M.F.C. Guedes da Silva, J. Krol, M.C. Oliveira, P. Smolenski, A.J.L. Pombeiro, A.M. Kirillov, Inorg. Chem. 55 (2016) 1486–1496.
[108] S.W. Jaros, M.F.C. Guedes da Silva, M. Florek, P. Smolenski, A.J.L. Pombeiro, A. M. Kirillov, Inorg. Chem. 55 (2016) 5886–5894.
[109] S.J. Zamisa, B. Omondi, J. Coord. Chem. 69 (2016) 3043–3052.
[110] P. Smolenski, S.W. Jaros, C. Pettinari, G. Lupidi, L. Quassinti, M. Bramucci, L.A. Vitali, D. Petrelli, A. Kochel, A.M. Kirillov, Dalton Trans. 42 (2013) 6572–6581.
[111] C. Pettinari, F. Marchetti, G. Lupidi, L. Quassinti, M. Bramucci, D. Petrelli, L.A. Vitali, M.F.C. Guedes da Silva, L.M.D.R.S. Martins, P. Smolenski, A.J.L. Pombeiro, Inorg. Chem. 50 (2011) 11173–11183.
[112] P. Smolenski, C. Pettinari, F. Marchetti, M.F.C. Guedes da Silva, G. Lupidi, G.V. Badillo Patzmay, D. Petrelli, L.A. Vitali, A.J.L. Pombeiro, Inorg. Chem. 54 (2015) 434–440.
[113] A.M. Kirillov, S.W. Wieczorek, A. Lis, M.F.C. Guedes da Silva, M. Florek, J. Krol, Z. Staroniewicz, P. Smolenski, A.J.L. Pombeiro, Cryst. Growth Des. 11 (2011) 2711–2716.
[114] S.W. Jaros, P. Smolenski, M.F.C. Guedes da Silva, M. Florek, J. Krol, Z. Staroniewicz, A.J.L. Pombeiro, A.M. Kirillov, CystEngComm 15 (2013) 8060–8064.
[115] (a) Y.R. Hristova, B. Kember, P. Besenius, Tetrahedron 69 (2013) 10525–10533;
(b) B. Bertrand, A. Casini, Dalton Trans. 43 (2014) 4209–4219.
[116] (a) Recent articles describing medicinal application of Au-PTA derivatives include: E. Vergara, E. Cerrada, A. Casini, O. Zava, M. Laguna, P.J. Dyson Organometallics 29 (2010) 2596–2603;
(b) E. Vergara, A. Casini, F. Sorrentino, O. Zava, E. Cerrada, M.P. Rigobello, A. Bindoli, M. Laguna, P.J. Dyson, ChemMedChem 5 (2010) 96–102;
(c) L. Maiore, M.A. Cinellu, E. Michelucci, G. Moneti, S. Nobili, I. Landini, E. Mini, A. Guerri, C. Gabbiani, L. Messori, J. Inorg. Biochem. 105 (2011) 348–355;
(d) E. Vergara, E. Cerrada, C. Clavel, A. Casini, M. Laguna, Dalton Trans. 40 (2011) 10927–10935;
(e) C. Santini, M. Pellei, G. Papini, B. Morresi, R. Galassi, S. Ricci, F. Tisato, M. Porchia, M.P. Rigobello, V. Gandin, C. Marzano, J. Inorg. Biochem. 105 (2011) 232–240;
(f) E. Garcia-Moreno, S. Gascon, M.J. Rodriguez-Yoldi, E. Cerrada, M. Laguna, Organometallics 32 (2013) 3710–3720.
[117] E. Garcia-Moreno, E. Cerrada, M.J. Bolsa, A. Luquin, M. Laguna, Eur. J. Inorg. Chem. (2013) 2020–2030.
[118] E. Garcia-Moreno, S. Gascon, E. Atrian-Blasco, M.J. Rodriguez-Yoldi, E. Cerrada, M. Laguna, Eur. J. Med. Chem. 79 (2014) 164–172.
[119] R. Gavara, J. Llorca, J.C. Lima, L. Rodriguez, Chem. Commun. 19 (2013) 72–74.
[120] (a) J. Arcau, V. Andermark, E. Aguiló, A. Gandioso, A. Moro, M. Cetina, J. C. Lima, K. Rissanen, I. Ott, L. Rodriguez, Dalton Trans. 43 (2014) 4426–4436;
(b) A.J. Moro, B. Rome, E. Aguiló, J. Arcau, R. Puttreddy, K. Rissanen, J.C. Lima, L. Rodriguez, Org. Biomol. Chem. 12 (2015) 2026–2033.
[121] E. Aguiló, R. Gavara, C. Baucells, M. Guitart, J.C. Lima, J. Llorca, L. Rodriguez, Dalton Trans. 45 (2016) 7328–7339.
[122] B.J. Frost, W.-C. Lee, K. Pal, T.H. Kim, D. VanDerveer, D. Rabinovitch, Polyhedron 29 (2010) 2373–2380.
[123] D. Anselmo, R. Gramage-Doria, T. Besset, M.V. Escarcega-Bobadilla, G. Salassa, E.C. Escudero-Adan, M. Martinez Belmonte, E. Martin, J.N.H. Reek, A.W. Kleij, Dalton Trans. 42 (2013) 7595–7603.
[124] X. Tu, H. Truong, G.S. Nichol, Z. Zheng, Inorg. Chim. Acta 363 (2010) 4189–4196.
[125] S.E. Garcia-Garrido, J. Francos, V. Cadierno, J.-M. Basset, V. Pohlshettiwar, ChemSusChem 4 (2011) 104–111.
[126] W.-C. Lee, B.J. Frost, Green Chem. 14 (2012) 62–66.
[127] E. Bolyog-Nagy, A. Udvardy, F. Joó, A. Kathó, Tetrahedron Lett. 55 (2014) 3615–3617.
[128] A. Kumar Misra, E. Bokor, S. Kun, E. Bolyog-Nagy, A. Kathó, F. Joó, L. Somsak, Tetrahedron Lett. 56 (2015) 5995–5998.
[129] T.J. Sherbow, E.L. Downs, R.I. Saylar, J.J. Razink, J.J. Juliette, D.R. Tyler, ACS Catal. 4 (2014) 3096–3104.
[130] C. Delhomme, L.A. Schaper, M. Zhang-Presse, G. Raudaschl-Sieber, D. Weuster-Botz, F.E. Kühn, J. Organomet. Chem. 724 (2013) 297–299.
[131] P.-J. Debouttiere, V. Martinez, K. Philippot, B. Chaudret, Dalton Trans. (2009) 10172–10174.

Please cite this article in press as: A. Guerriero et al., Coordination chemistry of 1,3,5-triaza-7-phosphatricyclo[3.3.1.1]decane (PTA) and derivatives. Part III. Variations on a theme: Novel architectures, materials and applications, Coord. Chem. Rev. (2017), https://doi.org/10.1016/j.ccr.2017.09.024

[132] P.-J. Debouttiere, Y. Coppel, A. Denicourt-Nowicki, A. Roucoux, B. Chaudret, K. Philippot, Eur. J. Inorg. Chem. (2012) 1229–1236.
[133] M. Caporali, A. Guerriero, A. Ienco, S. Caporali, M. Peruzzini, L. Gonsalvi, ChemCatChem 5 (2013) 2517–2526.
[134] S. Moret, P.J. Dyson, G. Laurenczy, Nat. Commun. 5 (2014) 4017.
[135] L.C. Matsinha, P. Malatji, A.T. Hutton, G.A. Venter, S.F. Mapolle, G.S. Smith, Eur. J. Inorg. Chem. (2013) 4318–4328.
[136] A. Udvardy, A.C. Benyei, A. Kathó, J. Organomet. Chem. 717 (2012) 116–122.
[137] B. Gonzalez, P. Lorenzo-Luis, M. Serrano-Ruiz, E. Papp, M. Fekete, K. Csepke, K. Osz, A. Kathó, F. Joó, A. Romerosa, J. Mol. Catal. A: Chem. 326 (2010) 15–20.
[138] F. Scalambra, M. Serrano-Ruiz, A. Romerosa, Dalton Trans. 46 (2017) 5864–5871.
[139] A. Mena-Cruz, M. Serrano-Ruiz, P. Lorenzo-Luis, A. Romerosa, A. Kathó, F. Joó, L.M. Aguilera-Saez, J. Mol. Catal. A: Chem. 411 (2016) 27–33.
[140] N. Ahlsten, H. Lundberg, B. Martin-Mature, Green Chem. 12 (2010) 1628–1633.
[141] A. Bermejo Gomez, P. Holmberg, J.-E. Bäckvall, B. Martin-Matute, RSC Adv. 4 (2014) 39519–39522.

Please cite this article in press as: A. Guerriero et al., Coordination chemistry of 1,3,5-triaza-7-phosphatricyclo[3.3.1.1]decane (PTA) and derivatives. Part III. Variations on a theme: Novel architectures, materials and applications, Coord. Chem. Rev. (2017), https://doi.org/10.1016/j.ccr.2017.09.024